DESIGN, FABRICATION, PACKAGING AND TESTING OF THIN FILM THERMOCOUPLES FOR BOILING STUDIES

A Thesis

by

NIPUN SINHA

Submitted to the Office of Graduate Studies of
Texas A&M University
in partial fulfillment of the requirements for the degree of

MASTER OF SCIENCE

August 2006

Major Subject: Mechanical Engineering

DESIGN, FABRICATION, PACKAGING AND TESTING OF THIN FILM THERMOCOUPLES FOR BOILING STUDIES

A Thesis

by

NIPUN SINHA

Submitted to the Office of Graduate Studies of
Texas A&M University
in partial fulfillment of the requirements for the degree of

MASTER OF SCIENCE

Approved by:

Chair of Committee,	Debjyoti Banerjee
Committee Members,	N.K.Anand
	Victor M. Ugaz
Head of Department,	Dennis O'Neal

August 2006

Major Subject: Mechanical Engineering

ABSTRACT

Design, Fabrication, Packaging and Testing of Thin Film Thermocouples for Boiling Studies. (August 2006)

Nipun Sinha, B.E., Panjab University

Chair of Advisory Committee: Dr. Debjyoti Banerjee

Boiling is the most efficient form of heat transfer. Thermo-fluidic transport mechanisms at different length and time scales govern the nature of boiling. This study was conducted to enhance the understanding of the surface temperature variations and fluctuations during boiling. Microfabricated thin film thermocouples were used in this study.

The main aim of this study was to develop a repeatable procedure for fabrication of thin film thermocouples and to test them by measuring surface temperatures during various boiling regimes. Since thin film thermocouples are known to provide reliable measurements at very fast response rates, they were selected for this study. Small temperature fluctuations at high sampling rates were studied in boiling experiments conducted using PF-5060 as the boiling medium. An experimental apparatus was fabricated for conducting these experiments and it contained a viewing chamber which housed the copper block used for providing the heat for boiling. The substrate with thin film thermocouples was placed on top of this copper

block for sensing the temperature during boiling on its surface. The small size of these thermocouples was another big advantage as they were expected to cause minimal interference to the temperature distribution and the transport phenomenon during boiling.

This thesis reports the design evolution of the thermocouples according to the need of packaging and describes the fabrication process with sufficient detail so that it can be easily reproduced given the same facilities and environment. The results of testing show that they can be used for monitoring and analyzing surface temperature variations and fluctuations during various boiling regimes with better temporal resolution.

To my parents and my sister

for their love and support

ACKNOWLEDGEMENTS

I thank Dr. Debjyoti Banerjee for his continued support towards achieving my research goals. He has shown tremendous interest in me and my research and without the freedom he has given me, in terms of both thinking and resources, I wouldn't have been able to come this far.

I would also like to thank Dr. N.K. Anand and Dr. Victor M. Ugaz for having interest in my research and for showing personal interest in my work. I would also like to thank them for assisting me when I needed help.

I would also like to thank the employees of the Material Characterization Facility: Dr. William Lackowaski (Former Manager), Yulia Vasileva (Research Assistant) and Shyamashree Chaterjee (Former Research Assistant) for their help.

Finally, I would like to thank my parents for their love and support, without which none of this would have been possible.

TABLE OF CONTENTS

Page

ABSTRACT iii

DEDICATION v

ACKNOWLEDGEMENTS vi

TABLE OF CONTENTS vii

LIST OF FIGURES ix

LIST OF TABLES xiii

CHAPTER

I INTRODUCTION 1

1.1 History of Thin Films 1
1.2 Background of Thin Film Thermocouples 4

II DESIGN AND FABRICATION OF THIN FILM THERMOCOUPLES 6

2.1 Thin Film Thermocouple Design 6
2.2 Thin Film Thermocouple Fabrication 33

III PACKAGING OF THIN FILM THERMOCOUPLES 52

3.1 Packaging Methods 52

IV EXPERIMENTAL SETUP 67

4.1 Frame Structure 67

V EXPERIMENTAL PROCEDURES 79

5.1 Calibration Experiments 79
5.2 Boiling Experiments 81

CHAPTER Page

VI DATA REDUCTION 88

VII RESULTS AND DISCUSSION 91

7.1 Calibration Experiments 91
7.2 Boiling Experiments 109

VIII CONCLUSIONS 124

REFERENCES 126

VITA 131

LIST OF FIGURES

FIGURE Page

2.1. Photomask Obtained from Health Science Center and a Similar Photomask Attached on a Glass Slide Ready for Use in Photolithography 9

2.2. Locators Used for Alignment of Subsequent Photolithographic Layers 11

2.3. Alumel Design: First Generation 13

2.4 Chromel Design: First Generation 14

2.5 Bond Pad Design: First Generation 15

2.6 Full Design: First Generation 16

2.7 Alumel Design: Second Generation 19

2.8 Chromel Design: Second Generation 20

2.9 Full Design: Second Generation 21

2.10 Alumel Design: Third Generation 23

2.11 Chromel Design: Third Generation 24

2.12 Full Design: Third Generation 25

2.13 Alumel Design: Fourth Generation 27

2.14 Chromel Design: Fourth Generation 28

2.15 Full Design: Fourth Generation 29

2.16 Alumel Design: Fifth Generation 31

2.17 Chromel Design: Fifth Generation 32

2.18 Full Design: Fifth Generation 33

FIGURE Page

2.19 Non-programmable Spin Coater 36

2.20 Quintel Mask Aligner Used for Both The Layers of Photolithography 38

2.21 Reactive Ion Etcher Used for Oxygen Plasma Cleaning 40

2.22 Metal Evaporator Used in This Study 42

2.23 Wafer Holder with Traces for the Four Wafers and the Substrate Used for Composition Analysis is Shown in This Image 43

2.24 Chuck for Holding the Sources for Depositing the Layers 44

2.25 Sources Used for Deposition 45

2.26 Schematic Showing the Steps Used for the Fabrication of Thin Film Thermocouples 47

2.27 Last Four Steps of Fabrication of Thin Film Thermocouples 50

3.1 Initial Attempts at Using Pressure Contacts 54

3.2 4523A Digital Manual Wire Bonder 56

3.3 Picture of the Wedge, Spool and Sample Holder for the Wire Bonding Apparatus 59

3.4 Two Methods of Resistance Arc Welding for Thin Film Thermocouples 62

3.5 The Figure Shows the Use of Two Pairs of Alligator Clips 64

3.6 Apparatus for Welding Using Alligator Clips 66

4.1 An Assembled Look at the Apparatus that is Used for Conducting the Experiments 67

FIGURE Page

4.2 Drawing Sheets for the Vertical L-Beams.. 69

4.3 Drawing Sheets for Horizontal L-Beams 70

4.4 Drawing Sheets for Side L-Beams.. 71

4.5 Assembled Back View of the Apparatus... 72

4.6 Steel Jacket Design 73

4.7 Copper Block Design 74

4.8 Schematic Block Diagram of the Experimental Apparatus............. 76

4.9 Picture of Apparatus for Pool Boiling Experiments......................... 78

5.1 Lab View Block Diagram for Temperature Calibration 84

5.2 Lab View Block Diagram for Temperature Measurement 87

7.1 Survey of Alumel Sample I 93

7.2 Survey of a Chromel Sample I 94

7.3 Survey of the Alumel Sample II.. 97

7.4 Nickel Scan of Alumel Sample.. 98

7.5 Aluminum Scan of Alumel Sample.. 99

7.6 Survey of Chromel Sample II... 100

7.7 Nickel Scan of Chromel Sample.. 101

7.8 Chromium Scan of Chromel Sample 102

7.9 Calibration Curve Obtained by Wire Bonding................................. 106

FIGURE Page

7.10 Calibration Curve Obtained by the First Method of Resistance Arc Welding 107

7.11 Calibration Curve Obtained by Second Method of Resistance Arc Welding 108

7.12 Log-Log Curve Showing Heat Flux Values 113

7.13 Curve Showing the Heat Transfer Coefficient 114

7.14 Curve Showing the Thermal Resistance Values 115

7.15 Pictures of the Apparatus Showing Stages of Boiling at Various Superheats 116

LIST OF TABLES

TABLE Page

7.1 Composition Analyses of TFT Layers 95

7.2 Results of Calibration of Thin Film Thermocouple Packaged by Wire Bonding 103

7.3 Results of Calibration of Thin Film Thermocouple Using First Method of Resistance Arc Welding 104

7.4 Results of Calibration of Thin Film Thermocouple Using Second Method of Resistance Arc Welding 105

7.5 Data Obtained from the Pyrex Wafer Experiment 109

7.6 Heat Flux and Heat Transfer Coefficient Calculation from Thermocouple Data 110

7.7 Thermal Resistance and Rate of Heat Transfer Values 111

CHAPTER I

INTRODUCTION

The study of thermal phenomenon at the micro scale in multi-phase flows necessitates the development of thermography devices which can provide high spatial and temporal resolution. These devices can also be used to monitor temperature non-uniformities (e.g., "hot spots") on packages of high heat flux electronics devices. Accurate and continuous monitoring of such high performance systems is required; since high heat fluxes can affect the performance and capability of a system adversely. Integrated miniaturized arrays of sensors need to be fabricated and monitored, to be able to observe the changes accurately and to control them. In multi phase flow studies, techniques like optical thermography cannot be used because of the optical interference caused by the constituent phases. The design, fabrication and testing of thin film thermocouples will be explored in this study for monitoring temperature fluctuations on a boiling surface.

1.1 History of Thin Films

Thin films have a long history of engineering applications. One of the

---

This thesis follows the style and format of ASME Journal of Heat Transfer.

ancient methods of forming thin films was the beating of gold to form 'gold leaf.' Even in early times armies used to quench their heated arrows in poisonous liquid so that a thin poisonous film would form on them. Faraday in 1857 was, most probably, the first person to use evaporated thin films, when he exploded metal wires in various environments (oxygen, hydrogen). Faraday must have done some depositions at sub-atmospheric pressures. It was in 1887 that Nahrwold reported the formation of platinum films by Joule heating under vacuum. He is credited to be the first person to use thermal vaporization to form films under vacuum.

The cathodic sputtering process was first mentioned by Grove in 1842. Thin films remained to be a field of academic interest till better vacuum technology was developed. In mid 1940's when industrial scale vacuum equipment was developed, growth in this field occurred and this helped in the application of thin films in the industry. For the process of actual growth and nucleation of thin films many articles and reviews can be found, especially describing the kinetics of thin films, like Hirth *et al.* [1], Lewis [2], Sigsbee [3], Rhodin [4], Thompson (1990) [5], Thompson (2000) [6], Sato [7] and Maissel *et al.* [8].

As the technology progressed the field of thin films started to grow by leaps and bounds and this attracted a lot of attention from the scientists and researchers at that time. To promote this field the journal Thin Solid Films

was started in July 1967. With such emphasis on this field it had become necessary to define what is considered as a thin film and what is not [9]. The editorial statement of Thin Solid Films [10] contains the following definition, "The term *Thin Solid Films* covers layers of solid matter extending from those measured in atomic or molecular dimensions up to layers or multi-layers several tens of microns thick." Many books like Leaver *et al.* [11] explain thin film to be just a layer of material. Many definitions also state that thin films have a thickness varying from a few nanometers to as high as one micrometer (µm). The main caveat in these definitions is that they describe thin films to be less than 1µm. The definition supported does not consider the dimension of the thin film as the most important criteria. The status of a film being thick or thin depends on the property for which the film is being fabricated. For example, if a single layer of magnetic atoms is fabricated they can exhibit bulk properties, so they are considered as bulk natured (even though, according to thickness criteria, they are considered thin film).

Thin films exhibit properties which vary from the bulk state. These properties are dependent on the various parameters like the method of production, grain size, surface finish, etc. So the correct process is to be followed, so that the required properties are attained. Considerable research efforts are in progress on the methods of thin film production, study and

understanding of their properties. Information on past research in this filed are available in Kay [12], Yaffe [13], Monteiro[14], Heavens [15] and Berry *et al.* [16].

1.2 Background of Thin Film Thermocouples

The concept of thin film thermocouples (TFTs) was first reported in the 1930's by Harris *et al.* [17]. Various combinations of thermocouple elements have been studied and analyzed in Marshall *et al.* [18]. TFT have been used for various surface temperature measurements by Bullis *et al.* [19], Assanis *et al.* [20], Debey *et al.* [21], Tian *et al.* [22] and Laugier [23], due to their inherent advantages over wire-bead type thermocouples. The use of thin films for surface temperature measurement provides the advantage that they can be fabricated on surfaces where placement of a beaded thermocouple may interfere with the functioning of the object, e.g., aerodynamic structures where the surface roughness is of extreme importance and cannot be compromised. TFT have extremely small thermal inertia when compared to conventional beaded thermocouples, resulting in fast thermal response, as reported by Chu *et al.* [24]. The small thermal inertia also causes minimal interference of the surface temperature distribution, as reported by Chu *et al.* [25]. Thus, TFT provide more accurate measurement of surface temperatures than beaded thermocouples according

to Bullis *et al.* [19]. Numerical methods were used by Tian *et al.* [22] to determine the distortions in temperature field caused by introduction of TFT on a surface. They found out that the presence of TFT had minimal effect on the surface temperature distribution.

The TFTs were developed to study surface temperature fluctuations in boiling and multi-phase flows primarily for their fast response (high temporal resolution) and the capability for implementation in high density architecture (high spatial resolution). Park *et al* [26] fabricated an array of T-Type thin film thermocouples to measure temperature in a 1cm x 1cm area. The material choice of TFT in elevated temperature applications is guided by the possibility of inter-metallic interactions and environmental interactions as explained by Kreider *et al*. [27] and Kreider *et al*. [28]. Homogeneity of material composition affects the calibration and performance of TFT. Therefore, packaging (primarily interconnect fabrication) is crucial for reliable performance and ensuring measurement accuracy of TFT. The solution to this problem has been reported in the literature in the form of parallel gap welding by Holanda *et al.* [29] and spot welding by Zupan *et al.* [30].

CHAPTER II

DESIGN AND FABRICATION OF THIN FILM THERMOCOUPLES

2.1 Thin Film Thermocouple Design

Thin film thermocouples were designed to investigate surface temperatures during various boiling regimes. The aim of this study was to study the surface temperatures at the micro scale. For this reason, the design of the thin film thermocouples was of utmost importance. The design provided with the required resolution for temperature measurement.

So, the major aims of the design were to measure temperature with high spatial and temporal resolution. Thin film thermocouples exhibit a faster response rate and can be designed to achieve high spatial resolution as compared to beaded thermocouples. Many limiting factors had to be considered while designing the thin film thermocouples. The resolution of the mask aligner was crucial to achieving the minimum feature size required for the boiling experiments. The required spatial resolution was of the order of tens of microns. The fabrication process of thin film thermocouples involved multi layer photolithography and metal deposition, which will be described in the fabrication section. Multi level masking steps had a bearing on the design, since alignment issues were tackled in the design. Two sets of

locators on the four corners of the masks were designed. The size of these locators was also crucial to minimize alignment errors.

The access to mask making facilities was a major limiting factor. Actually, the size of the masks and their availability were the two most important factors in the whole process of designing masks. These factors along with the packaging limitations, that will be discussed later, were the major motivators for the evolution of the designs of thin film thermocouples, used in this study.

A total of five generations of mask design were explored in this study. The various generations of design will be discussed in the following sections.

2.1.1 First Generation

The salient features which are used to distinguish each design are as follows:

a. Number of Junctions: 36
b. Number of Layers (Number of masks needed for full design): 3
c. Size of Alumel and Chromel lines:

   Alumel: 30 µm

   Chromel: 50 µm
d. Size of Bond Pads: 500 µm
e. Number of Bond Pads: 72
f. Description:

As mentioned earlier, this design had 3 layers. For fabrication of thin film thermocouples, by definition, we need two different layers to form the junction at the end. This design had the usual Alumel and Chromel layers that were used for making the junction of the K-Type thin film thermocouple. This design had an additional layer which comprised of bond pads. This layer had 72 bond pads which had to be aligned with the 36 thermocouples that were fabricated at nearly the center of the wafer, in an area of 1 cm^2, with a pitch of 0.2 cm. This layer was fabricated using Aluminum.

For the fabrication, three different layers required three different masks. Two of them were made in Texas A&M University by HSC Communications at the Texas A&M University System Health Science Center in College Station. One was made by Photo Sciences, Inc. Torrance, California. The mask made by Photo Sciences was a Chrome/Soda Lime mask, of 4” x 4” x 0.09” dimensions, containing bond pads. The major constraint that was present in this design, and all the designs that followed this one, were the dimensions of the photomask that was made by the Health Sciences Center. The Health Sciences Center could reduce an 8.5” x 11” page to a 3.6cm x 2.4cm photographic negative film. A negative as well as a positive image

could be obtained in the process. Fig. 2.1 shows the photomask and its size.

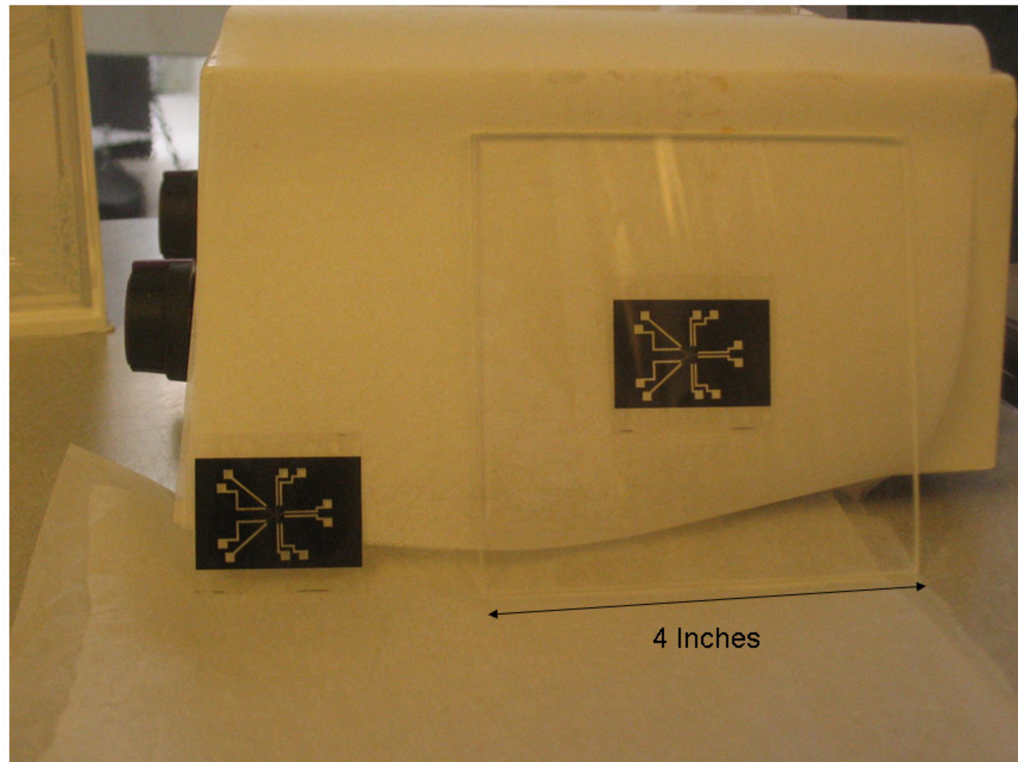

Fig. 2.1 Photomask Obtained from Health Science Center (on left) and a Similar Photomask Attached on a Glass Slide Ready for Use in Photolithography (on right).

g. Limitations:

There were many limitations in this design. First, the lead time for mask fabrication was a major consideration. The process of designing the mask according to the design rules, ordering the mask from an

offsite location and resolving the design conflicts before fabrication, usually added to the lead time. Also, the cost of mask fabrication was an important factor. Second, there were three layers involved in this process so the probability of misalignment was higher. Third, the presence of Aluminum bond pads served as a parasitic junction (which proved to be a problem during wire bonding as well). In view of the constraints imposed by the initial design, the second generation of mask was designed.

h. Locator Design:

For the alignment of different metal layers, alignment marks were placed on the four corners of the design. Fig. 2.2 (a) and (b) show the two sets of alignment marks used in the designing process. The three layers and the complete design are shown in Figs. 2.3 to 2.6.

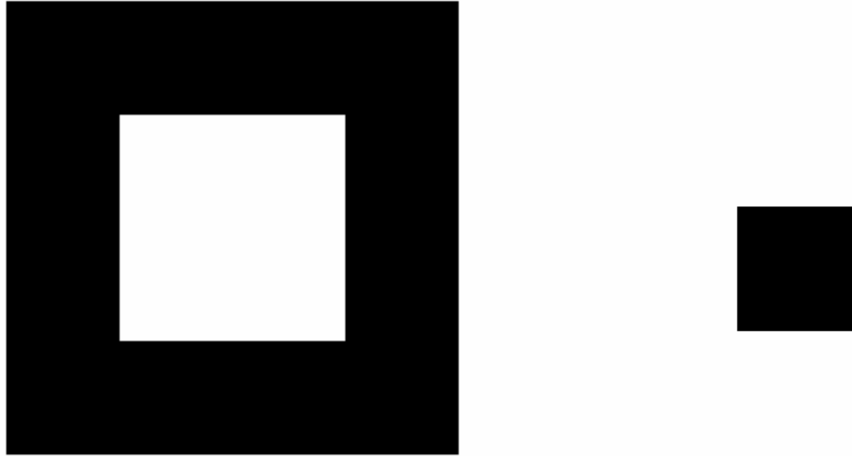

(a) Pair of locators used for alignment.

Fig. 2.2 Locators Used for Alignment of Subsequent Photolithographic Layers.

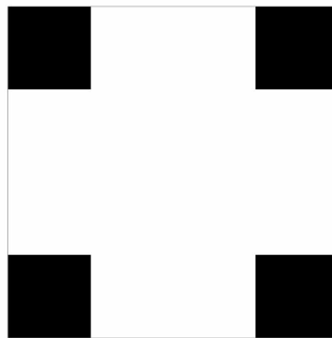

(b) Second Pair of locators for alignment.

Fig. 2.2 Continued.

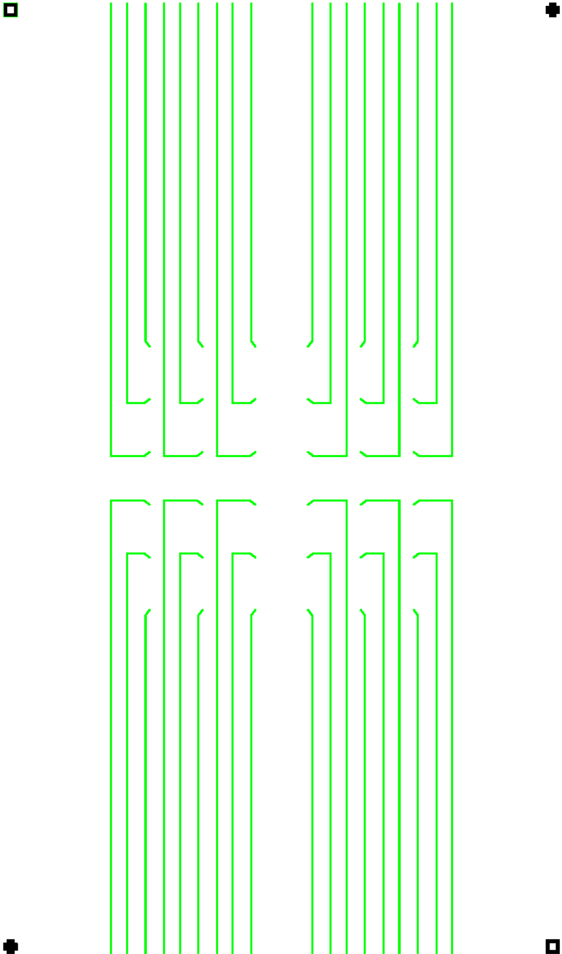

Fig. 2.3 Alumel Design: First Generation.

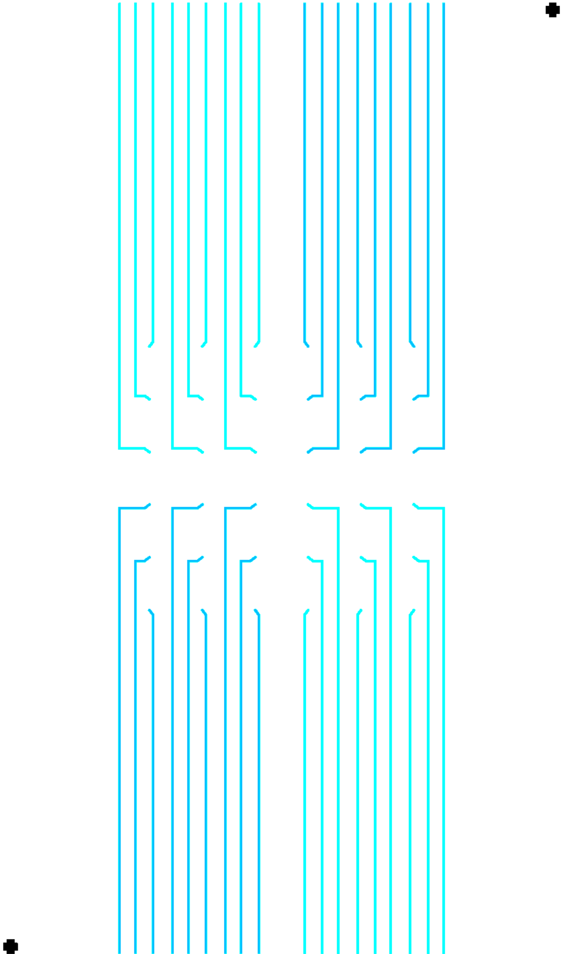

Fig. 2.4 Chromel Design: First Generation.

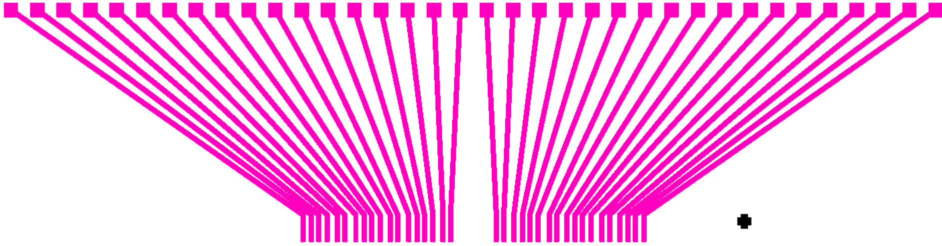

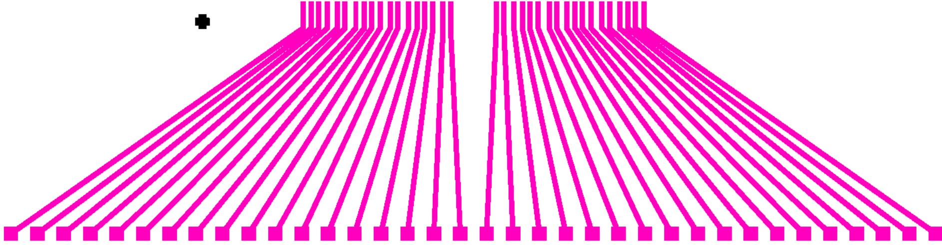

Fig. 2.5 Bond Pad Design: First Generation.

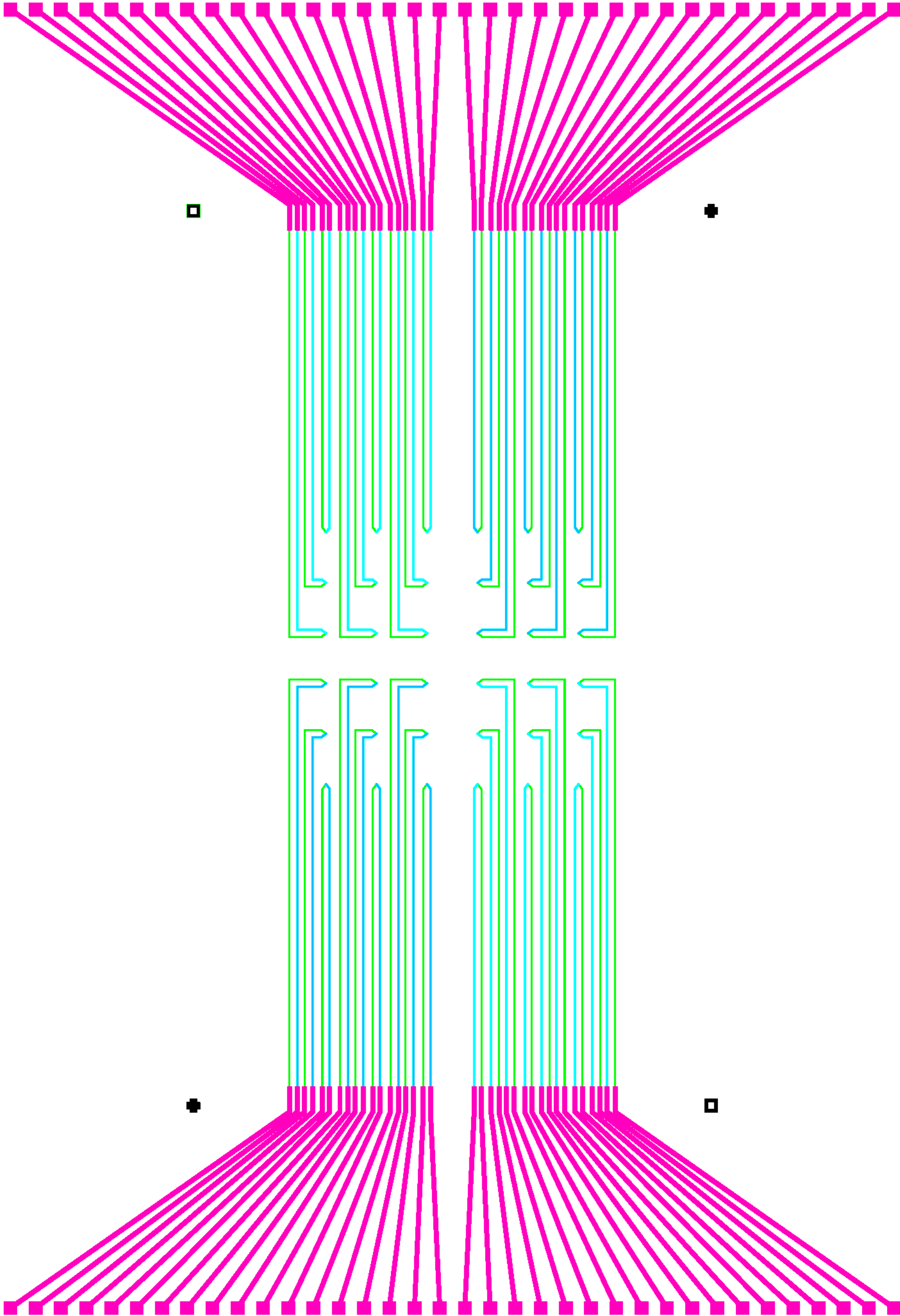

Fig. 2.6 Full Design: First Generation.

2.1.2 Second Generation

The salient features of this design are as follows:

a. Number of Junctions: 36

b. Number of Layers (Number of masks needed for full design): 2

c. Size of Alumel and Chromel lines:

   Alumel: 50 µm

   Chromel: 50 µm

d. Size of Bond Pads: 500 µm

e. Number of Bond Pads: 72

f. Description:

   In this design the three layer mask design was changed to a two layer mask layout. This design obviated the need for a mask that had to be fabricated off campus. Both the masks that were required in this case were made on campus at Texas A&M University. Photomasks were fabricated at the Texas A&M University Health Science Center. This design had a circular outlay of the bond pads and this gave the

unique flexibility of fitting all the 72 bond pads in the desired area of 36 x 24 mm^2. The layers of the design are shown in Figs. 2.7 to 2.9. This design overcame the drawbacks of the previous design. This design enabled a smaller lead time for mask fabrication, less alignment errors since only one alignment step was involved and eliminated parasitic junctions since Aluminum bond pads were not used.

g. Limitations:

The biggest limitation of this design was that the bond pads were very close to each other and this caused difficulty in packaging. Packaging was successful using conventional wire bonding using Aluminum wires. Other packaging methods were also tried and were not very successful as the bond pads were small in size and methods like manual welding and soldering could not be done successfully.

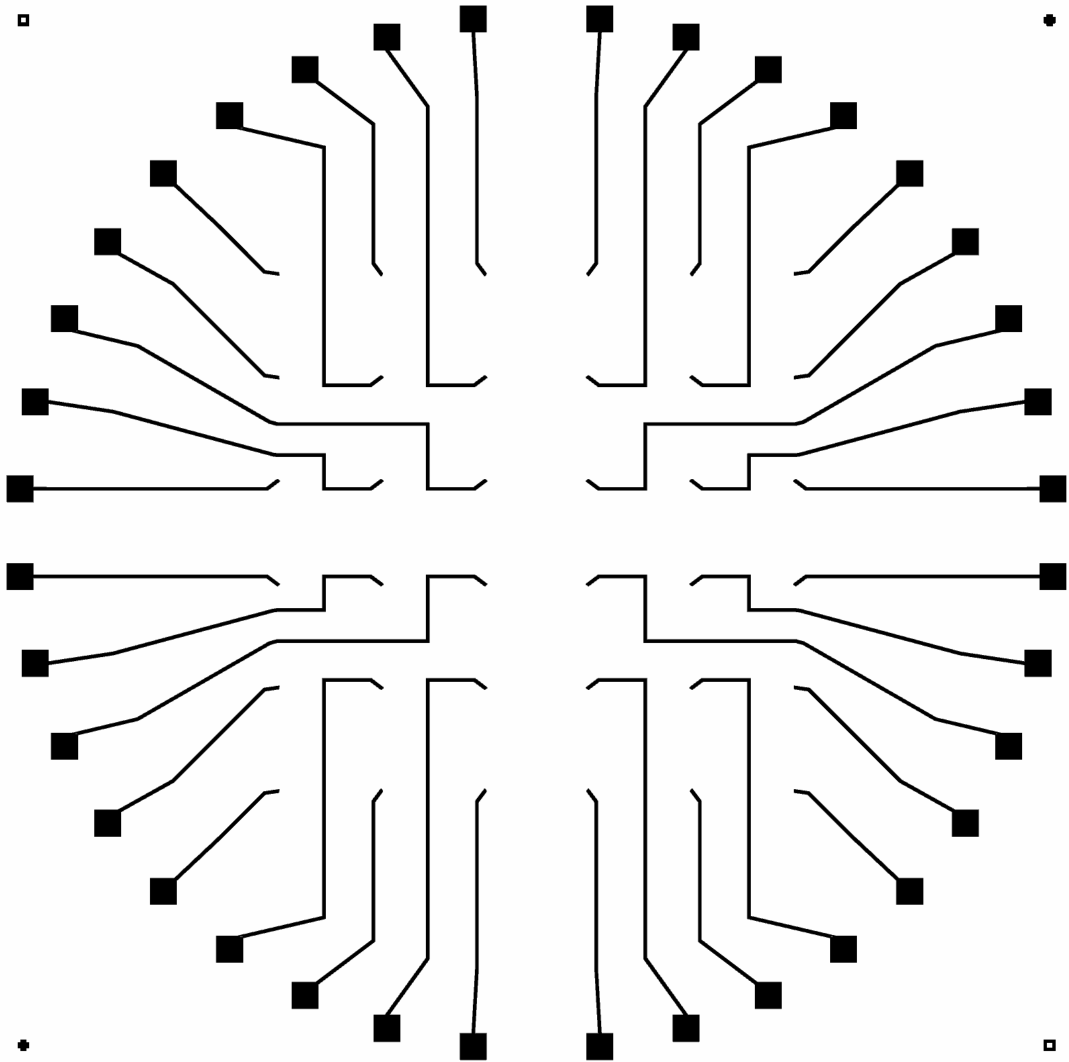

Fig. 2.7 Alumel Design: Second Generation.

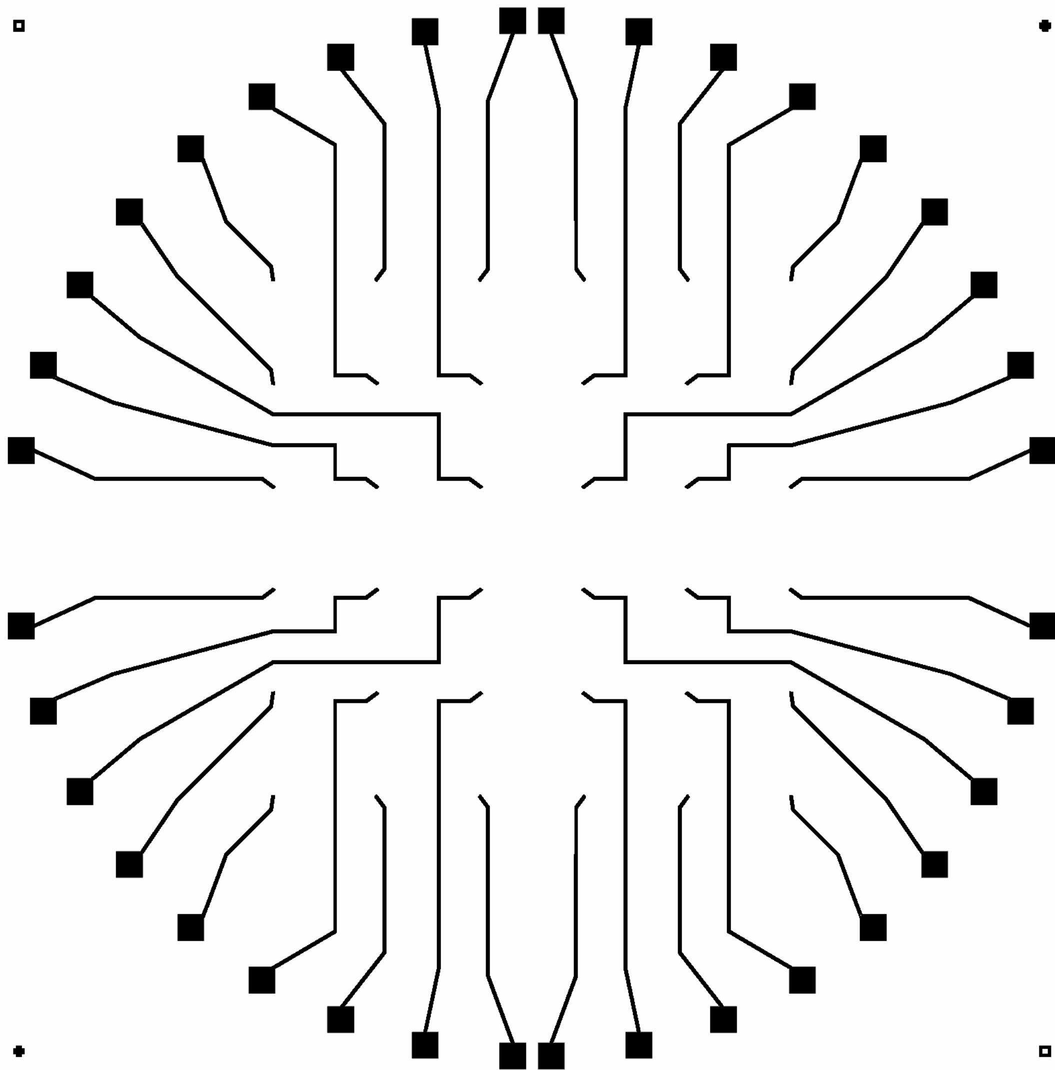

Fig. 2.8 Chromel Design: Second Generation.

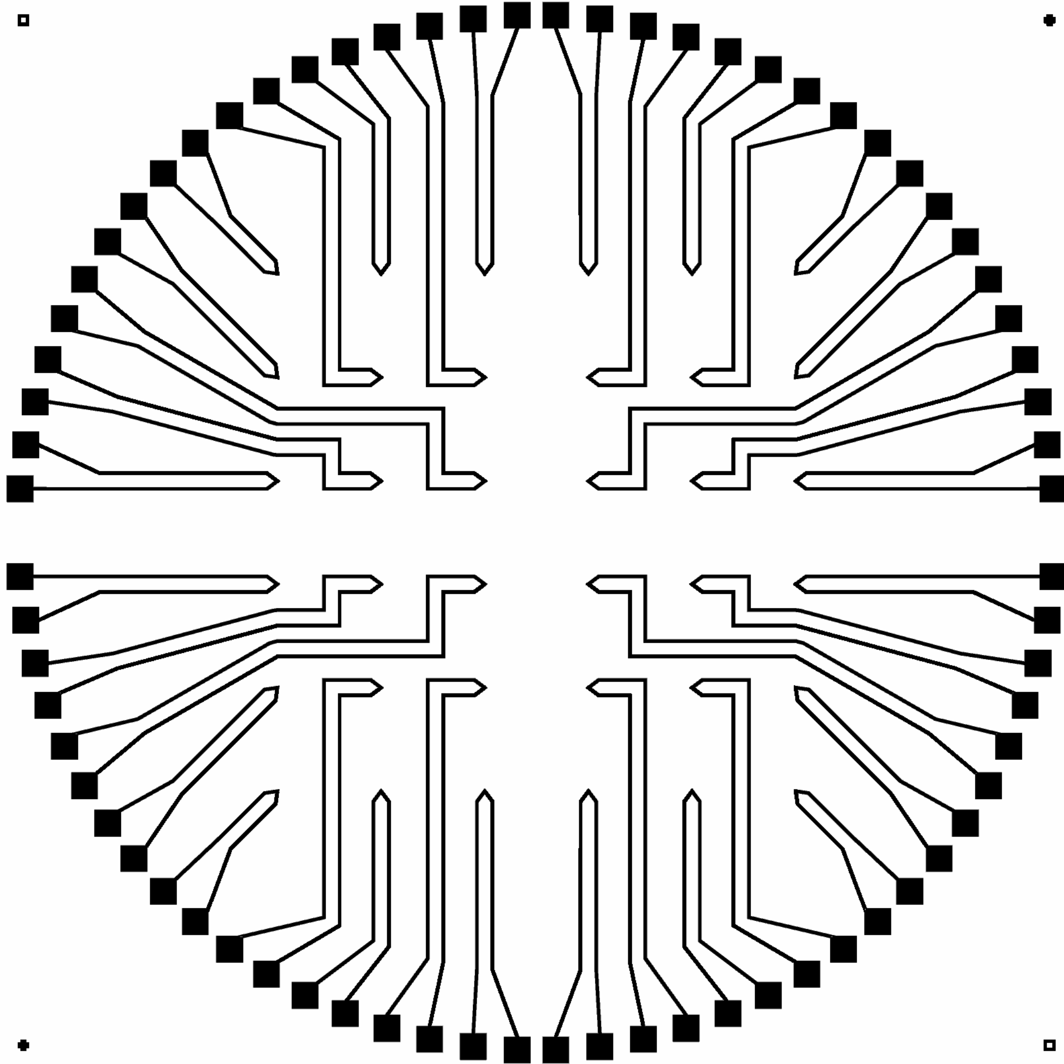

Fig. 2.9 Full Design: Second Generation.

2.1.3 Third Generation

The salient features of this design are as follows:

a. Number of Junctions: 10

b. Number of Layers (Number of masks needed for full design): 2

c. Size of Alumel and Chromel lines:

   Alumel: 50 µm

   Chromel: 50 µm

d. Size of Bond Pads: 1000 µm

e. Number of Bond Pads: 20

f. Description:

   To overcome the limitation imposed by small bond pads the size of the bond pads was increased to 1mm x 1mm from 0.5mm x 0.5mm. The number of thermocouples was, therefore, decreased to accommodate the increasing size of the bond pads. The layers of the design are shown in Figs. 2.10 to 2.12.

g. Limitation:

   This design tackled the limitations imposed by the previous designs. Subsequent designs were explored to further increase the size of the bond pads and to increase the yield of the microfabrication process.

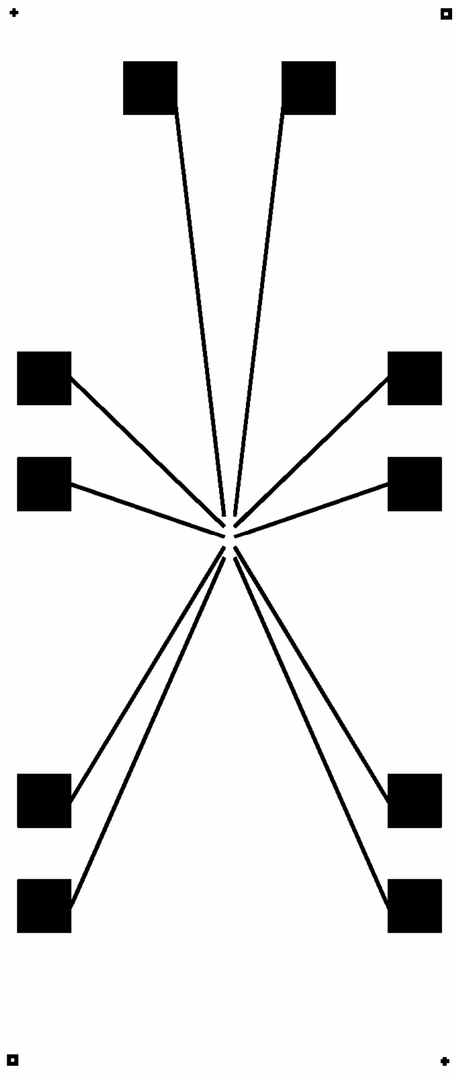

Fig. 2.10 Alumel Design: Third Generation.

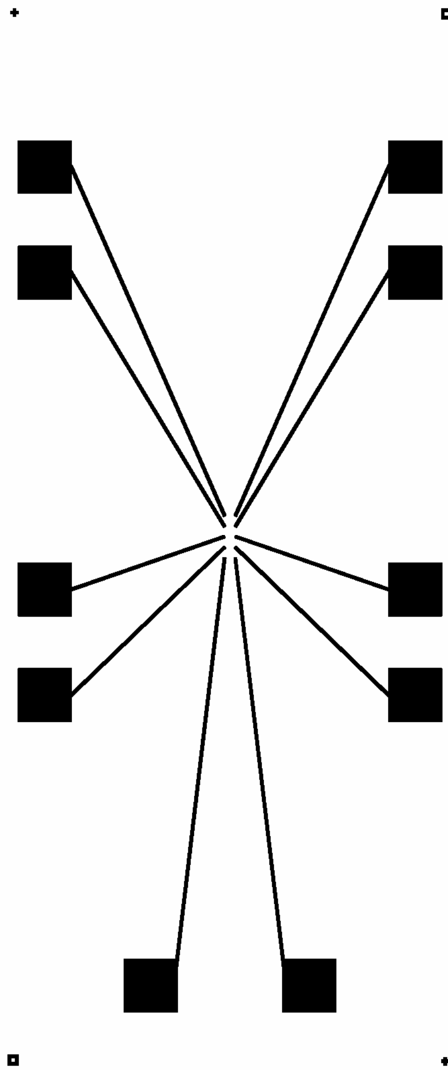

Fig. 2.11 Chromel Design: Third Generation.

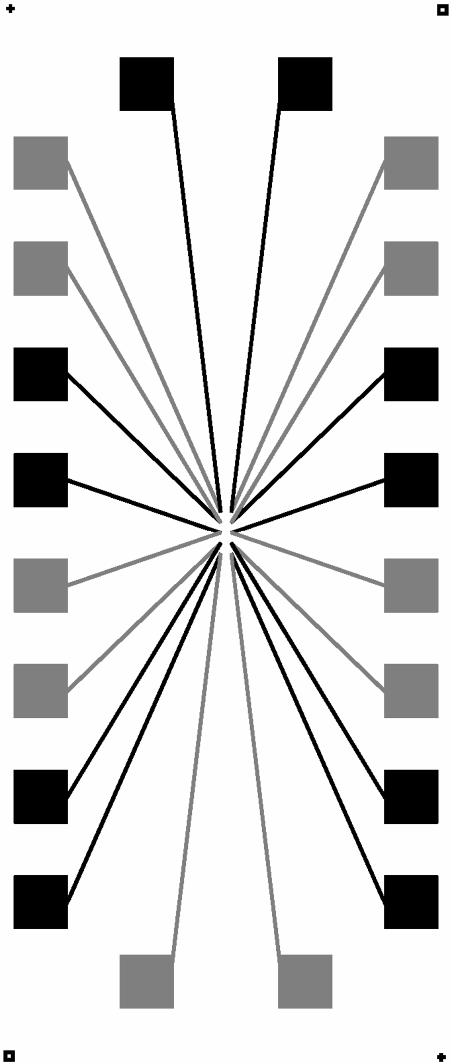

Fig. 2.12 Full Design: Third Generation.

2.1.4 Fourth Generation

The salient features of this design are as follows:

a. Number of Junctions: 10

b. Number of Layers (Number of masks needed for full design): 2

c. Size of Alumel and Chromel lines:

   Alumel: 50 μm

   Chromel: 50 μm

d. Size of Bond Pads: 2000 μm

e. Number of Bond Pads: 20

f. Description:

   This design was an improvement from the previous design as it has bond pads of 2mm x 2mm size. In this design bond pads moved further outward. The size of the junction and the number of junctions were retained from the previous design. The layers of the design are shown in Figs. 2.13 to 2.15.

g. Limitation:

   The major limitation of this design was that discontinuities were found to occur in some of the thermocouples during lift off. This occurred since the long and thin (50 μm) metal lines lacked the structural rigidity to survive the strains imposed by the lift-off process.

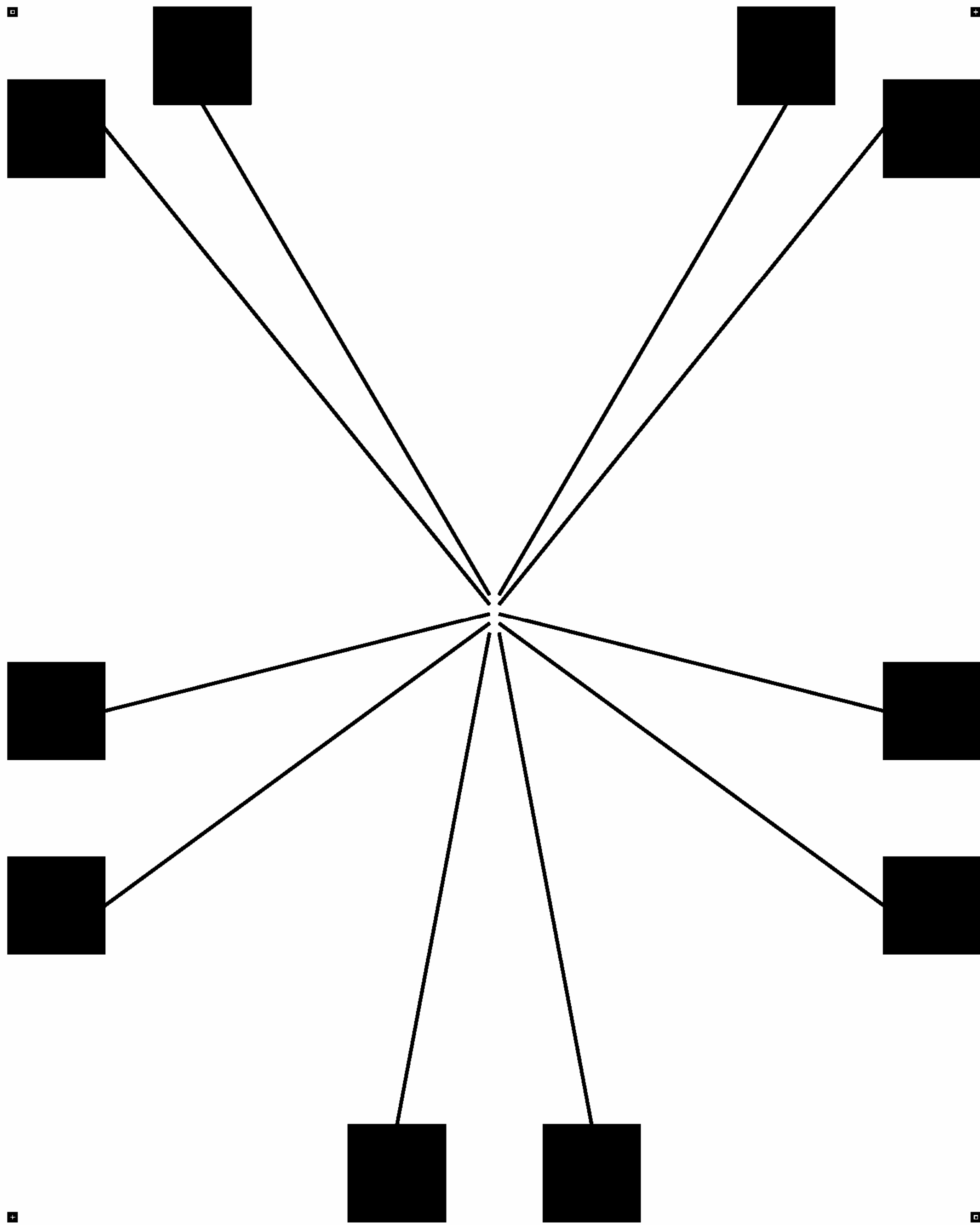

Fig. 2.13 Alumel Design: Fourth Generation.

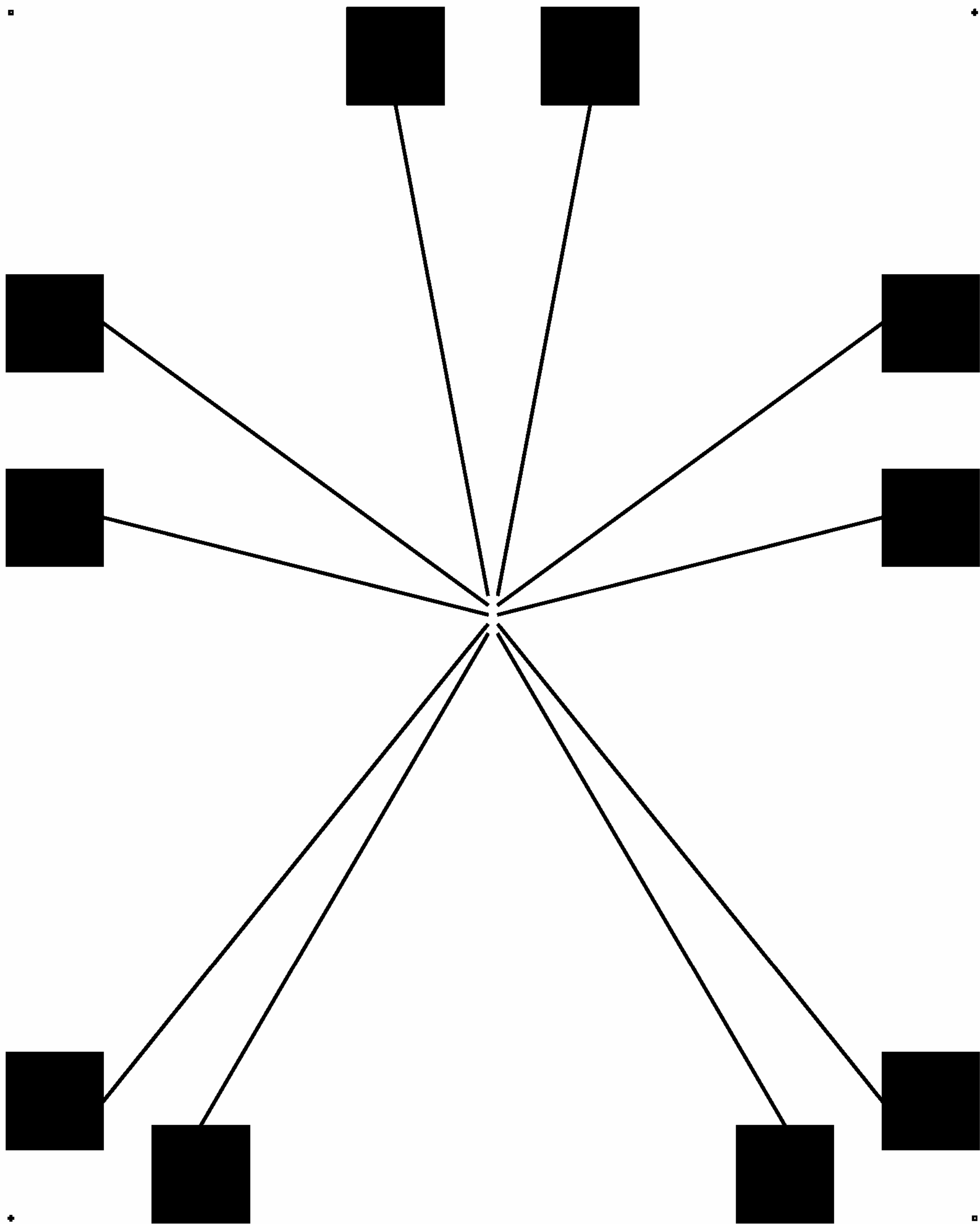

Fig. 2.14 Chromel Design: Fourth Generation.

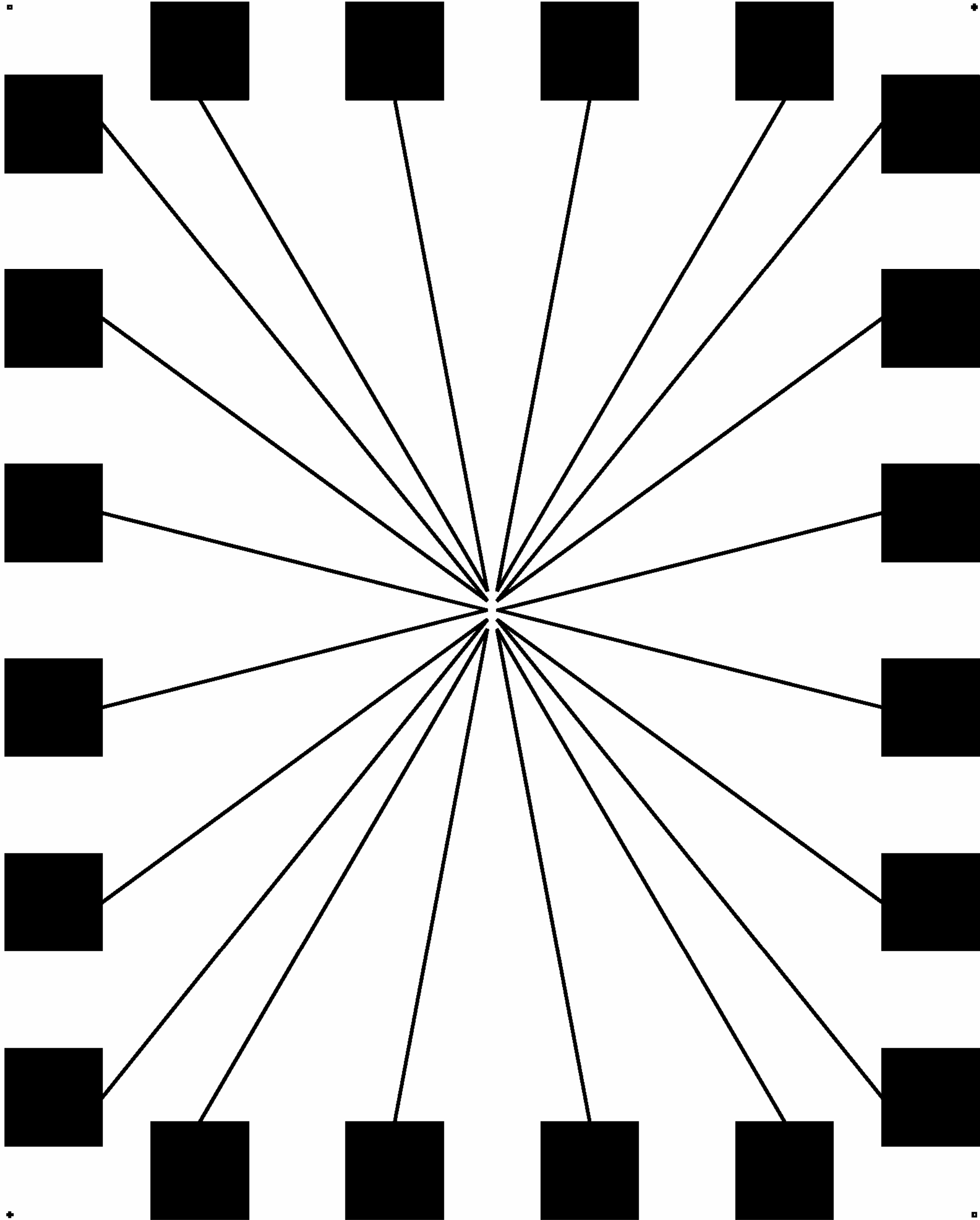

Fig. 2.15 Full Design: Fourth Generation.

2.1.5 Fifth Generation

The salient features of this design are as follows:

a. Number of Junctions: 10

b. Number of Layers (Number of masks needed for full design): 2

c. Size of Alumel and Chromel lines:

   Alumel: 50 μm

   Chromel: 50 μm

d. Size of Bond Pads: 2000 μm

e. Number of Bond Pads: 20

f. Description:

   The difference between this design and the previous design was the presence of thicker metal lines. The thickness of the metal lines ranged from 50 to 5000 microns. This design provided sufficient structural rigidity to all the metal layers and improved the yield of the fabrication process. The layers of the design are shown in Figs. 2.16 to 2.18.

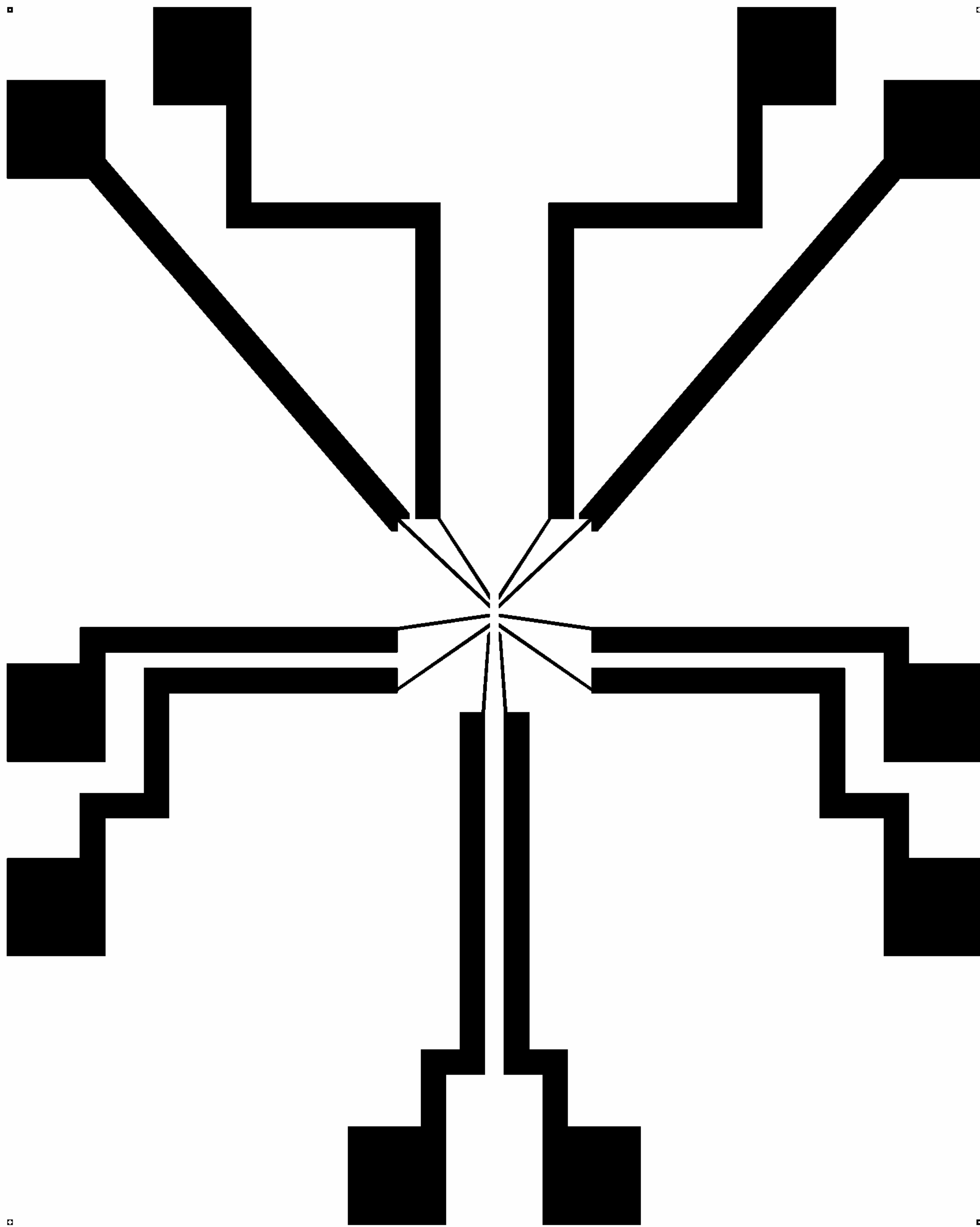

Fig. 2.16 Alumel Design: Fifth Generation.

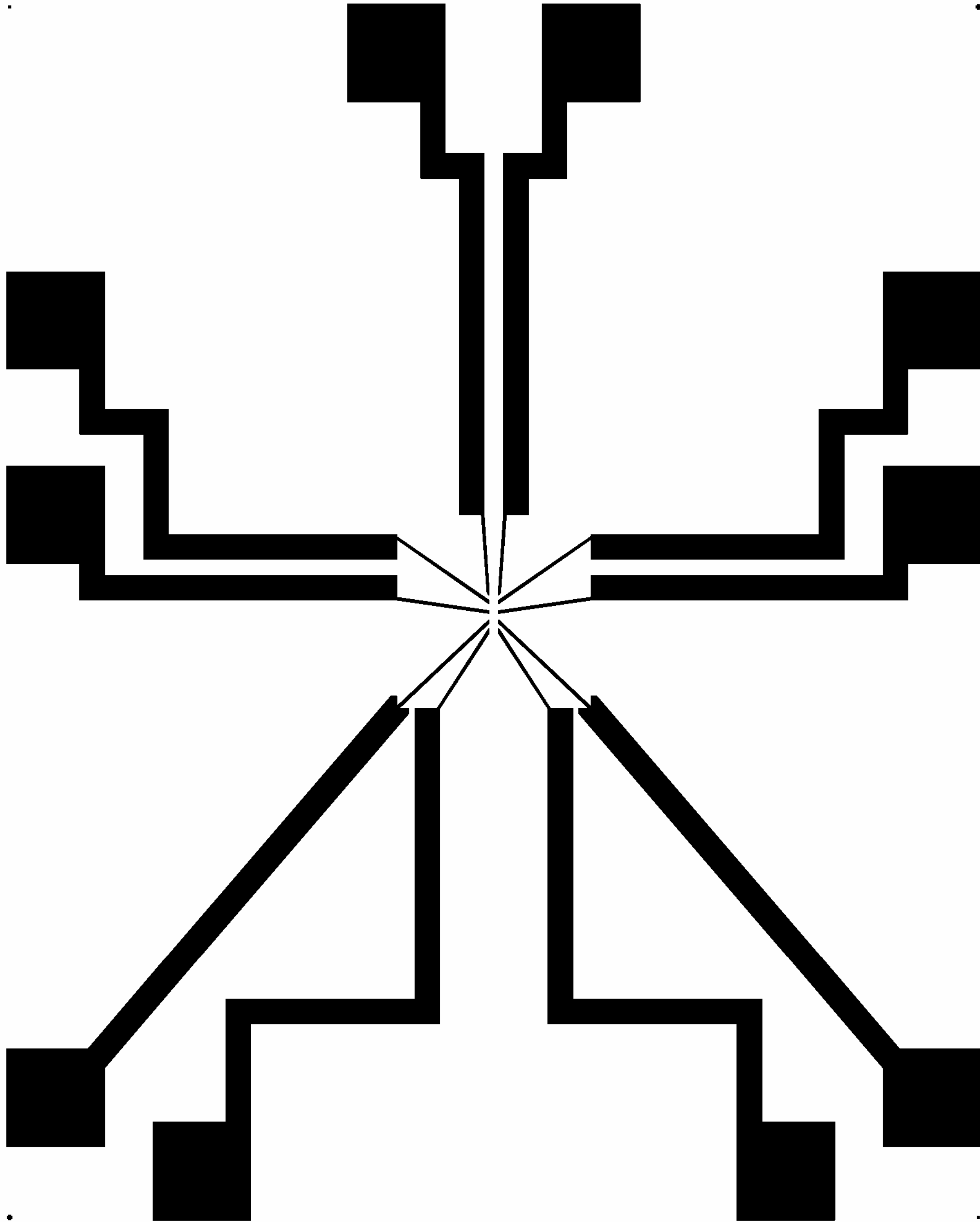

Fig. 2.17 Chromel Design: Fifth Generation.

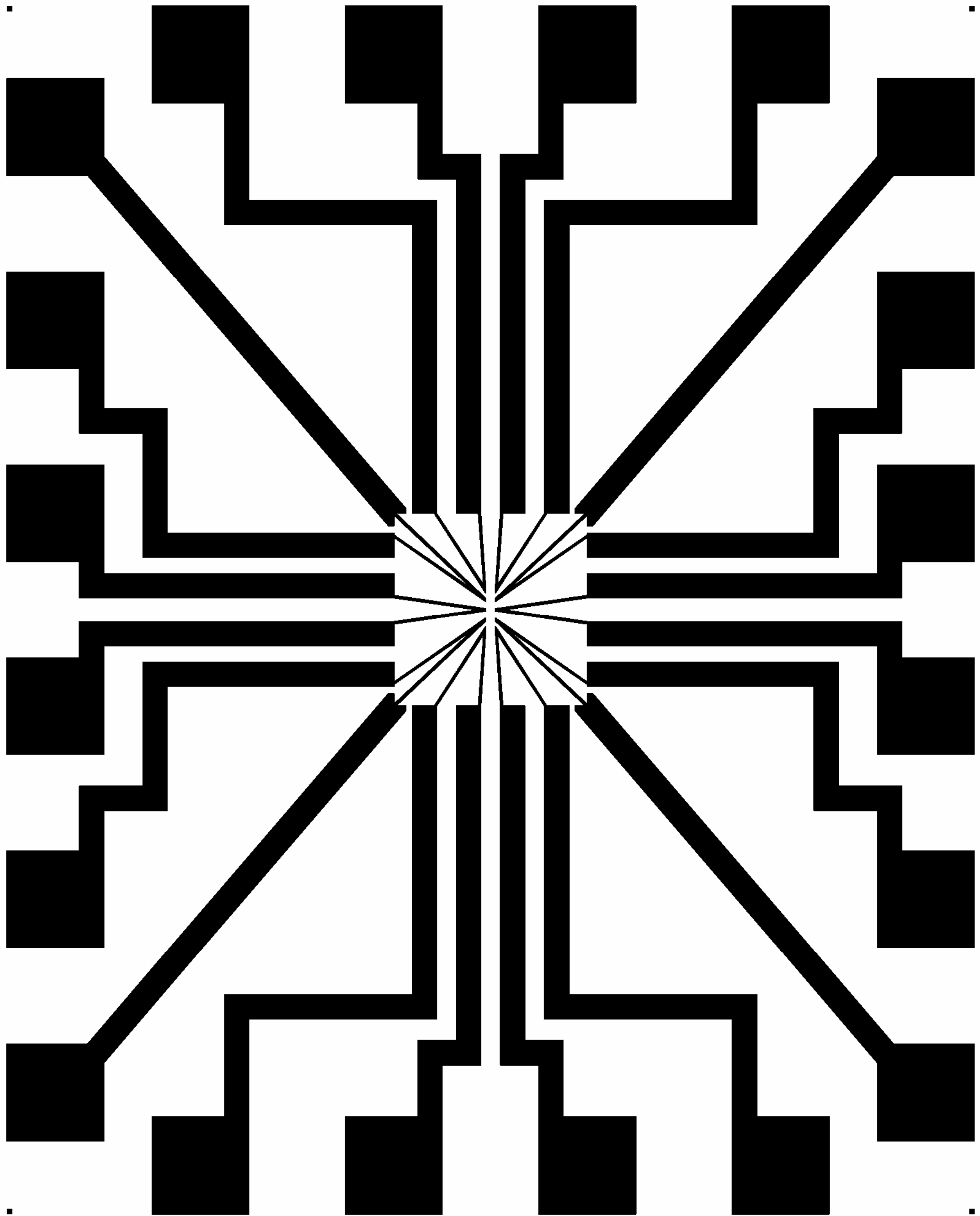

Fig. 2.18 Full Design: Fifth Generation.

2.2 Thin Film Thermocouple Fabrication

Thin film thermocouples were fabricated on campus, in Texas A&M University, using the Class 1000 Cleanroom at the Material Characterization Facility. The following portion of the thesis describes the fabrication processes for thin film thermocouples (TFTs), on silicon as well as Pyrex wafers. The steps involved in the microfabrication process were:

1. First Layer Photolithography
2. Oxygen Plasma Cleaning (De-Scum)
3. Metal Deposition
4. Lift-off
5. Second Layer Photolithography
6. Oxygen Plasma Cleaning (De-Scum)
7. Metal Deposition
8. Lift-off

2.2.1 First Layer Photolithography

The different steps in photolithography were:

a. Cleaning: The substrate was first cleaned using Acetone and then rinsed using Iso-propanol. The substrate was dried using pressurized nitrogen from a nozzle gun.

b. Heating: After the basic process of cleaning, the substrate was heated on a hot plate maintained at 200 ˚C for 5 minutes. This step was used to evaporate any volatile impurities that might be present on the surface of the substrate.

c. Photoresist Spin Coating: For this purpose a SCS P6204 (8-in. bowl) Non-programmable Spin Coater was used. The substrate was held by a vacuum chuck. The device also provided control over the speed of spinning, acceleration, deceleration and total time of spinning. This was used for spinning of the photoresist on the wafer. The time of spinning and the speed at which the wafer should be spun was determined by the graph that was provided by the photoresist manufacturer. The graph showed the thickness of the photoresist layer at different spinning speeds. Shipley 1827 (positive photoresist) was used in this study. The speed of spinning used in this study was fixed at 3000 rpm for 60 seconds. These timings and speeds were programmed before the wafer was mounted on the chuck. The vacuum was also checked before mounting the wafer. The thickness, the acceleration and the deceleration with which the photoresist was spun on the wafer had an effect on the edge effects caused by spin coating. Fig. 2.19 shows the spin coater used in this study.

Fig. 2.19 Non-programmable Spin Coater.

d. Pre Exposure Baking: After spin coating, the wafer was heated for 60 seconds at 115 ˚C on a hot plate.

e. Exposure: For pattern transfer from the photo mask to the wafer a Quintel Q4000 Mask Aligner was used. The photo mask was mounted on a glass plate by attaching it to one side of the glass slide using sticky tape. Following pre-exposure bake the wafer was mounted on the chuck. After mounting of the chuck to a given position under the

glass slide, the chuck was raised so that it came into contact with the photo mask. Contact exposure was performed using the mask aligner. The exposure time was set according to the photoresist being used and the amount of energy required for desired exposure. In this study exposure times ranged from 8 seconds to 30 seconds. This mask aligner used UV light of wavelength: 365 nm. The mask aligner has other features such as microscopes with split view which were used for performing alignment of metal layers in subsequent photolithographic steps. After exposure the chuck disengages automatically and the wafer was dismounted. Fig. 2.20 shows the Mask Aligner used in this study.

In this step over exposure was used. Over exposure implies that the photoresist was exposed to the UV light for a period longer than what it was supposed to be. This was done to facilitate the lift off process by optimizing the resist profile for easier access of the stripping chemicals to the resist. According to experience, this step proved to be very instrumental in the proper fabrication of the thermocouples.

Fig. 2.20 Quintel Mask Aligner Used for Both the Layers of Photolithography.

f. Developing: Following the exposure step the wafer was submerged in a developer solution. In this study MF-319 (by MicroChem) was used as the developer. The development time depended on the exposure time that was used. In this study the development time ranged from 40 seconds to 90 seconds.

g. Cleaning: After the development process, the wafer was rinsed with DI water and then dried using pressurized nitrogen.

This completes the process of photolithography for the first metal layer.

2.2.2 Oxygen Plasma Cleaning (De-Scum)

Oxygen plasma cleaning was performed using a March Plasma Systems Model CS-1701 reactive ion etcher (RIE). The oxygen plasma has higher selectivity to organic contaminants than the silicon surface. This selectivity helped to remove photoresist residues which were not removed during photoresist development. The settings used for the RIE for oxygen plasma cleaning were:

Pressure: 0 mTorr

Power: 350 W

Endpt: 100

Time: 10 seconds

Temperature: 0˚ C

BP/RP: 80 milliTorr

Gas 1(Oxygen): 20 sccm

Fig. 2.21 shows the RIE instrument used in this study. The process of oxygen plasma de-scum reduces the height of the photoresist but does not significantly reduce it to heights where it would affect the subsequent

processes. De-scum helps to remove photoresist in the exposed region of the wafers and helps to improve the yield for the lift-off process.

Fig. 2.21 Reactive Ion Etcher Used for Oxygen Plasma Cleaning.

2.2.3 Metal Deposition

One of the most important processes for the fabrication of TFT’s was metal evaporation. The process of deposition of the components of the TFT’s was carried out by using a BOC Edwards Auto 306 Metal Evaporation

Chamber. This chamber had two vacuum pumps which were used to pump down the system to low pressures where the process of evaporation of the metal was performed. The process pressure was approximately 10^{-6} torr. At such low pressures heating of the metal to its melting point causes evaporation and the vapors thus produced were deposited on the sample. The sample was placed above the metal source. The distance between the source and the substrate was an important criterion for categorizing and selecting a metal evaporator. The mounting plate contained the wafer substrates and was placed on top of the source. This plate was rotated throughout the process to ensure uniform deposition on all of the wafers. This system had the capability to provide 4 different sources for deposition. In this study only two sources: (Chromium as adhesion layer and Alumel or Chromel) were used for any particular deposition step. Fig. 2.22 shows a picture of the metal deposition instrument used for this study and Fig. 2.23 shows the mounting plate for the substrates. Fig. 2.24 shows the chuck on which the sources were placed and Fig. 2.25 shows the sources used for deposition, before and after use (from left to right). The left most source shows the bare tungsten bars, the next source was a used Alumel source and the other two sources were used Chromel sources.

Fig. 2.22 Metal Evaporator Used in This Study.

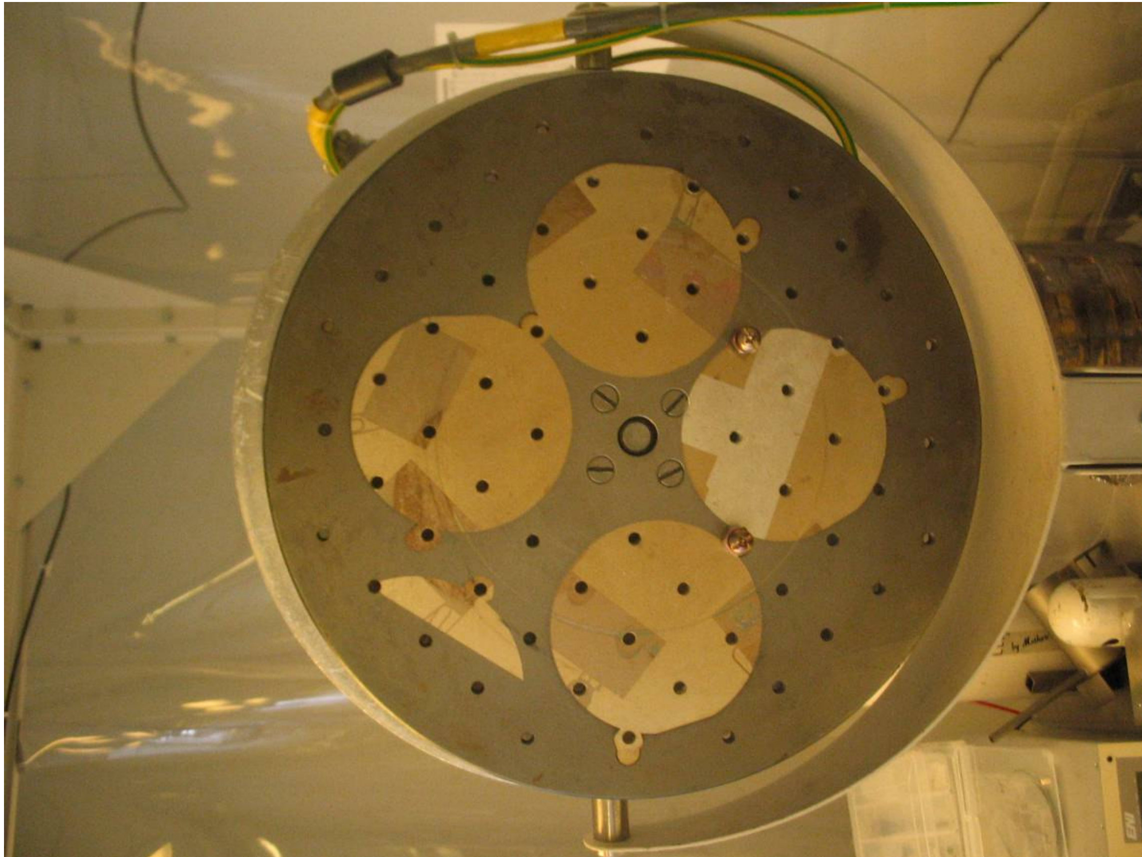

Fig. 2.23 Wafer Holder with Traces for the Four Wafers and the Substrate Used for Composition Analysis is Shown in This Image.

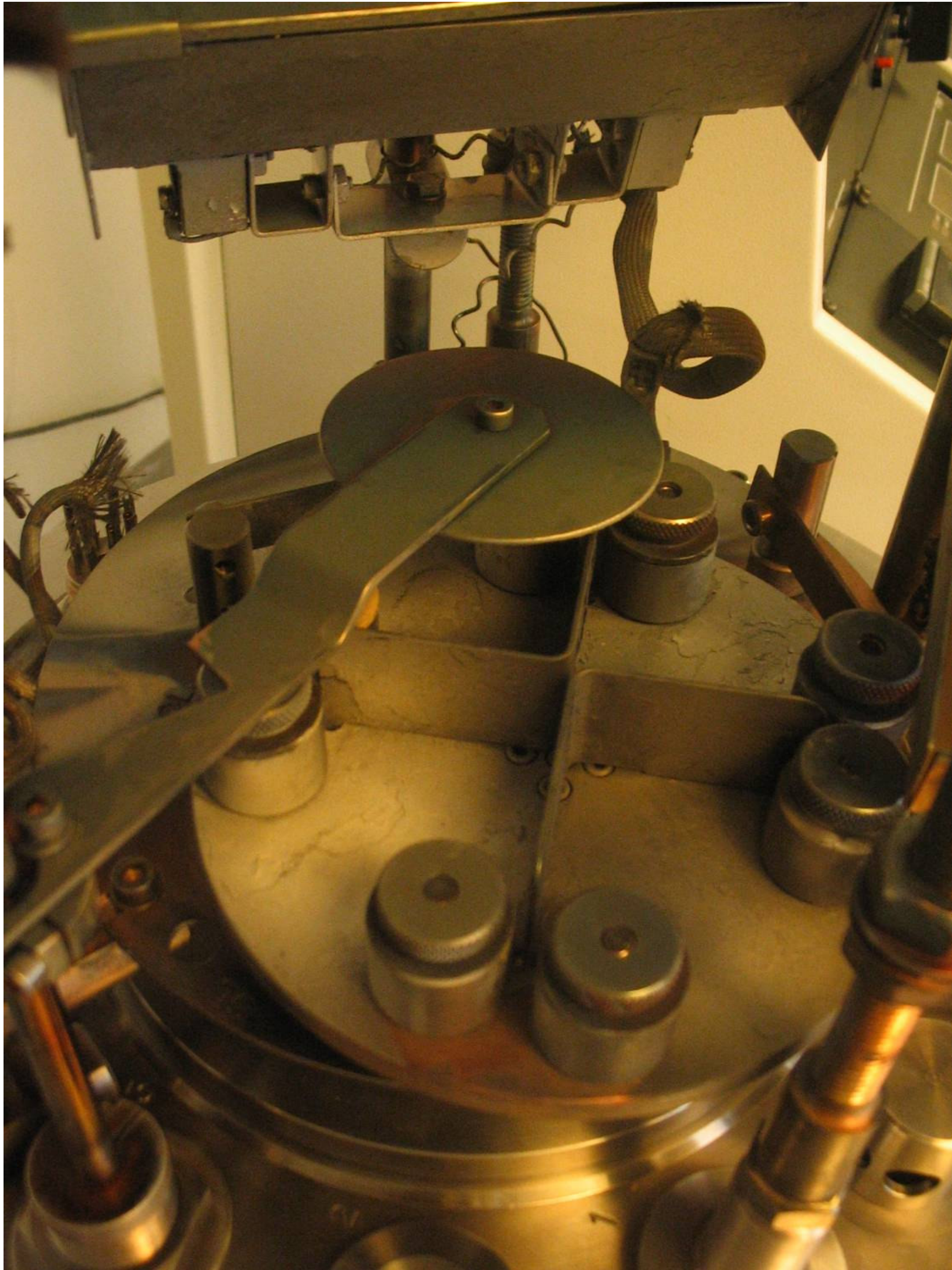

Fig. 2.24 Chuck for Holding the Sources for Depositing the Layers.

Fig. 2.25 Sources Used for Deposition. (Left from Right: Bare Tungsten Bars before Use, Used Alumel Source and Two Used Chromel Sources.)

Chromium was used as an adhesion layer and was used to increase the adhesiveness of the targets to the substrate. The thickness of the chromium adhesion layer used in this study ranges from 5-20 nanometers. The thickness of the Alumel/Chromel layers was in excess of 200 nanometers.

The surface inside the metal evaporator was cleaned before the deposition step. The sources were then mounted and the samples were fixed to the plate. The plate was then placed inside the metal evaporation

chamber. A Kevlar jar was placed and an implosion guard was placed surrounding the jar (to minimize damage in the event of an implosion). The system was evacuated after closing the lid of the evaporator, the system required 3-4 hours to attain process vacuum. After the desired pressure was attained, the metal evaporation process was started. For monitoring evaporation the target material z-value and density were specified. The specification of these parameters enabled the system to calculate the rate of deposition of the source. The system used for this study was a resistive heating system that heated the metals to their melting point for evaporating the material. For this purpose current was passed through a boat or tungsten rods. Following the completion of the deposition process the instrument required additional time to cool down. This minimized oxide layer formation when the chamber was vented.

2.2.4 Lift-off

This was the final step that was performed in the fabrication process. After the deposition, the photoresist was removed using either Acetone or Remover PG. Remover PG (by MicroChem) was used more extensively in this study since this provided faster lift-off. Also the lift-off using Remover PG was cleaner (compared to acetone liftoff). The temperature of the bath was critical for the effective performance of the Remover PG. An ultra sonic

bath was used for this purpose. Care was taken during the lift-off process to prevent complete removal of the deposited metal. So this process required continuous monitoring. The ultrasonic baths were maintained at 65 ˚C for the effective performance of the Remover PG. Remover PG was washed off using Iso-Propanol and then the sample was dried using a nitrogen gun. Fig. 2.26 (a) – (d) shows the process schematically, till the lift-off stage.

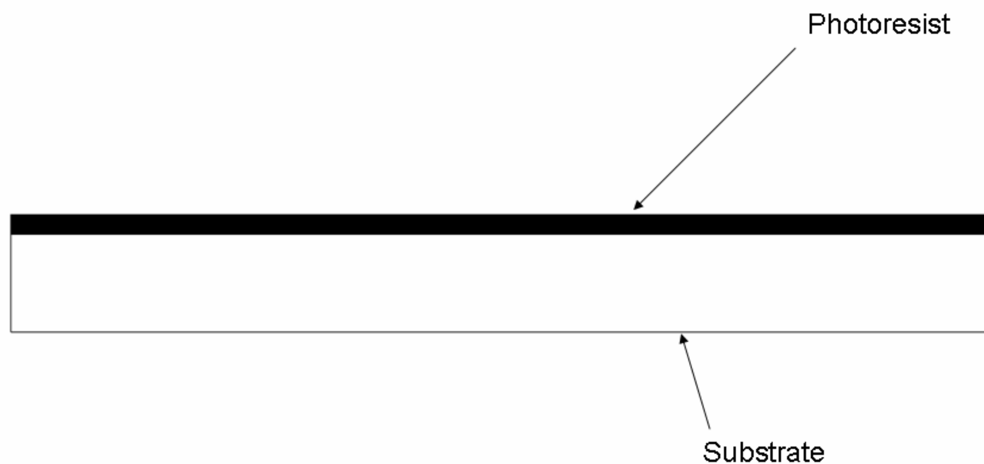

(a) Spun Photoresist

Fig. 2.26 Schematic Showing the Steps Used for the Fabrication of Thin Film Thermocouples.

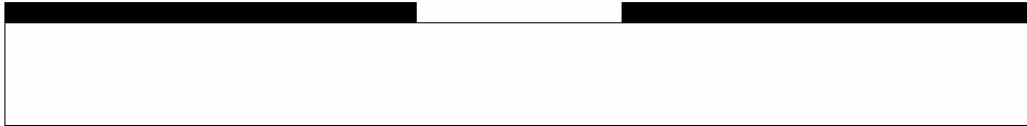

(b) Photolithography

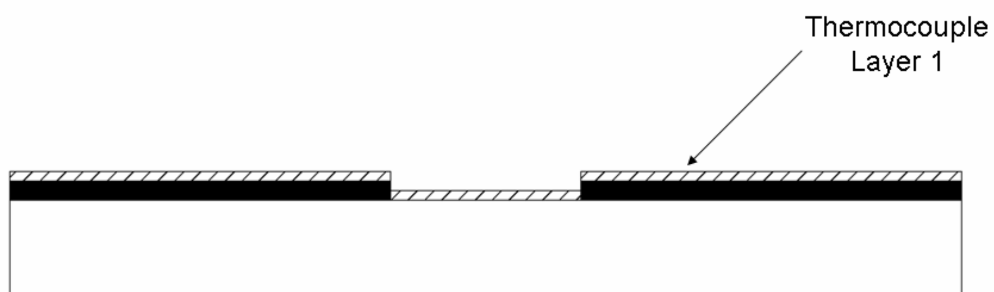

(c) Metal Deposition of First Layer

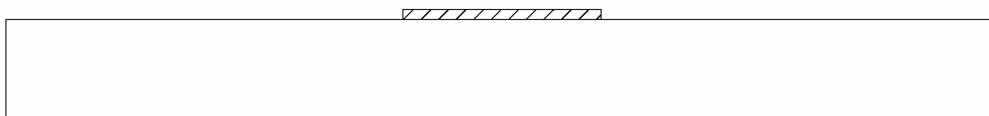

(d) Lift off of First Layer.

Fig. 2.26 Continued.

2.2.5 Second Layer Photolithography

This was one of the most important steps in the whole process and was sometimes very time consuming. The second set of leads for the thermocouples was fabricated in this step to form the junctions on the wafer. The process of fabrication was similar to the earlier photolithographic step. With the major difference being that, this time the partially fabricated wafer was used in place of a brand new wafer and the split view mode of the microscope in the mask aligner was used to achieve the alignment. Precise alignment was required for forming the thermocouple junctions. A Quintel 4000 Mask Aligner was used to achieve this. Alignment marks in the masks enabled precise alignment. After aligning the markers and ensuring that the junctions were being formed the substrate was exposed to the UV light for the required time.

2.2.6 Oxygen Plasma Cleaning (De-Scum)

The same parameters as in the earlier step were used and the results were also similar as mentioned earlier.

2.2.7 Metal Deposition

The second metal layer of the thermocouple was deposited using the metal evaporator. The adhesion layer of chromium was also used in this case and deposition thickness was in excess of 200 nanometers.

2.2.8 Lift-off

The lift-off process had to be performed in the same fashion. Ultra sonic baths with Remover PG were used in this case as well for the lift-off. This process was followed by a packaging method so that the wafer could be used for testing. Fig. 2.27 (a) - (d) shows the steps of fabrication of the II layer schematically.

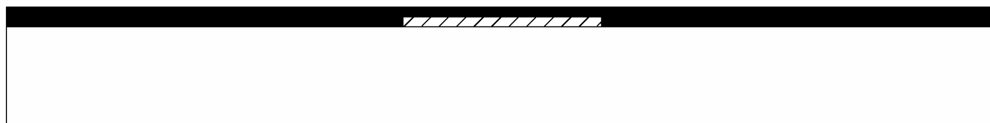

(a) Spun Photoresist for Second Layer of Photolithography.

Fig. 2.27 Last Four Steps of Fabrication of Thin Film Thermocouples.

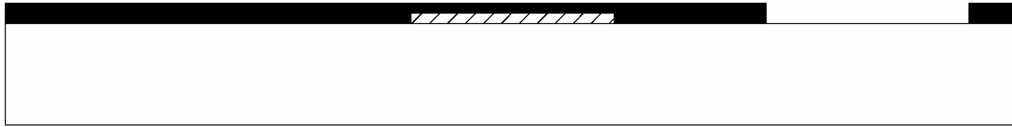

(b) Second Layer Photolithography.

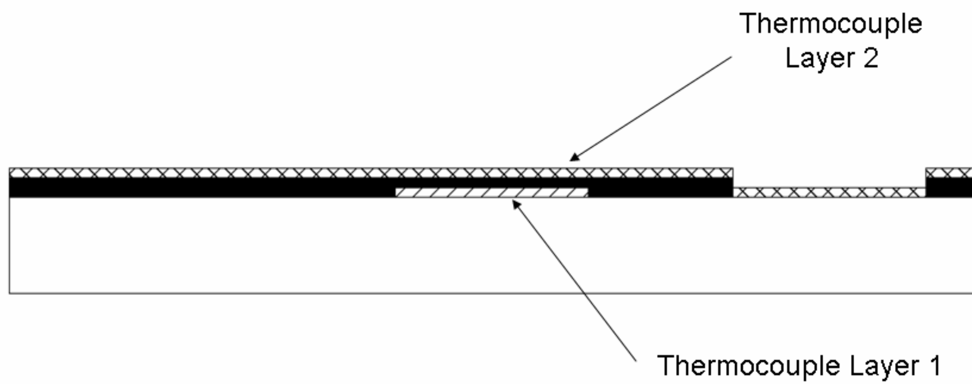

(c) Metal Deposition of Second Layer of Thermocouple.

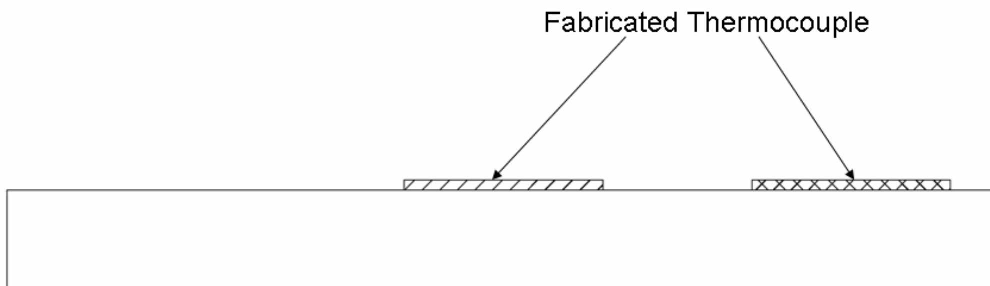

(d) Lift off of the second layer.

Fig. 2.27 Continued.

CHAPTER III

PACKAGING OF THIN FILM THERMOCOUPLES

3.1 Packaging Methods

Packaging steps were performed to connect the fabricated thin film thermocouples to the data acquisition apparatus. In a commercial application, it is commonly believed that packaging is usually the most costly step or procedure.

Several interconnect fabrication strategies were explored, including: pressure contacts, wire bonding (of Aluminum wires) and resistance arc welding. These are reported below.

3.1.1 Pressure Contacts

Pressure contacts were initially explored to connect the wires to the bond pads. In this method the alumel and chromel wires were attached to the ends of a multimeter lead and positioned in such a way that the ends of these wires touched the bond pads, as shown in Fig. 3.1. The multimeter leads acted as supports for the alumel and chromel wires which extended to a thermocouple reader.

Using the support of the multimeter leads the ends of the wires were fixed at a particular position. When these ends made contact with adjacent bond pads the potential difference across the thermocouple could be read. In Fig. 3.1 two thermocouple readers were used. One reader was used for measuring the temperature of the beaded thermocouple that was attached on the surface of the wafer and the other one measured the temperature of the thin film thermocouple. The whole assembly was done on top of a hot plate.

The inherent weakness and feebleness of the contact led to unreliable and unrealistic intermittent fluctuations in temperature data at high temperatures. Such inconsistency in data implied that a different method of acquiring information was required. Therefore, this strategy for packaging was abandoned.

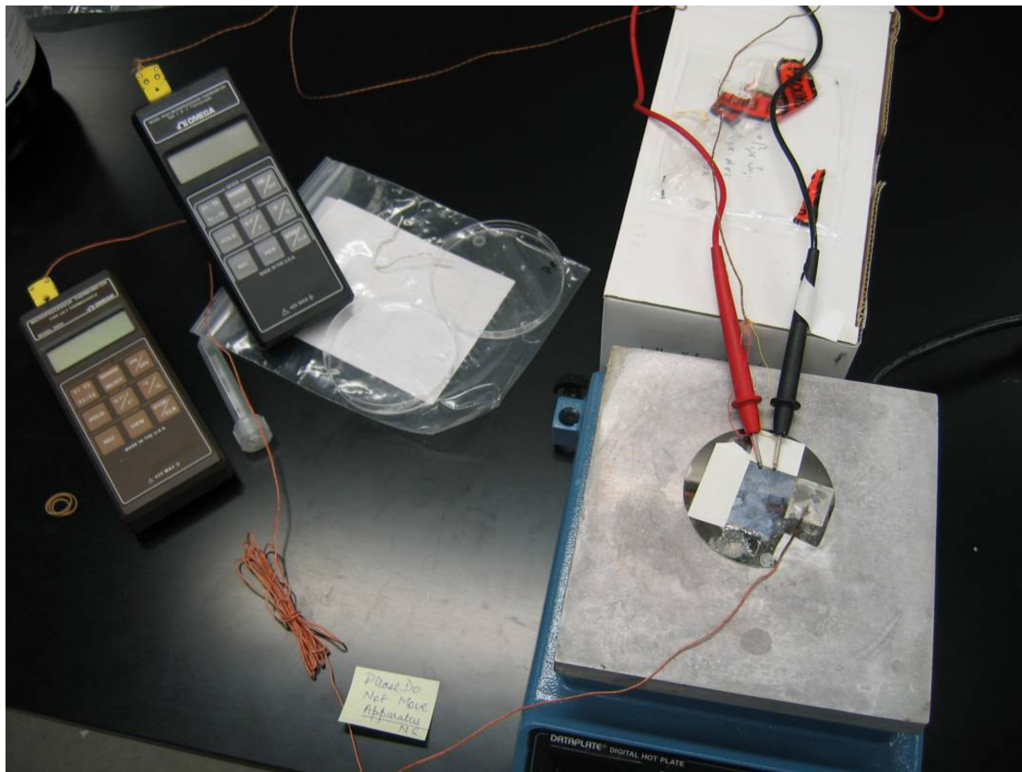

Fig. 3.1 Initial Attempts at Using Pressure Contacts.

3.1.2 Wire Bonding

Wire bonding is conventionally used for packaging of interconnects in the microelectronics industry. However, this technique is limited to low melting point materials such as Gold (1064 ˚C) and Aluminum (660 ˚C) wires. Wire bonding of Chromel and Alumel (melting point for both of them is greater than 1400 ˚C) wires of 75 micrometer (3 mil.) diameter was explored on a Kulicke & Soffa Ltd. 4523A Digital Manual Wire/Wedge Bonder, shown in Fig. 3.2. Since these alloys melt at higher temperatures

than Gold or Aluminum, successful wire bonding could not be achieved with Chromel and Alumel wires. Hence, Aluminum wires (25 micrometer diameter) were initially used for wire bonding on the microfabricated bond pads. The values of the various parameters used for achieving a successful Aluminum wire bond were:

Vertical Feed (90°)

Power Setting of 2.62

Time Setting of 2.0

Force Setting of 1.4

Since the bond strength with the 25 micrometer wire was low, wire bonding was performed using a thicker bond wire (75 micrometers diameter). The bonding parameters for these wires were as follows:

Vertical feed (90°)

Power Setting of 6

Time Setting of 3.0

Force Setting of 3

Fig. 3.2 4523A Digital Manual Wire Bonder.

The initial setup was very important, so that the correct search heights were set. Search heights varied widely according to the height of the holder on which the sample was mounted. Nearly every time wire bonding was performed some amount of optimization of the parameters of force or power was required. The settings that have been mentioned earlier are an approximate average of the settings that were observed to work over a period of time. A rule of thumb for wire bonding was that when the wedge was lowered for making a bond it should be at a height at which it just sandwiches the wire between the surface and the wedge. At that position the wedge can be released to ultrasonically form the bond.

Wire bonding is conventionally used for making interconnects, so it is usually used to join two different metal surfaces by a wire. In this study wire bonding was used to make one bond and keep one end free for connecting to the alumel or chromel wire (which would then connect to the data acquisition system).

The normal programming of the wire bonder requires two set of parameters for the formation of the bond. The bonder was adjusted to either cut the wire off, leave a tail or to form another bond on the same bond pad. This required that the initial length of the wire being bonded was of sufficient length for it to be able to be attached to the Alumel or Chromel wire for connecting to the data acquisition system.

The heterogeneity in thermocouple material composition at the bond pad due to packaged interconnects resulted in parasitic junction potentials being introduced into the sensor element. These parasitic junctions interfered with successful thermography operations. As a result other methods of packaging were also explored. This method was also used for packaging but alternate methods using, resistance arc welding were also used. Fig. 3.3 shows a closer view of the sample holder, wedge and spool, used for wire bonding.

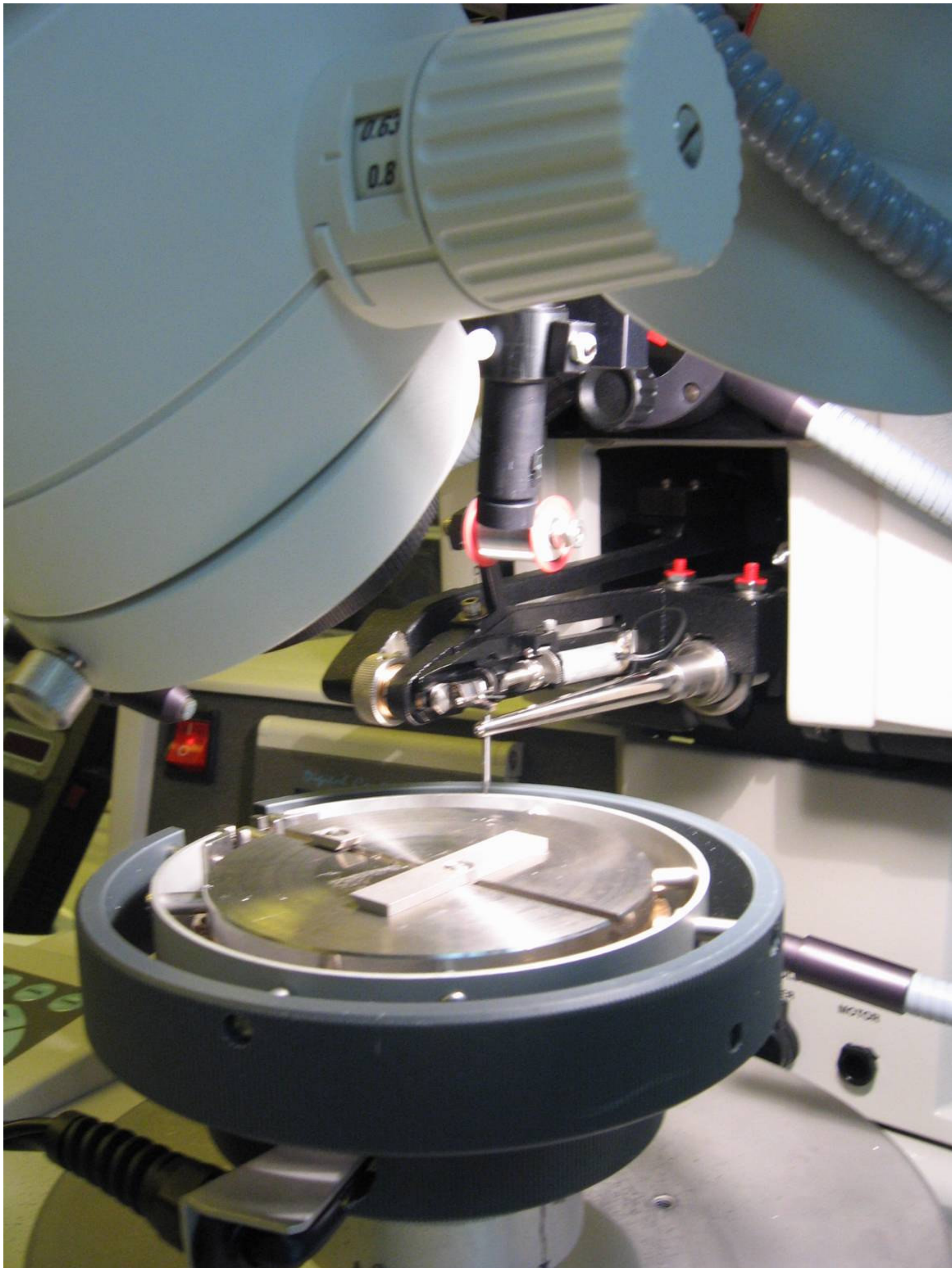

Fig. 3.3 Picture of the Wedge, Spool and Sample Holder for the Wire Bonding Apparatus.

3.1.3 Resistance Arc Welding Method

In conventional resistance arc welding method, an arc is sustained in a small gap between an electrically conducting substrate brought in close proximity to a wire or rod held at high electric potential. The heat generated from the arc melts the tip of the wire. The melted tip is brought in contact with the conducting substrate and it subsequently cools by loosing heat to the ambient and solidifies to form a physical bond between them. After trying the previously mentioned strategies for achieving reliable packaging for the thin film thermocouples, resistance arc welding was explored for the bonding of the Chromel and Alumel wires to the bond pads.

Initially, a DC supply (0-340V, 0-0.1A) was explored; as the arcs produced by using DC sources are known to have better bonding characteristics. The DC source produced considerable arcing. However, the low current rating of the DC power supply was an impediment to continued use of the instrument. The DC source was not able to handle the sudden change in current flow that occurred during the arcing. Hence, the use of an AC supply was explored. The apparatus was tailored for small scale micro resistance arc welding. A standard variable transformer by Staco Energy Products Co. with an Input: 120V 50/60 Hz, Output: 0-120/140V and a rating of 0.7KVA with 5 amps was used. A 5 amp slow blow fuse was connected in series with the transformer input for safety. The alumel/chromel wire that

was to be welded was fixed onto a wooden ledge and another wire was fixed onto the wafer so that it touched the thin film thermocouple. The transformer was used to control the current supply. The wafer substrate (containing the microfabricated TFT and the bond pads) was placed on a multi-jack. The multi-jack was used to slowly raise the wafer and to progressively decrease the gap between the wafer and the wire for striking an electric arc. When the wire was in close proximity to the bond pad the circuit was completed and the arc was formed. Immediately after formation of an electric arc the wire was bonded to the bond pad and the transformer was switched off (within a few seconds). Failure to switch off the transformer would cause the whole length of the wire to become red hot. The bond formed using thin wires was inherently weak due to small amount of melted material present at the bond in the resistance arc welding process. To enhance the mechanical strength of the interconnects a conducting epoxy (Pyro-Duct 598-A by Aremco Products, Inc.) with high temperature rating was dispensed on the bond pads. The conductive epoxy degraded in presence of moisture and also reacted explosively when in contact with water. To improve the limits of operability an additional layer of a non conductive high temperature resistant epoxy (JB Weld) was applied. This packaging strategy for forming interconnects resulted in better performance of the TFT. Using a similar method for bonding, the wire was bent at the tip so that it becomes

parallel to the surface of the bond pad. This strategy of bending the wire was adopted to form multiple arcs in a single attempt and to obtain multiple melt zones. Fig. 3.4 shows a schematic of both these methods.

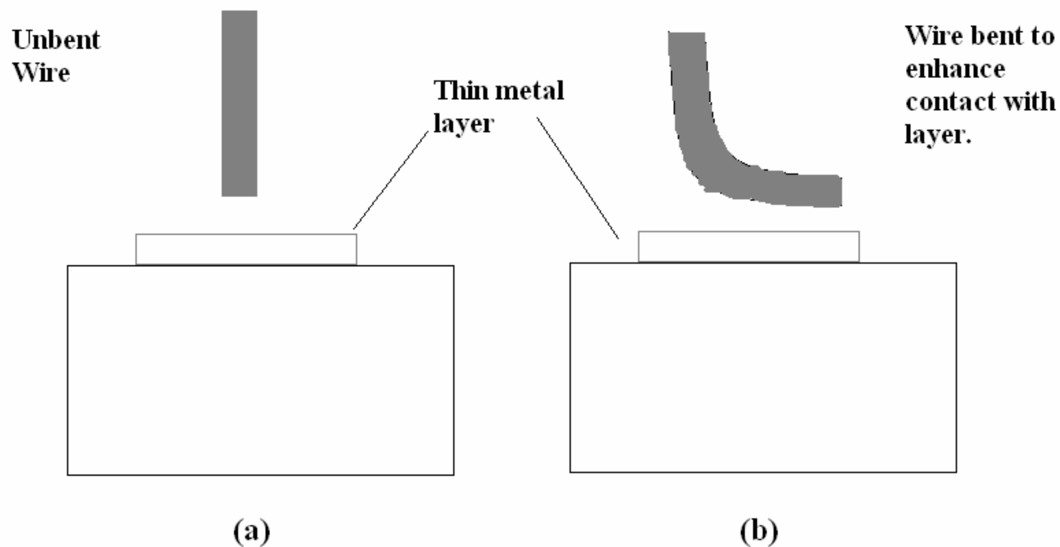

Fig. 3.4 Two Methods of Resistance Arc Welding for Thin Film Thermocouples. (a) Using the Straight Wire. (b) Using Bent Wire.

Another strategy that was used to achieve resistance arc welding for the packaging of thin film thermocouples was the use of two different diameter wires.

The wires were first cleaned at the bare ends using as 400 grit sandpaper to eliminate the surface contaminants and achieve better contact between the two surfaces. The two different diameter wires used in this study were: 125 micrometer and 500 micrometer. The thick (500 micrometer diameter) wire was attached to the 125 micrometer diameter wire of the same kind (Chromel or Alumel) using a thermocouple welder. The thick wire was used to make contact with the bond pads. Two wires of the same kind (Chromel or Alumel) were placed on a bond pad and held in position using alligator clips. This involved application of two pairs of alligator clips. A pair of metal alligator clips was used to keep the wires in position and in contact with the bond pad and another pair was used to supply the current to the wires from the transformer using copper wires. Fig. 3.5 shows the arrangement of these wires.

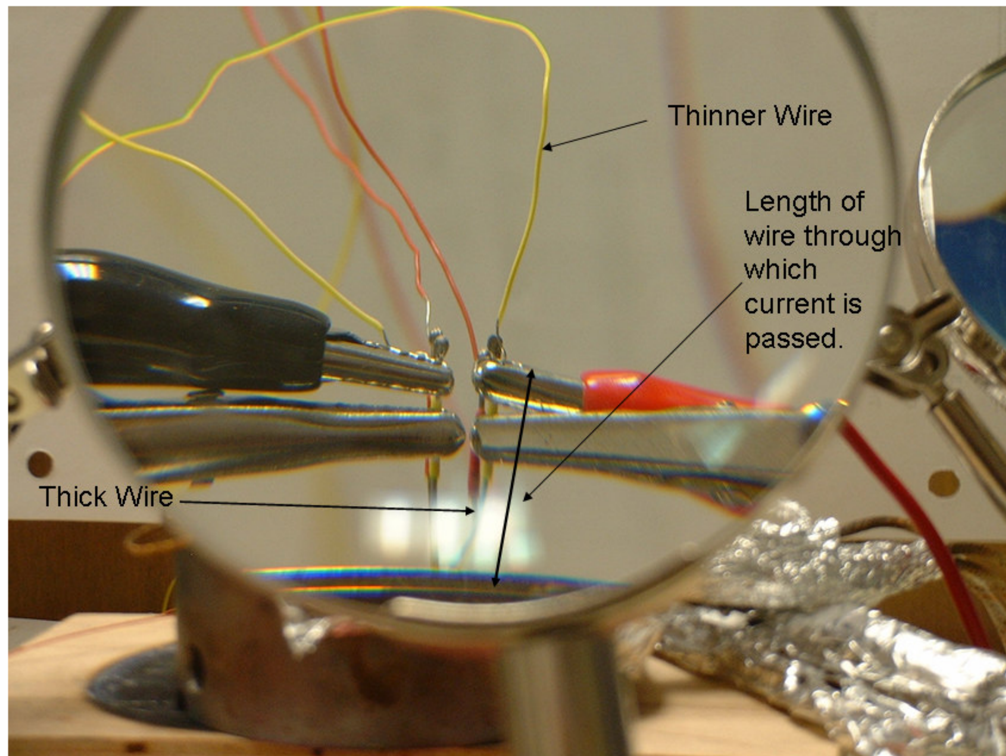

Fig. 3.5 The Figure Shows the Use of Two Pairs of Alligator Clips. The Metal Bodied Pair is Used to Hold the Thick Wire in Place and the Red and Black Clips (touching the bare wire) are Used to Supply the Current to the Wires. (Source: Sinha *et al.* [32])

While keeping the length of the thicker wire small (~1 to 2 cm) current was passed through only the thick wire using the alligator clips (as described and shown earlier). The wire was bonded to the bond pad of similar material (Chromel or Alumel).

The size of the microfabricated bond pads was 1mm x 1mm and the wires were welded onto the bond pad. The silicon wafer substrate (containing the microfabricated TFT and the bond pads) was placed on a multi-jack. The multi-jack was used to slowly raise the wafer to progressively decrease the gap between the wafer and the wire tip for striking an electric arc. Immediately after an electric arc causes the wire to bond to the bond pad, the transformer was switched off (within a few seconds). The voltage drop in the weld was approximately 30% of the maximum voltage (~36V). Great care was taken to avoid the wires from touching each other and from arcing to form a bond mutually amongst them. Once the weld was formed an epoxy (JB Weld) was used over the weld to provide additional mechanical strength. Fig.3.6 shows the wafer placed on the copper block that was placed on top of a multi-jack.

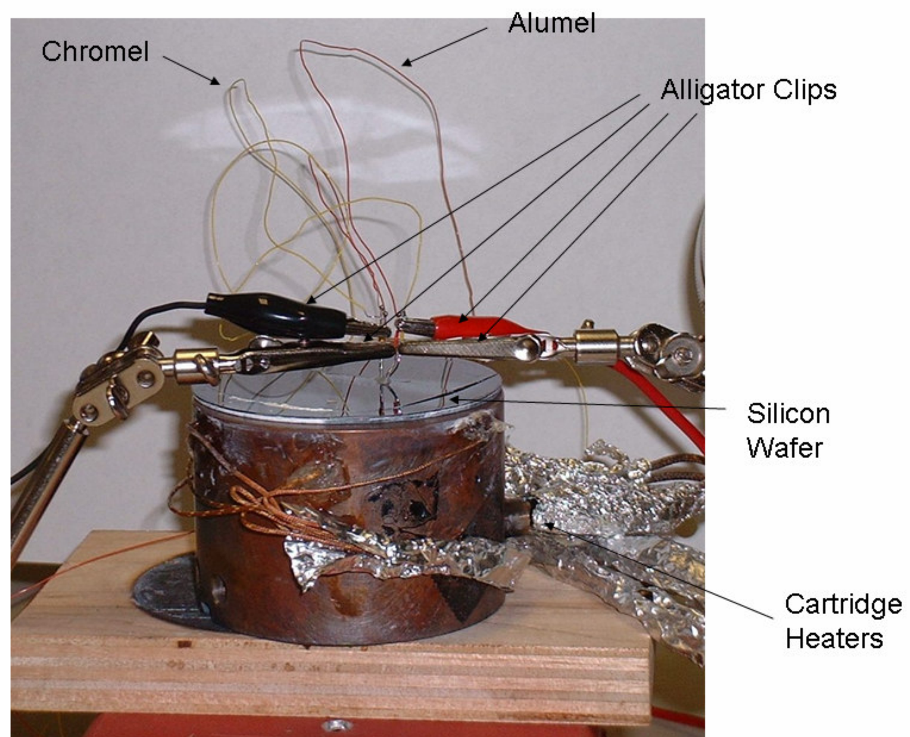

Fig. 3.6 Apparatus for Welding Using Alligator Clips. (Source: Sinha *et al*. [32])

CHAPTER IV

EXPERIMENTAL SETUP

4.1 Frame Structure

The boiling experiments were conducted in a Viewing Chamber (shown in Fig. 4.1). The main functions of the viewing chamber were:

a. To provide a leak proof container for boiling experiments.

b. To provide a clear view of the boiling regime during experiments. Pyrex glass panels were mounted to provide viewing access.

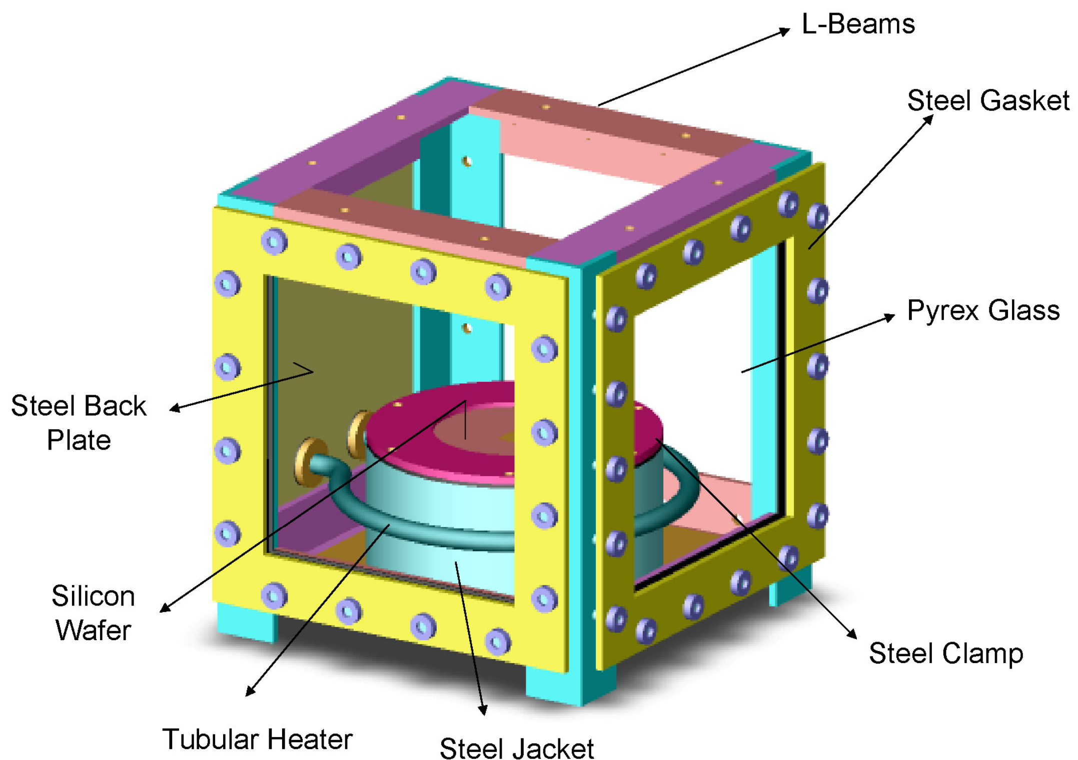

Fig. 4.1 An Assembled Look at the Apparatus that is Used for Conducting the Experiments. (Source: Ahn *et al*. [31])

Steel L-Beams of 1/8 inch thickness and 1 inch width were used to form the skeletal structure of the chamber. These were cut according to the required size and welded together to get the structure shown. Fig.4.2. shows the layout of the four vertical L-beams.

Fig. 4.3 shows the layout (generated by SolidWorks) for the Horizontal L-Beams. Fig. 4.4 shows the layout for Side L-beams. In total 12 L-beams were used for making of the apparatus. Fig. 4.1 shows the assembly drawing of the L-beams. After assembly they form the viewing chamber. Fig. 4.5 shows the back view of the viewing chamber.

Steel plates were placed on the top and bottom surface. The top plate was attached using screws whereas the bottom plate was welded to ensure that there would be no leakages from the bottom. Holes were drilled in the top plate for replenishing the working fluid in the chamber while the experiments were in progress.

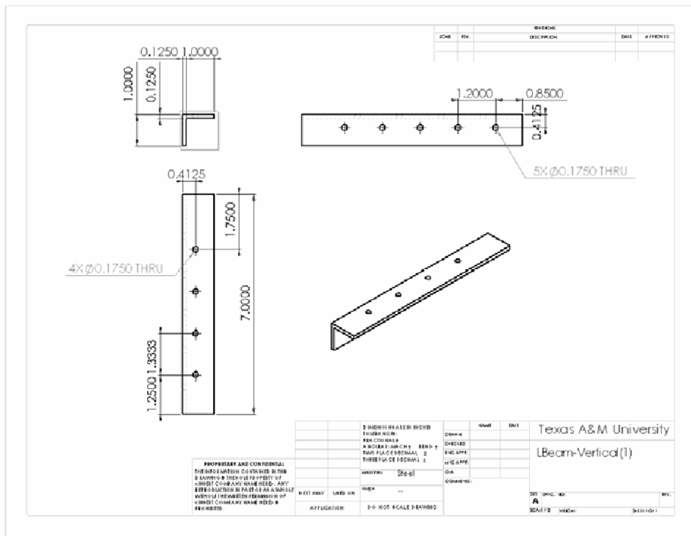

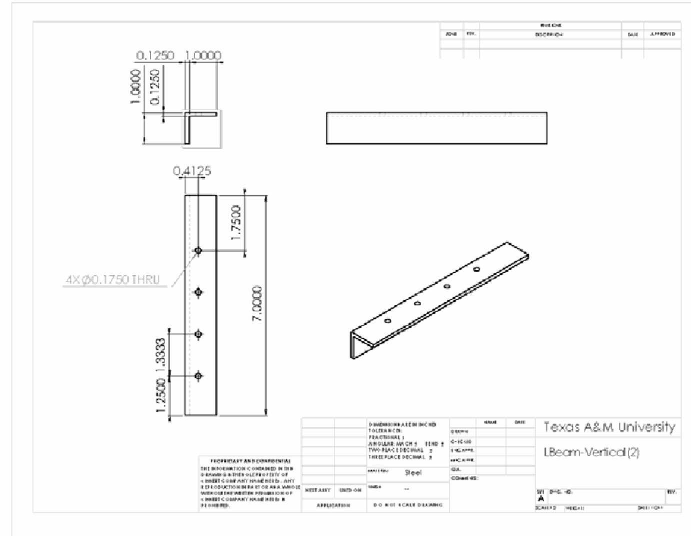

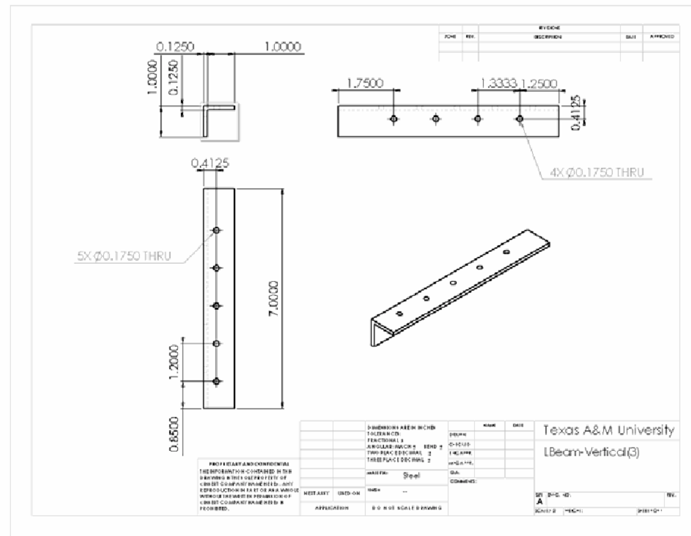

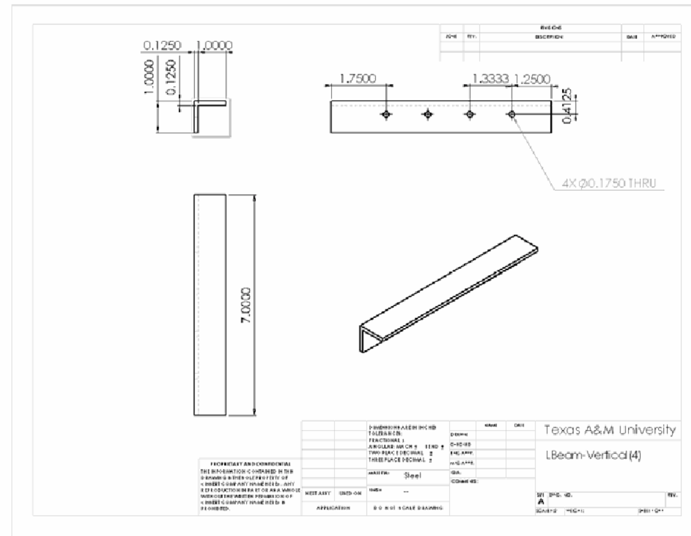

Fig. 4.2 Drawing Sheets (generated using SolidWorks) for the Vertical L-Beams.

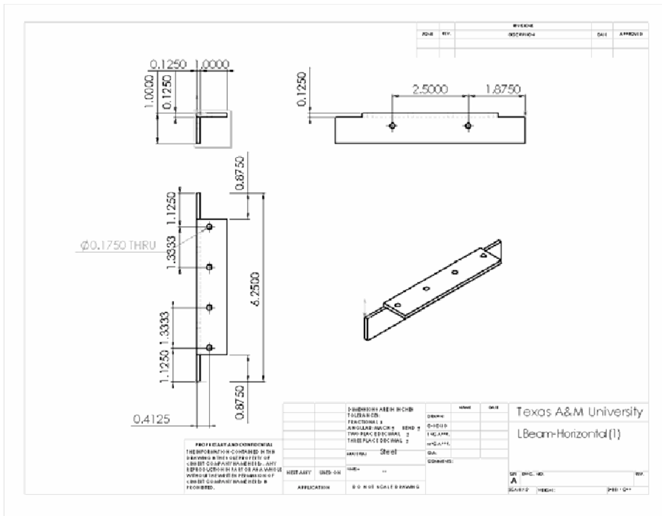

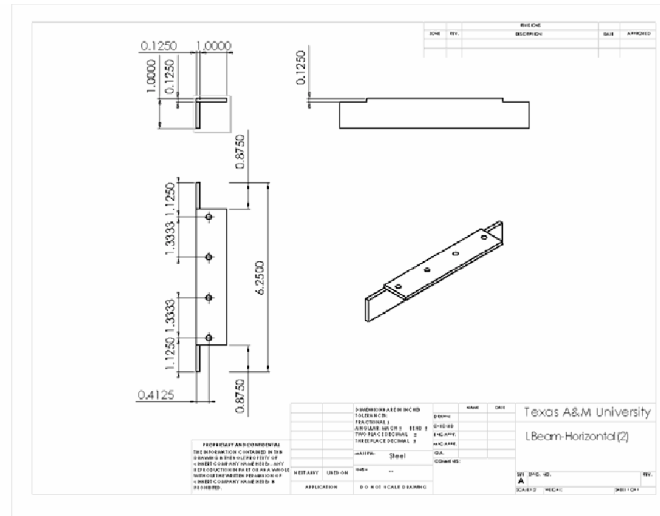

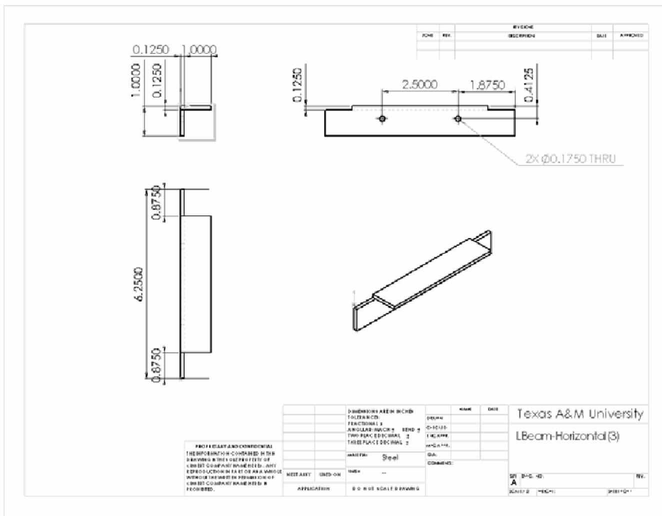

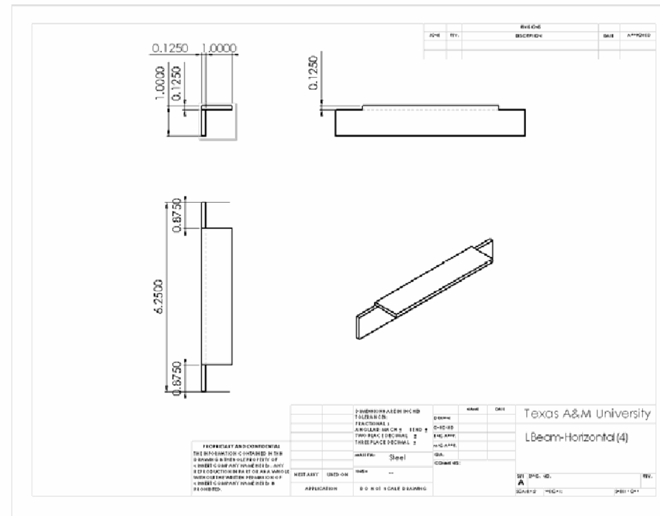

Fig. 4.3 Drawing Sheets for Horizontal L-Beams.

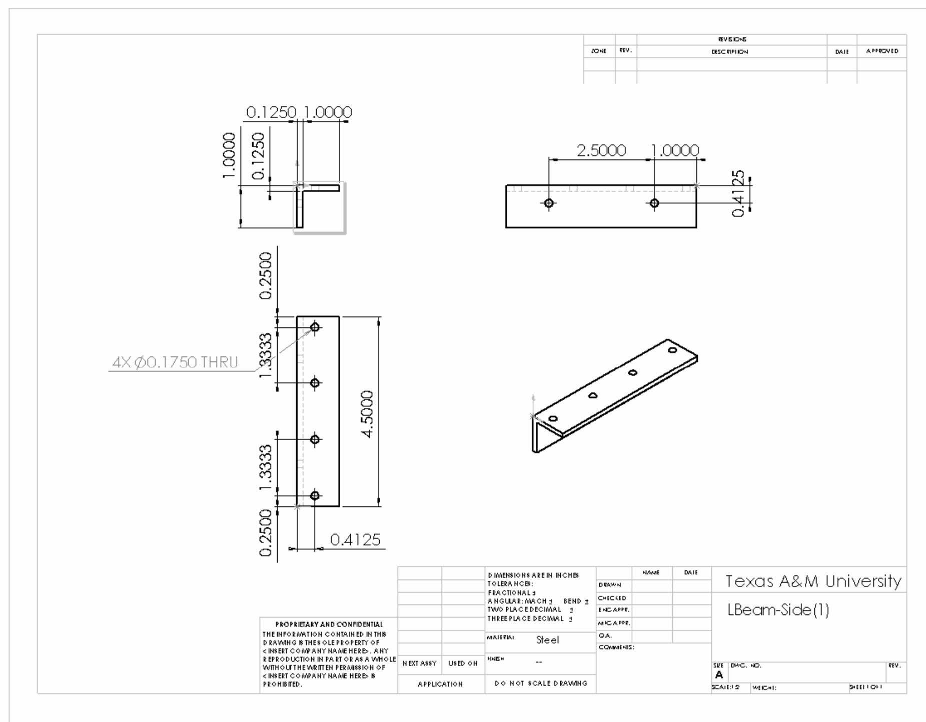

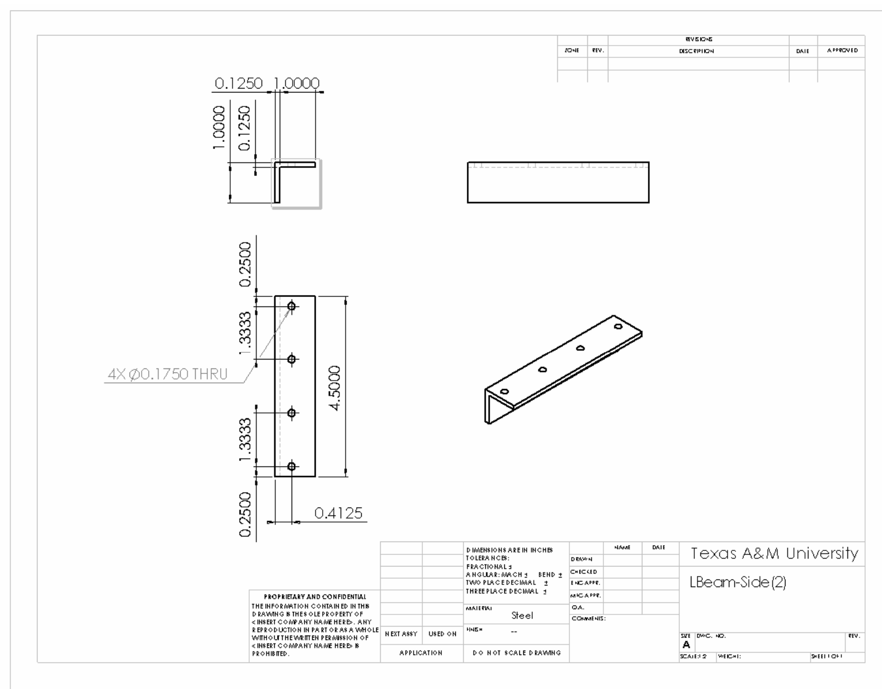

Fig. 4.4 Drawing Sheets for Side L-Beams.

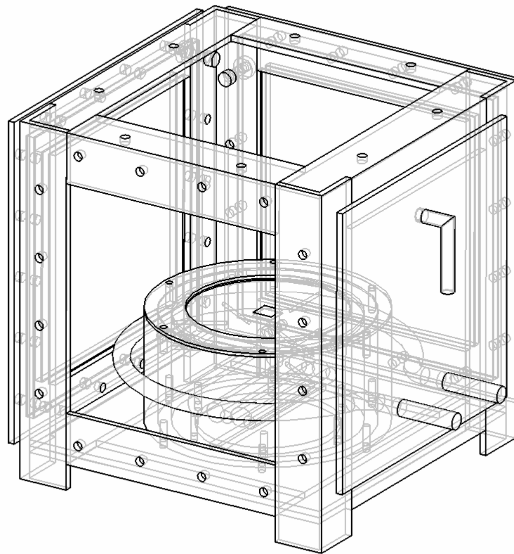

Fig.4.5 Assembled Back View of the Apparatus. Showing the Vent and Electrical Connections for the Tubular Heaters.

A chiller was also added to the system to prevent excessive loss of the boiling medium and for maintaining the temperature of the boiling medium. The chiller assembly provides recirculation of the coolant from a liquid bath and this circulation of the coolant at controlled temperatures gave us the ability to control the boiling liquid temperature. The bottom plate was also designed to provide access to wires for the heaters and the thermocouples. The bottom plate also had taps for mounting the steel jacket. The steel jacket covered the sides of the copper block. Holes were drilled in the top and bottom of the steel jacket, as shown in Fig. 4.6.

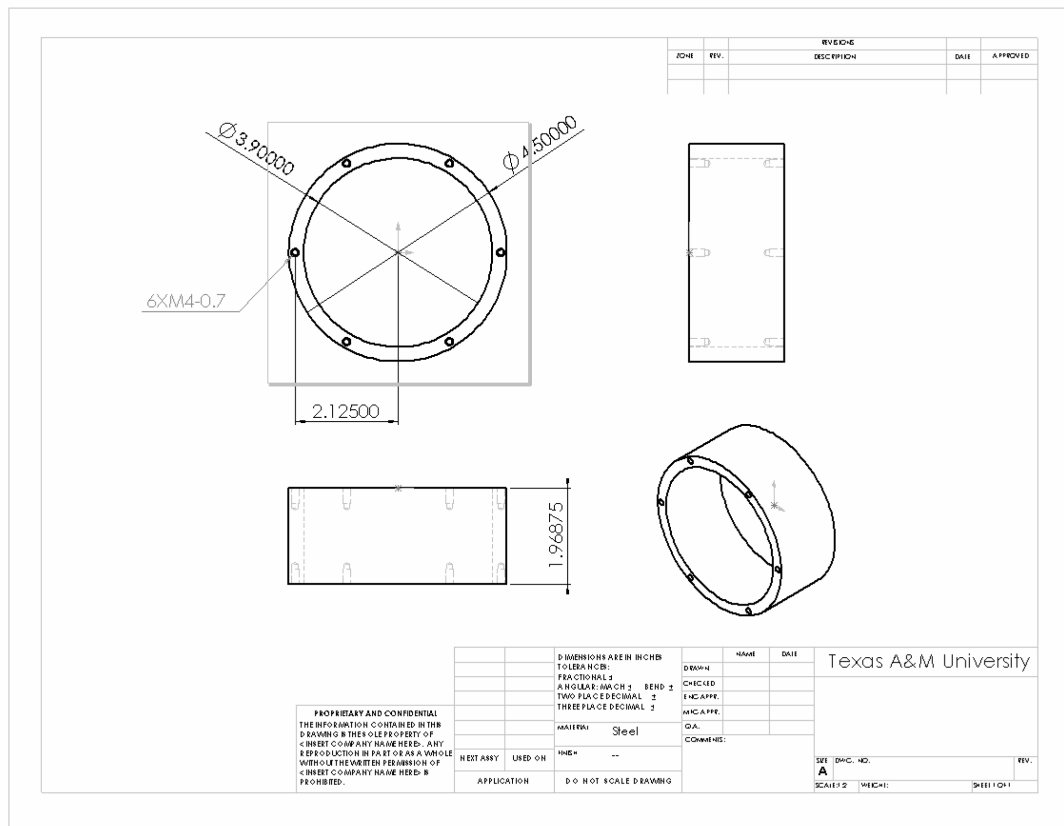

Fig. 4.6 Steel Jacket Design.

These screws were used to attach a steel clamp on the top of the steel jacket and the steel jacket to the bottom plate of the apparatus. As mentioned earlier, the copper block (99.9% pure, deoxidized) was placed inside the steel jacket. The copper block, shown in Fig 4.7, contained the cartridge heaters to provide the heat for the boiling experiments. Five cartridge heaters were used: three (500W) and two (300W) (Manufacturer: Watlow Inc.).

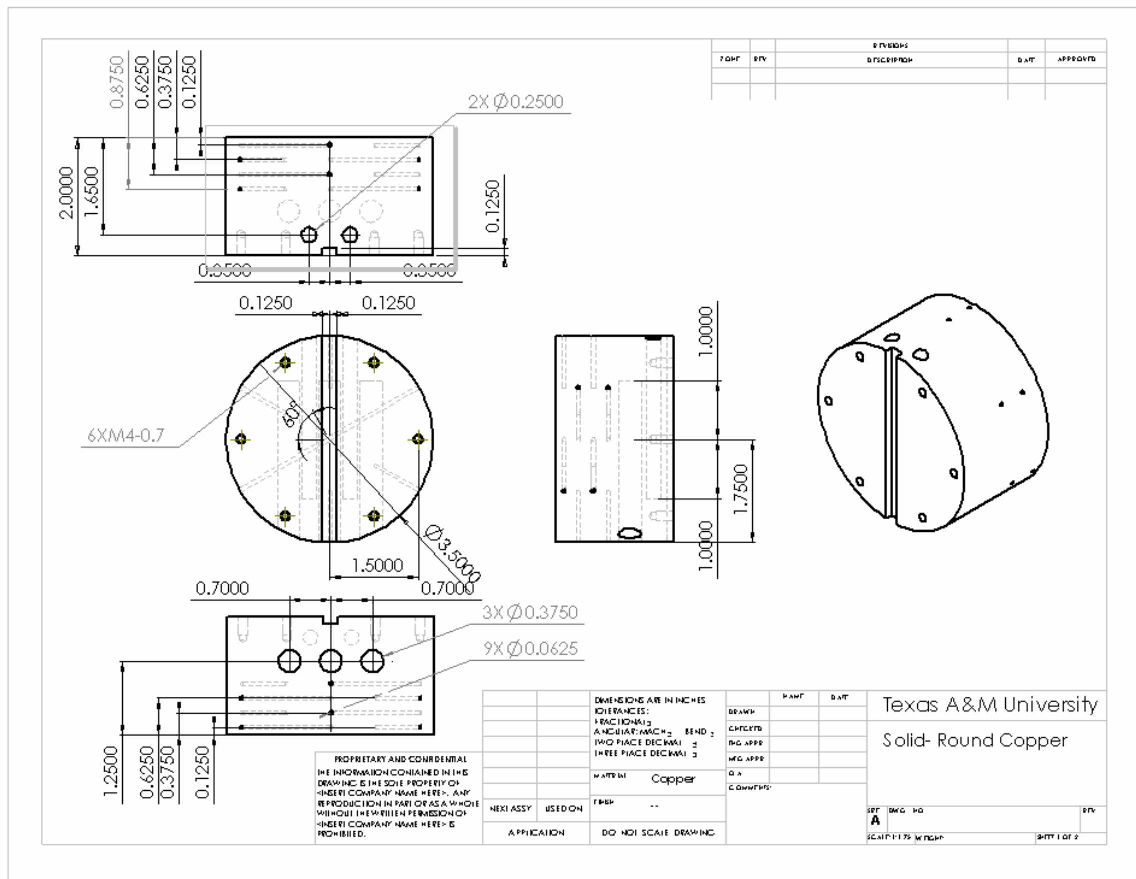

Fig. 4.7 Copper Block Design.

In the copper block, holes were drilled for inserting thermocouples. Twelve thermocouples were placed in the copper block at various heights and radial locations. These thermocouples were used to record the temperature distribution inside the copper block and obtain the heat flux through the copper block.

The thermocouple wires were connected to the data acquisition system and the wires from the cartridge heaters were connected to the power source

(variable transformer). One thermocouple was placed in the working fluid to measure the liquid bulk temperature. The wafer containing the thin film thermocouples was clamped on top of the copper block. A pyrex wafer was used between the copper block and the silicon wafer to filter out the electrical noise from the cartridge heaters. Thermal grease was applied on both the sides of the pyrex wafer with one side in contact with the copper block and the other side in contact with the silicon wafer, as shown in the magnified view in Fig. 4.8. Fig. 4.8 also shows the block diagram of the experimental apparatus. Fig. 4.8 also shows the drain line, vent line and supply line that were used for emptying the chamber, keeping the pressure inside at the atmospheric level and supplying extra PF-5060 when required, respectively. The figure also shows the power sources; data acquisition system and the digital camera for taking pictures during the experiment.

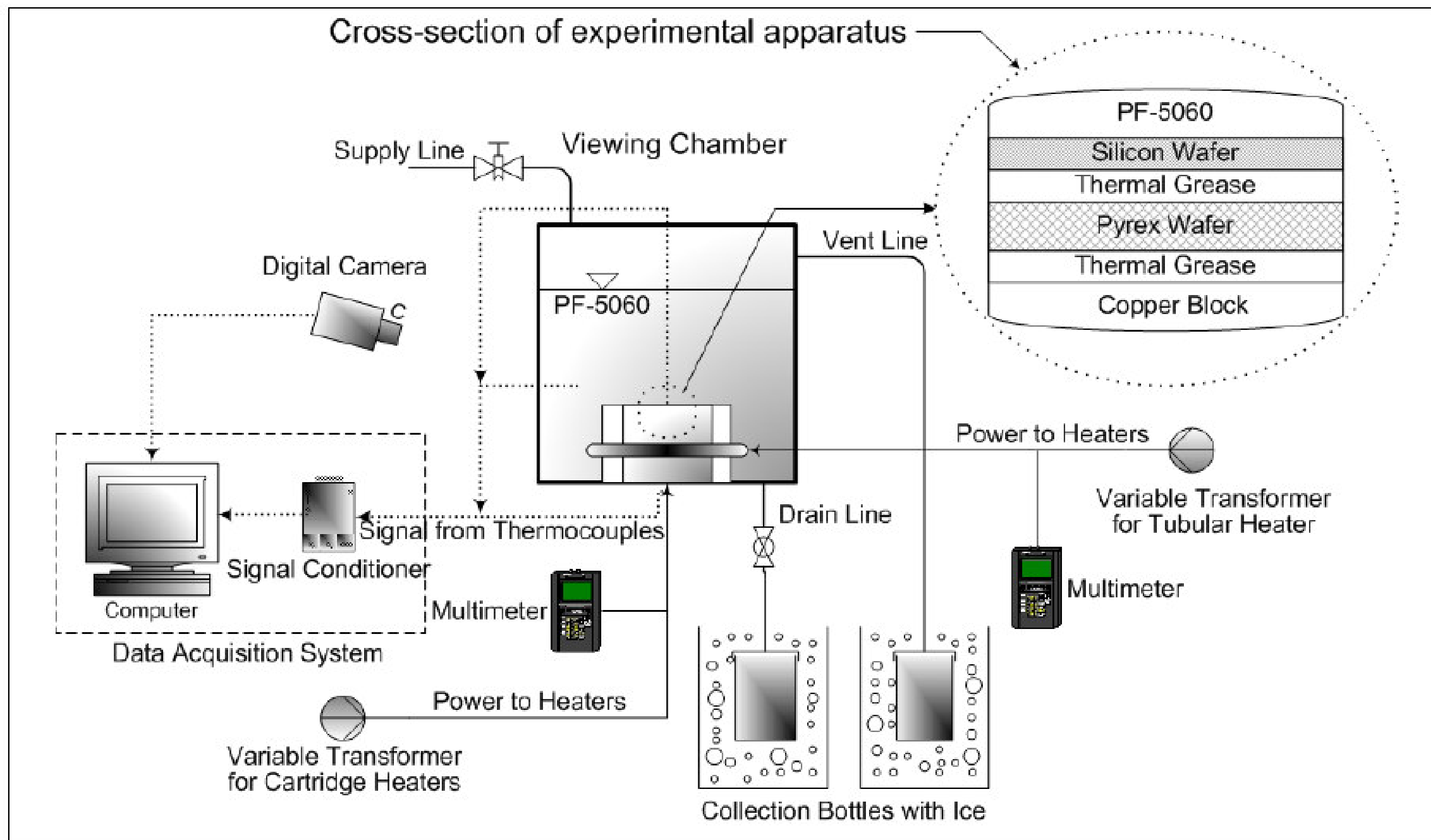

Fig. 4.8 Schematic Block Diagram of the Experimental Apparatus. (Source: Ahn *et al*. [31])

A rubber gasket was placed between the steel jacket and the wafer to prevent leakage and thermal stress cracking. The rubber gasket was also helpful in providing a seal with the silicon wafer.

Four holes were drilled on the back plate of the apparatus. Two holes were made for mounting the tubular heater, one hole was used to mount a vent and one hole was used to mount a drain line. To prevent cracking due to differential thermal expansion - the glass sheets were mounted between rubber gaskets on either side and clamped with steel square frames which were machined to appropriate size. A good seal was ensured by using rubber gaskets and the steel frame. A cross section of the viewing side consists of five layers (going from outside to inside): steel gasket, rubber gasket, pyrex glass, rubber gasket and then the steel frame structure. This provides a good seal for keeping the liquid in. Fig. 4.9 shows the actual picture of the apparatus as it was used for the experiments.

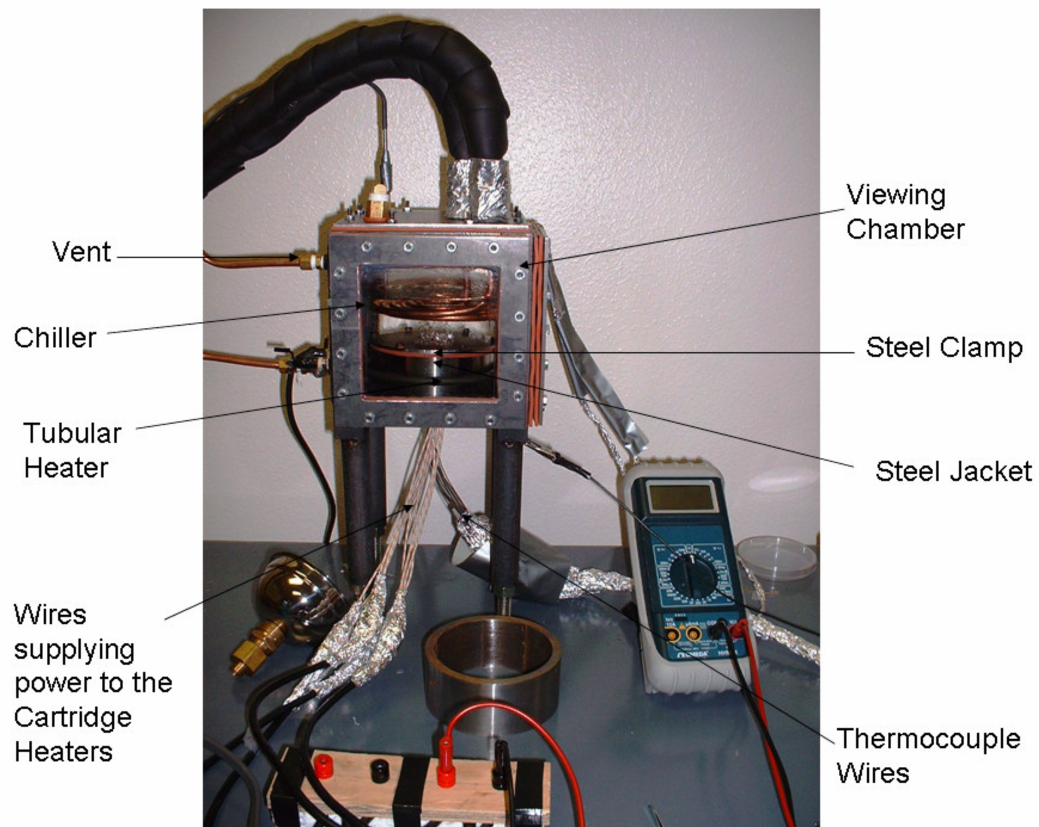

Fig. 4.9 Picture of Apparatus for Pool Boiling Experiments.

CHAPTER V

EXPERIMENTAL PROCEDURES

Two sets of experiments were performed:

1. Calibration experiments
2. Boiling Experiments

5.1 Calibration Experiments

Due to the vapor deposition process the chemical composition of thin film thermocouples was different from commercially available K-Type thermocouples. For this reason, calibration experiments were performed for thin film thermocouples using standard K-Type beaded thermocouples and the chemical composition was analyzed using an XPS. The calibration procedure was as follows:

a. The wafer was mounted on the copper heater apparatus. The copper heater apparatus has been described in the Experimental Setup (Chapter IV) of the thesis.
b. The calibration was done with respect to a standard beaded K-Type thermocouple. The K-Type thermocouple was made using a thermocouple welder and was attached on the surface of the wafer. The beaded thermocouple was attached in close proximity to the thin

film thermocouples. The beaded thermocouple was previously calibrated with respect to a standard NIST calibrated thermometer using a temperature controlled water bath.

c. The cartridge heaters were connected to a variable transformer (variac) (Type 1010, Input 120V 50/60Hz, Output: 0-120/140V, 10 Amp, 1.4KVA by Staco Energy Products Co.) and the variable transformer was used to control the current passing through the heaters.

d. Both, the packaged thin film thermocouple and the beaded thermocouple were connected to the data acquisition system (National Instruments TC-2095 (terminal block), NI SCXI-1000 (chassis) and a National Instruments PCI-6024E DAQ Board (200 kS/s, 12-Bit, 16 Analog Multifunctional DAQ) connected to a Pentium 4 based computer). LabView 6 software was used.

e. A voltage value was set for the cartridge heaters and the system was allowed to come to steady state. The voltage supplied to the cartridge heaters was measured by a voltmeter that was connected to the variable transformer.

f. After steady state conditions were achieved, the data acquisition system was used to record the temperatures for one or two minutes.

This data was averaged over time and was used for calibrating the thin film thermocouple with respect to the beaded thermocouple.

5.2 Boiling Experiments

The purpose of the thin film thermocouple was to measure the transient surface temperature of the silicon wafer during various stages of boiling.

a. After performing the calibration of the thin film thermocouples, the wafer was mounted on the heater apparatus and the chamber was tested for any leaks by filling it with PF-5060 (Performance Fluid-5060). The chamber was filled to a predetermined mark in each of the tests.
b. The chiller tubes were lowered into the viewing chamber. The temperature of the coolant was set depending on the kind of experiment being conducted. For example, if a subcooled experiment had to be conducted then the chiller would be lowered and submerged in PF-5060, to keep the liquid temperature below the saturation temperature. If a saturated boiling experiment had to be conducted the chiller was not submerged into the liquid pool. In saturated boiling experiments the chiller was used to condense the boiling liquid.

c. After leak testing, the tubular heater was switched on and the voltage was set to 75 Volts. This voltage supply was maintained to increase the bulk temperature of the fluid to 56 degrees C (which is the boiling temperature of PF-5060) and the fluid bulk temperature was maintained at that value for approximately 15 minutes. This step was done to eliminate the presence of tiny bubbles in the system which would otherwise lead to premature boiling.

d. With the fluid at saturation temperature the voltage of the tubular heater was lowered and the cartridge heaters were switched on. Cartridge heaters were controlled by a separate variable transformer. The system was allowed to come to steady state.

e. During the process of attainment of steady state, the bulk temperature of the liquid had to be closely monitored so that it was maintained at 56 degrees C.

f. As the voltage supply to the cartridge heaters was increased the voltage supply to the tubular heater was decreased. The only constraint being the maintenance of the bulk temperature at 56 degrees C.

g. Once steady state was achieved, the DAQ system (National Instruments SCXI-1102C Analog MUX, and PCI-6251 DAQ Board with Pentium-4 3.2 GHz computer, and using Labview 7.1 software) was used to record the readings for a period of two minutes. The sampling rate that was used for these readings was 200Hz.

h. These readings of various temperatures were used to calculate the heat flux at various values of voltage supply. This data gave the ability to construct the boiling curve for PF-5060.

The block diagrams of the programs used for calibration experiments and boiling experiments are shown and explained in the following section of the chapter:

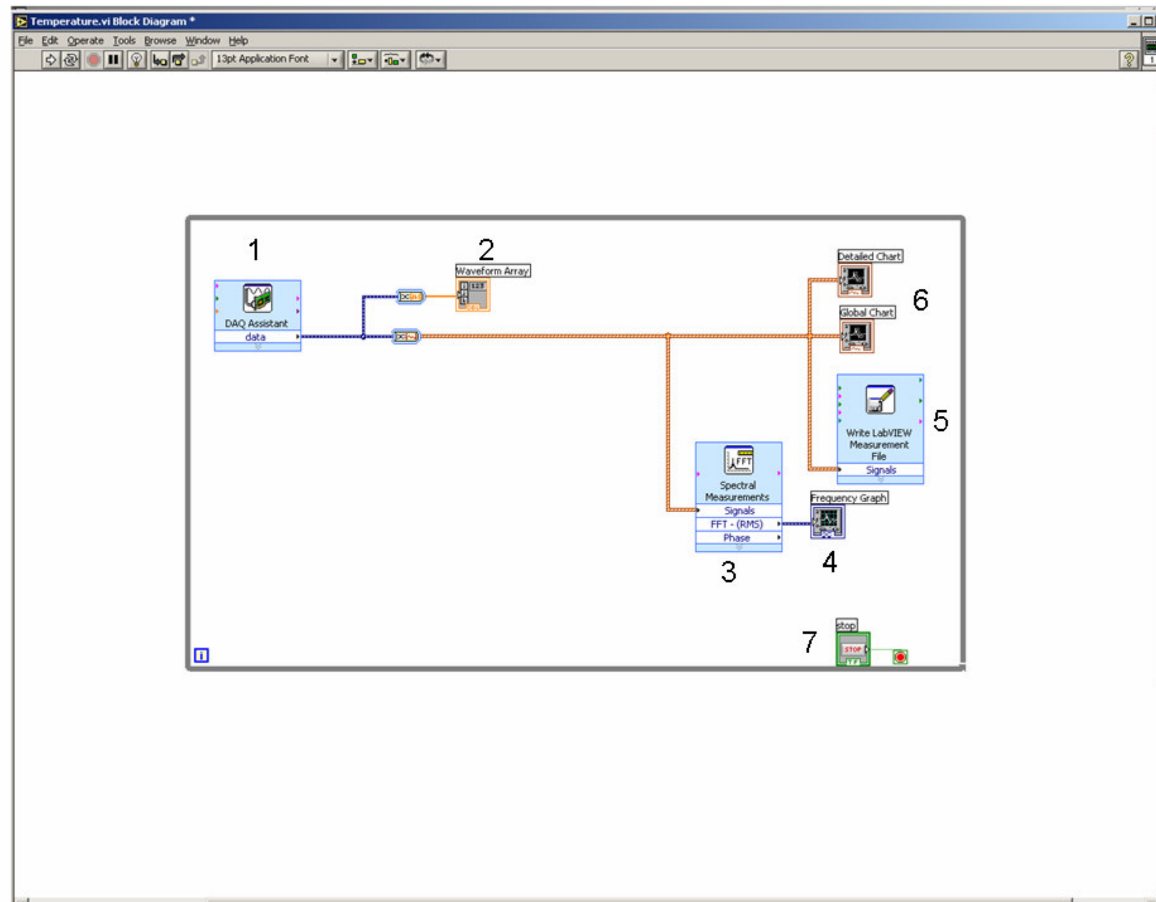

Fig. 5.1 Lab View Block Diagram for Temperature Calibration. Subunits 1-7: Show Various Components of the System.

Figure 5.1 shows the block diagram in Lab View for calibration of the thin film thermocouples. Subunit 1 represents the actual physical connection between the DAQ system and the thermocouples. Subunit 2 showed the waveform array, this was used to set the value of the thermocouples in the numeric form. Subunits 3 and 4 represent the part of the program used for applying FFT (Fast Fourier Transform) to the data acquired. Subunit 5 represents the unit used to output the values of the thermocouples to a data file. Subunit 6 represents the output graphs for the calibration curve. It shows the temperatures of the thin film thermocouples and the beaded thermocouple in graphical format. Subunit 7 is the stop switch.

Similarly, Figure 5.2 shows the block diagram used for the boiling experiments. Subunit 1 is used to specify the location of the calibration file.

A linear calibration was used and the file contained the values of the parameters a and b, where $y = ax + b$ and y represents the calibrated and x represents the non-calibrated temperatures. Subunit 2 is used to represent the physical connection between the thermocouples and the DAQ System. Subunit 4 displayed the graph for non-calibrated, raw temperature data. Subunit 3 was used to calibrate the actual raw data. The non-calibrated data was processed by Subunit 3 and by using the values from the calibration file the calibrated temperature data was obtained. Subunit 5 gave the values of the calibrated temperatures in the numeric form. Subunit 6 applied the FFT to the calibrated data for obtaining the frequency response in Subunit 7. Subunit 8 was used for writing the values of the calibrated temperatures to a file. At the same time Subunit 9 displayed the calibrated temperatures graphically and Subunit 10 was the stop switch.

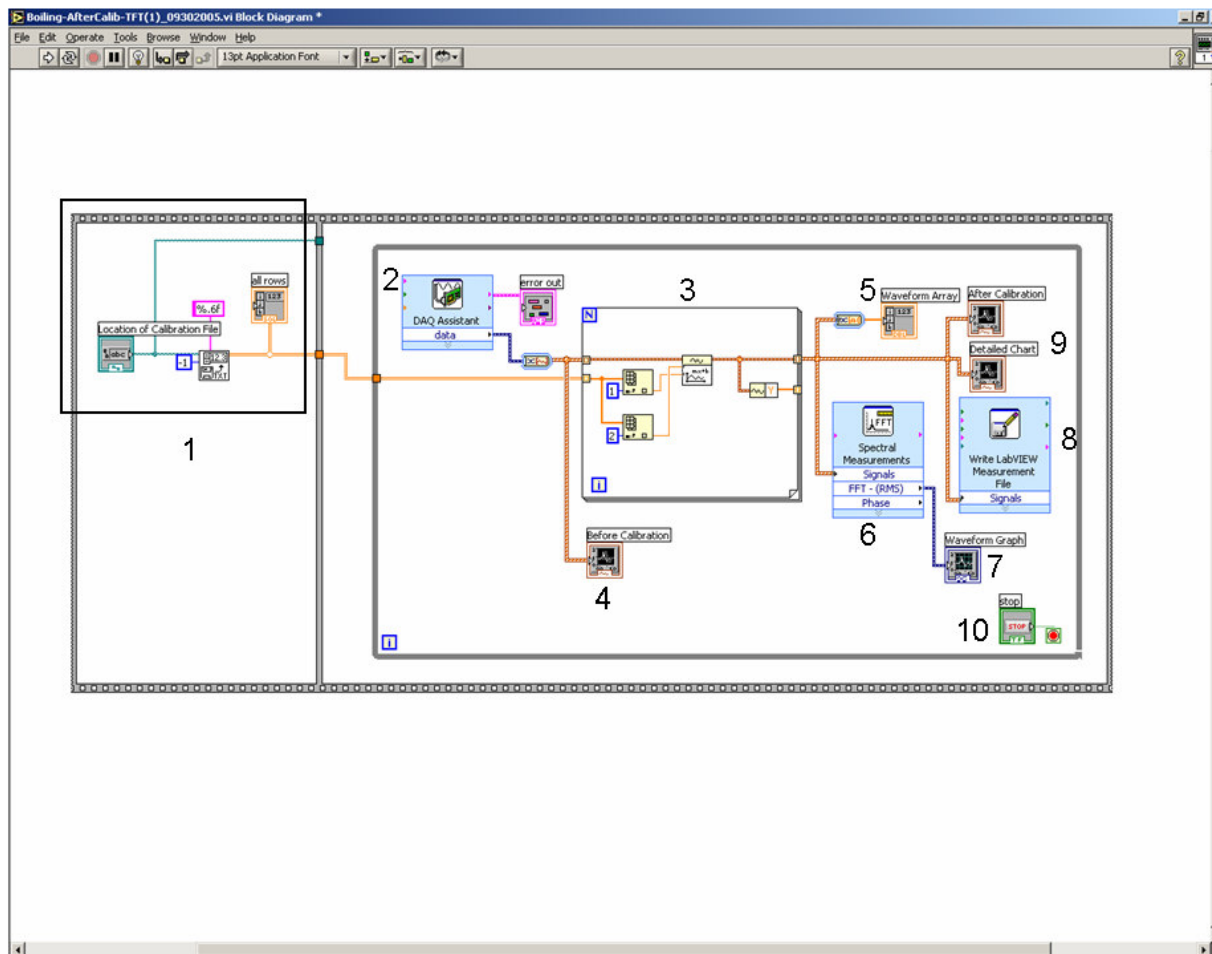

Fig. 5.2 Lab View Block Diagram for Temperature Measurement.

CHAPTER VI

DATA REDUCTION

The temperature data that was obtained from the boiling experiments was used to calculate the heat flux through the copper block. The temperature gradient through the copper block was used for the heat flux calculation, using the following formula:

$$q'' = -k \frac{\Delta T}{\Delta x}$$

where k is the thermal conductivity of copper (which was taken to be 400W/mK), ΔT was the difference in temperature between two thermocouples that were placed in the same vertical plane in the copper block and the distance between these thermocouples was Δx.

In the case of boiling the heat transfer coefficient was calculated in the following fashion:

$$h = \frac{q''}{T_w - T_{sat}}$$

where T_w represents the average wall temperature and T_{sat} represents the saturation temperature of the liquid boiling medium.

The thermal resistance between the copper block and the wafer was obtained by calculating the temperature difference between the top of the copper block (extrapolated by the data from the thermocouples in the copper

block) and the top of the wafer (data that was acquired from the thin film thermocouples on the surface). The formula used for this calculation was:

$$R = \frac{T_w - T_{Cu,Top}}{\dot{Q}}$$

where T_w represents the average wall temperature (the average temperature that was obtained from the thin film thermocouples) and $T_{Cu,Top}$ is the temperature of the top of the copper block (extrapolated from the temperature data). $\dot{Q}$ is the rate of heat transfer.

$$\dot{Q} = q''.A$$

where A is the cross sectional area of the copper block that was used for the study. As this area was used for calculation of thermal resistance between the copper block and the wafer, only the surface area of the wafer that was exposed to the liquid was considered.

The uncertainties in the heat flux and the heat transfer coefficient was also calculated using the Kline and McClintock method. The formula used for the calculation of uncertainty in the heat flux values was:

$$\frac{w_{q''}}{q''} = \sqrt{\left(\frac{w_k}{k}\right)^2 + \left(\frac{w_{T_2}}{T_2}\right)^2\left(\frac{T_2}{T_2 - T_9}\right)^2 + \left(\frac{w_{T_9}}{T_9}\right)^2\left(\frac{T_9}{T_2 - T_9}\right)^2 + \left(-\frac{w_{\Delta x}}{\Delta x}\right)^2}$$

$$\frac{w_{q''}}{q''} = \sqrt{\left(\frac{w_k}{k}\right)^2 + \left(\frac{w_{T_2}}{T_2 - T_9}\right)^2 + \left(\frac{w_{T_9}}{T_2 - T_9}\right)^2 + \left(-\frac{w_{\Delta x}}{\Delta x}\right)^2}$$

where w is the statistical uncertainty value for each variable. The correlation used for the calculation of the uncertainty in the heat transfer coefficient was:

$$\frac{w_h}{h} = \sqrt{\left(\frac{w_{q''}}{q''}\right)^2 + \left(-\frac{w_{T_W}}{T_W - T_{sat}}\right)^2 + \left(-\frac{w_{T_{sat}}}{T_W - T_{sat}}\right)^2}$$

The uncertainty value of the thermal conductivity was taken to be 1% of the thermal conductivity of copper (k) and the uncertainty value of the vertical distance between the thermocouples was taken to be 3% of the distance (Δx). The uncertainty in the two temperature values (T_2 and T_9) was calculated from the temperature data recorded at steady state, the uncertainty in the wall temperature (T_W) was calculated from the thin film thermocouple data and the uncertainty was taken to be 0.1 degrees C for the saturation temperature (T_{sat}).

CHAPTER VII

RESULTS AND DISCUSSION

7.1 Calibration Experiments

As mentioned previously (in Chapter III), various strategies were explored for packaging. Wire Bonding caused parasitic junctions, but, not very satisfactory results. Both methods used for resistance arc welding gave good results.

Composition of the thermocouples was analyzed using the XPS (X-Ray Photoelectron Spectrometer). For this purpose small pieces of broken silicon wafers were placed on the sample holder during metal deposition. Keeping small pieces, on the sample holder, allowed the processing of the same number of substrates that could be processed and at the same time provided the ability to analyze the composition using an X-ray Photoelectron Spectrometer.

7.1.1 X-Ray Photoelectron Spectrometer Analysis

The deposition of Alumel and Chromel was studied using the XPS (X-Ray Photoelectron Spectroscopy). A Kratos Axis Ultra Imaging X-Ray Photoelectron Spectrometer (XPS) was employed to analyze the composition of the deposited metal traces of the thin film thermocouple. Every time the

process of vapor deposition was performed to fabricate the thin film thermocouples a dummy sample was kept inside the vacuum chamber. This sample would have the same composition of deposited metals as the wafers that would be processed in the vapor deposition cycle. The analysis of these samples provided information about the chemical composition of the deposition. The deposited metal layers have a different composition compared to the target due to the different values for vapor pressures of the constituent metals, different partial pressures (including leaked gasses in the chamber) and different vapor diffusivities in the physical vapor deposition chamber for the component metals (Ni, Cr and Al).

The substrates were loaded into the XPS and the compositions of the deposited metal surfaces were analyzed. The spectrum of elements in the samples obtained from XPS measurements are plotted in Fig. 7.1 (Alumel) and 7.2 (Chromel). The spectral data shown in Figs. 7.1 and 7.2 were used to obtain the composition of the components of the TFT. The figure displayed here shows the survey curve (the curve which shows all the elements that are present on the surface) for one of the fabricated samples. The peaks shown indicate the presence of the constituent elements. The composition can be obtained by comparing the energies of these peaks with the known standard energies of ejected electrons from various elements in XPS. The survey represents general mapping which contains information about all the

components present on the surface. For detailed analysis, the instrument is capable of providing more specific information about certain regions of the spectrum.

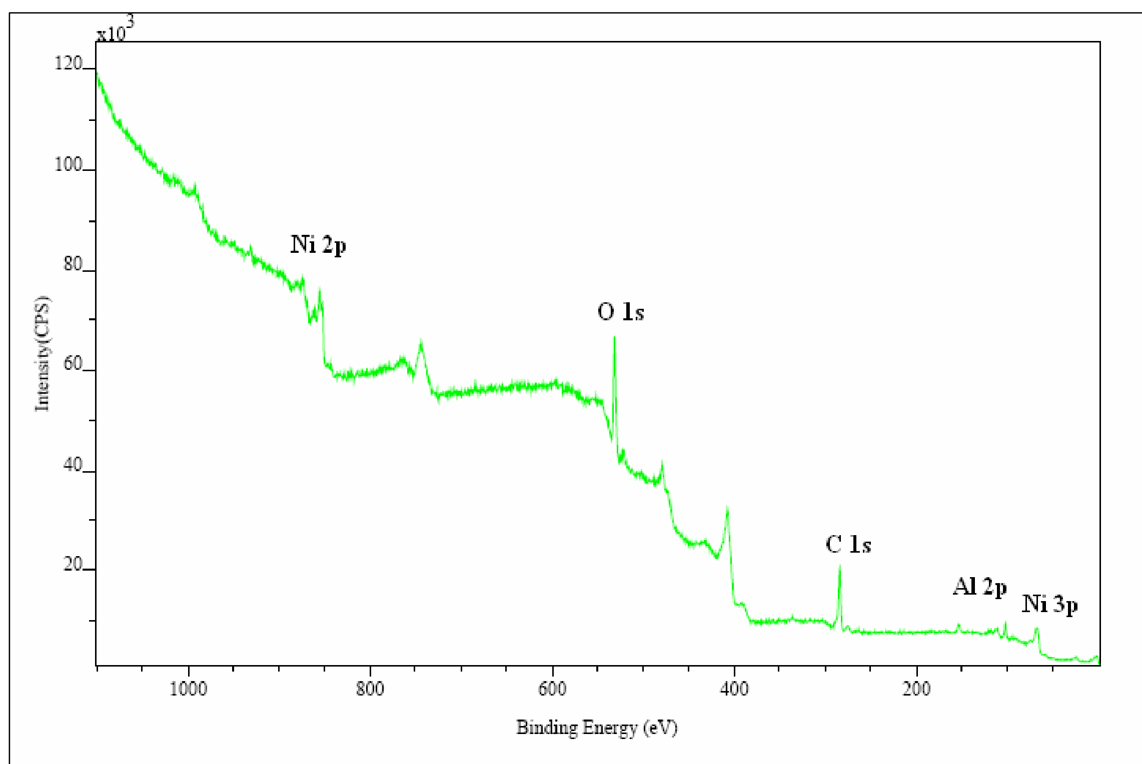

Fig. 7.1 Survey of Alumel Sample I. Ni 2p + Ni 3p (84.32%) and Al 2p (15.68%). (% Mass Concentration) (Source: Sinha *et al.* [32])

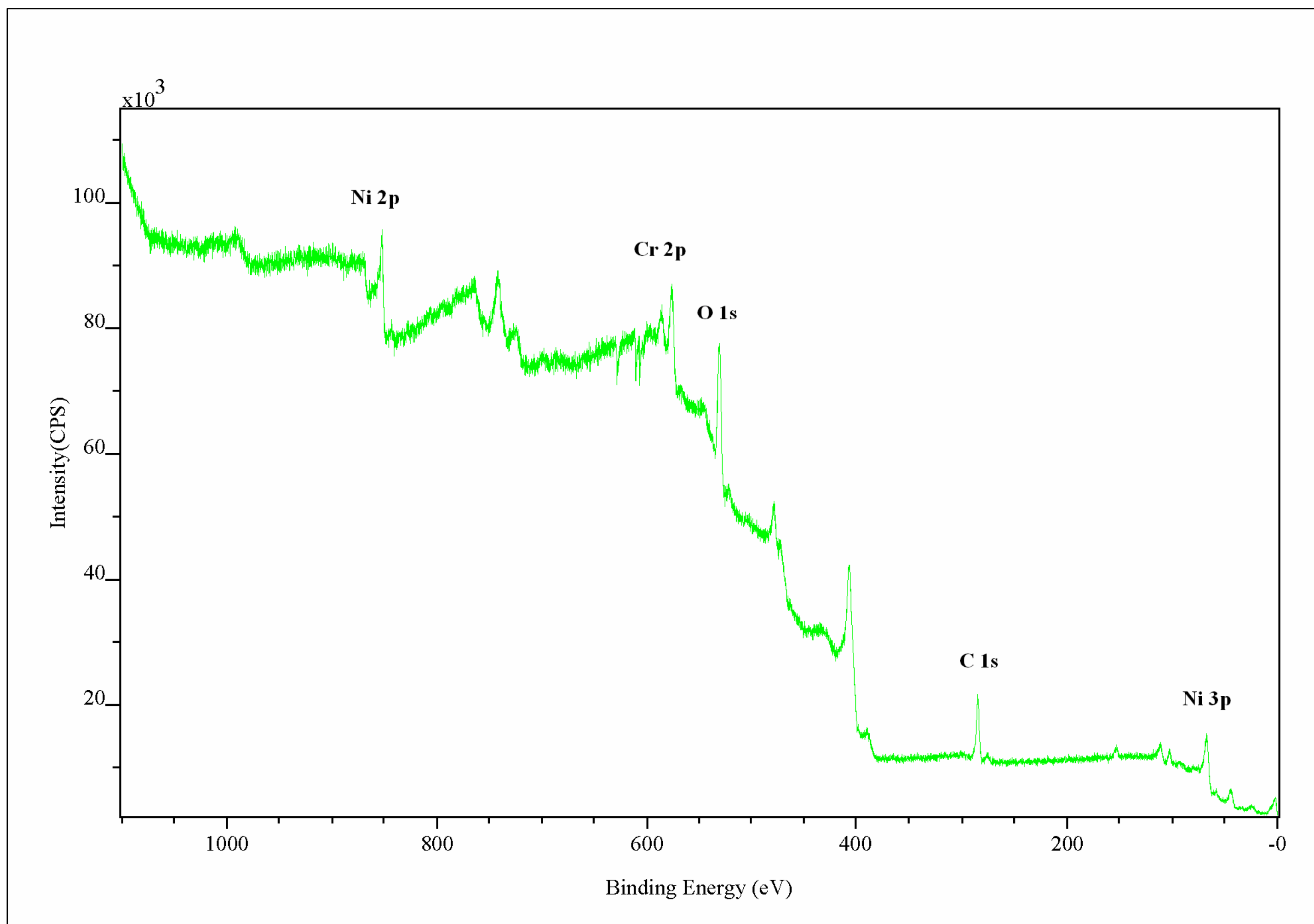

Fig. 7.2 Survey of a Chromel Sample I. Ni 2p + Ni 3p (80.8%) and Cr 2p (19.2%). (% Mass Concentration)

Table 7.1
Composition Analyses of TFT Layers (using XPS)

Alumel

	Atomic Concentration %		Mass Concentration %	
	Nickel	Aluminum	Nickel	Aluminum
Sample 1	66.52	33.47	81.22	18.77
Sample 2	71.17	28.82	84.32	15.68
Target	95	5	95	5

Chromel

	Atomic Concentration %		Mass Concentration %	
	Nickel	Chromium	Nickel	Chromium
Sample 1	78.85	21.15	80.8	19.2
Sample 2	76.4	23.6	78.52	21.48
Target	90	10	90	10

Table 7.1 shows the composition analyses of the thin film thermocouples component layers (Chromel and Alumel), measured using XPS. The measured values show that the composition of the deposited layers is significantly different from the composition of the target (reported by the manufacturer). These measurements show that the fabricated thin film thermocouples can potentially have a different thermoelectric response compared to conventional K-type thermocouples (used as the target material). Hence the thin film thermocouples were calibrated for temperature response using standard wire-beaded K-type thermocouples as reference under steady state conditions.

The figures 7.3-7.8 were generated from the XPS analysis. Figures 7.3-7.5 were generated by analysis of Alumel Sample. Figures 7.6-7.8 were generated by analysis of Chromel Sample.

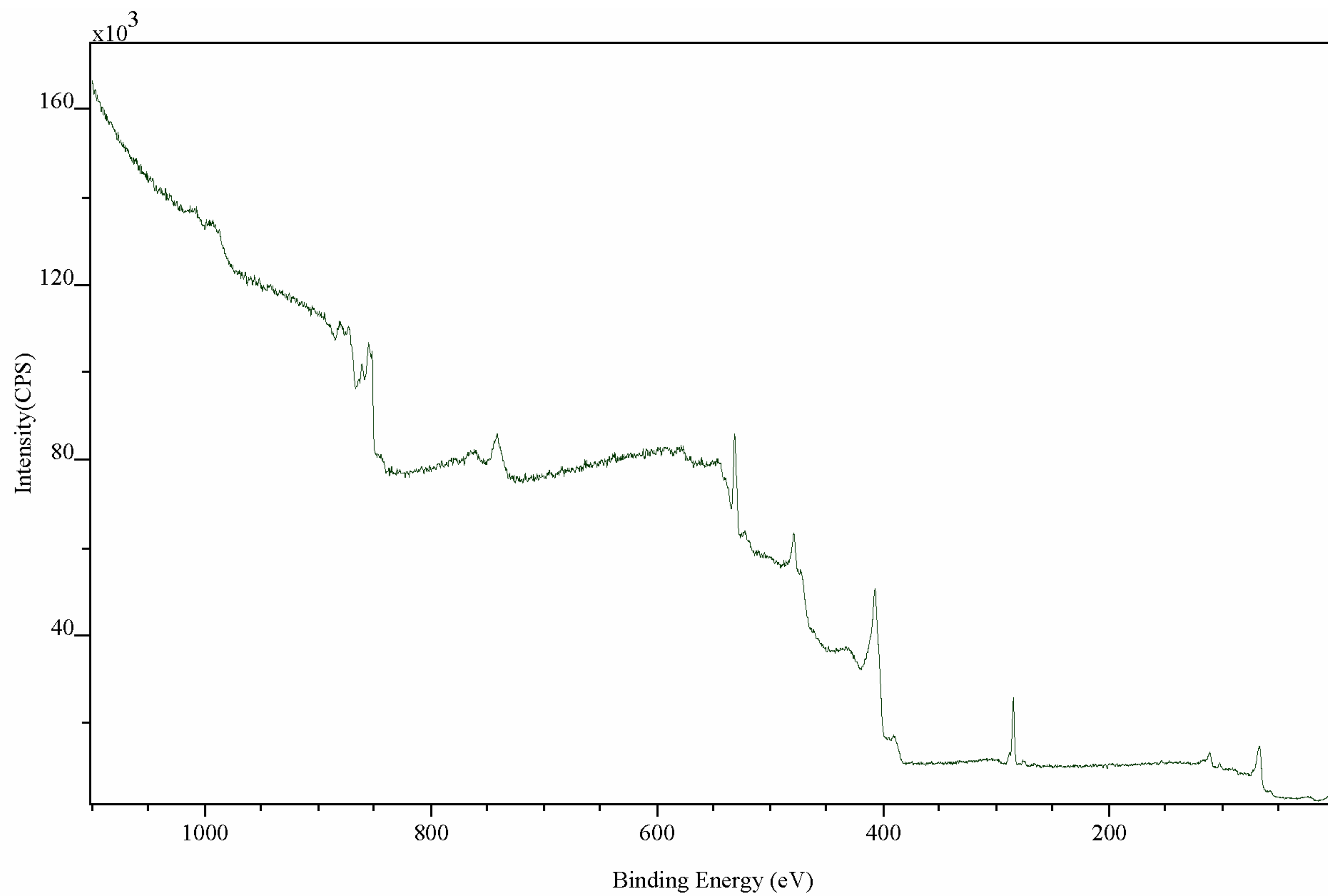

Fig. 7.3 Survey of the Alumel Sample II.

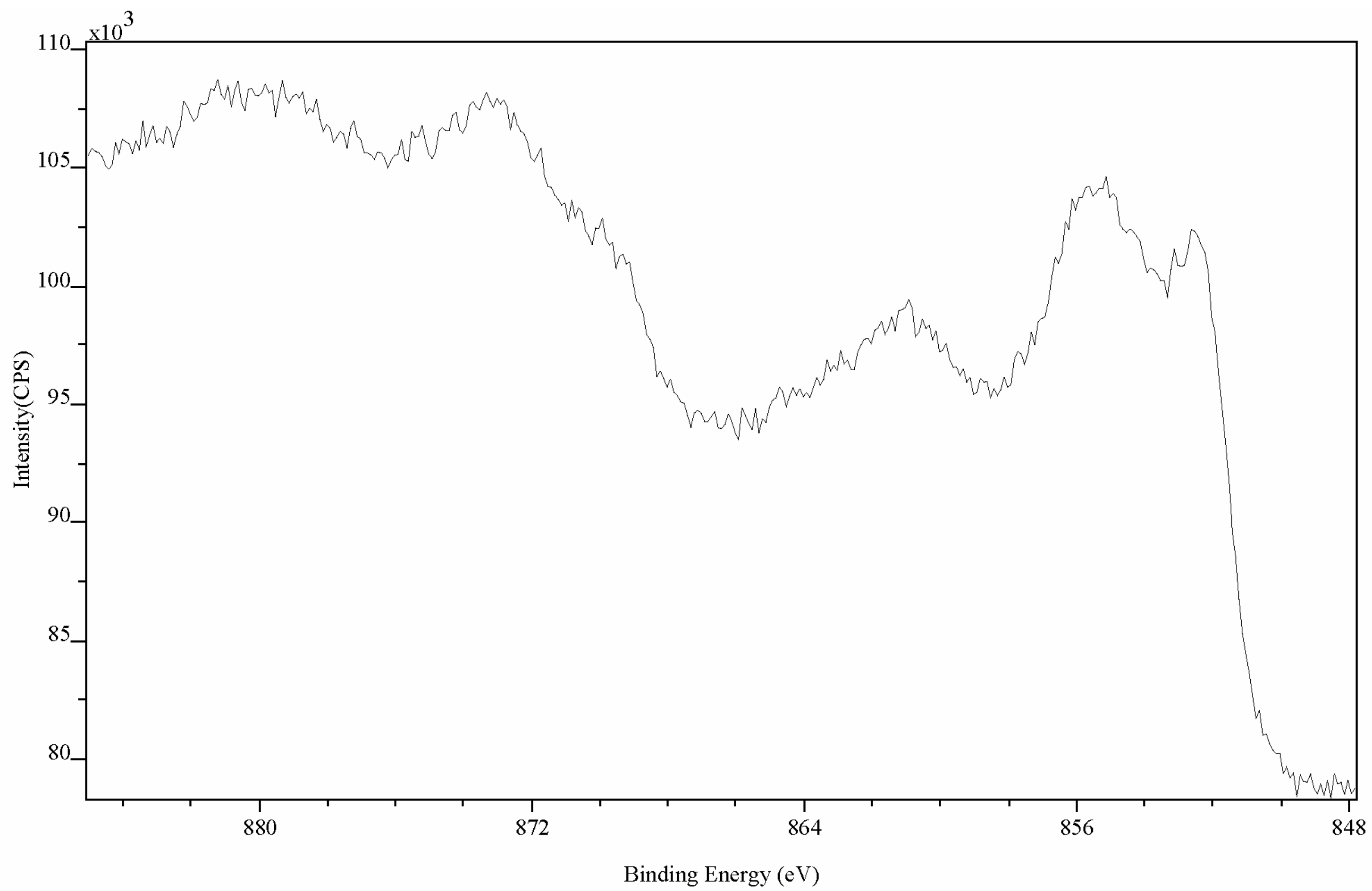

Fig. 7.4 Nickel Scan of Alumel Sample

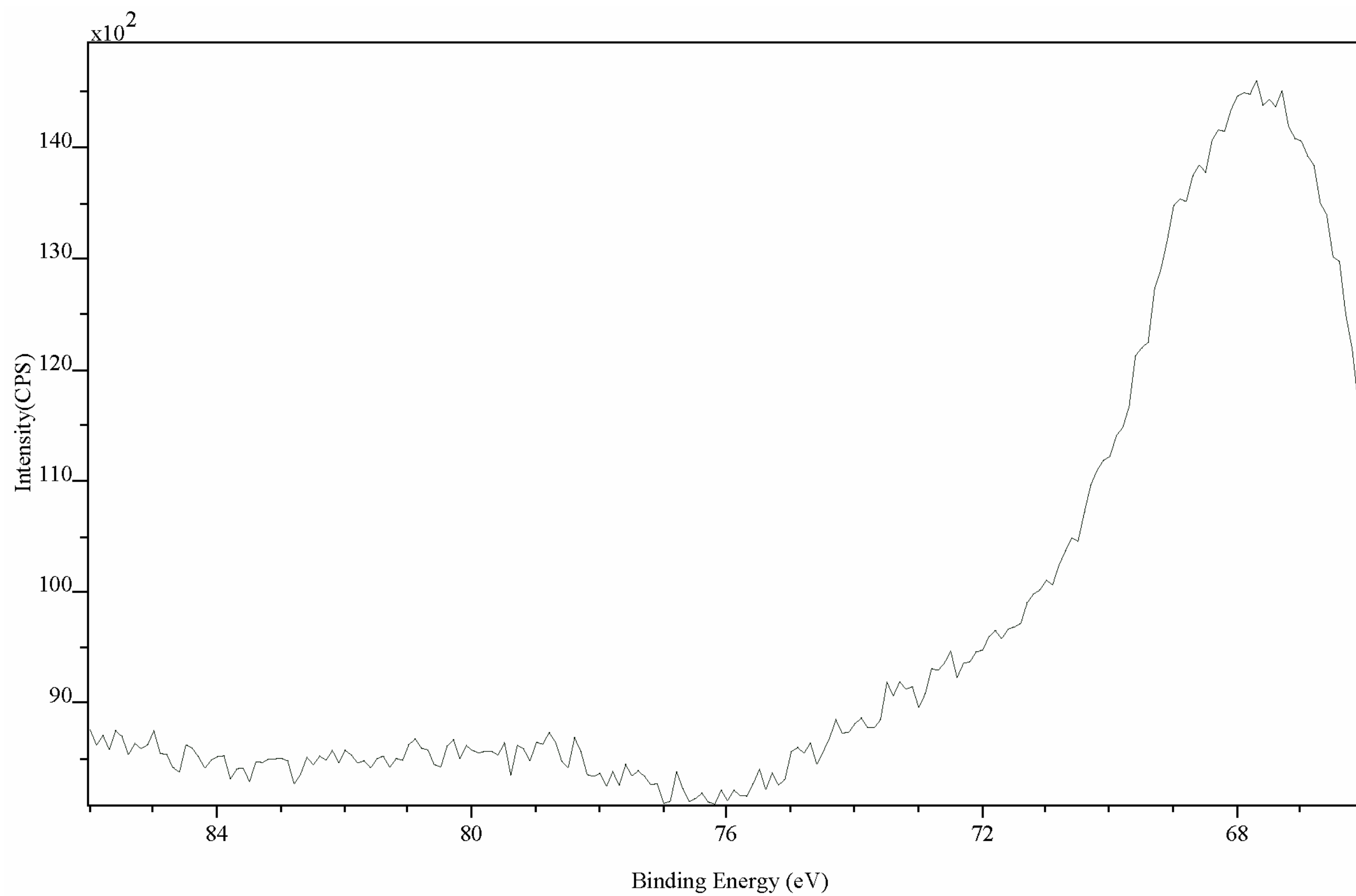

Fig. 7.5 Aluminum Scan of Alumel Sample

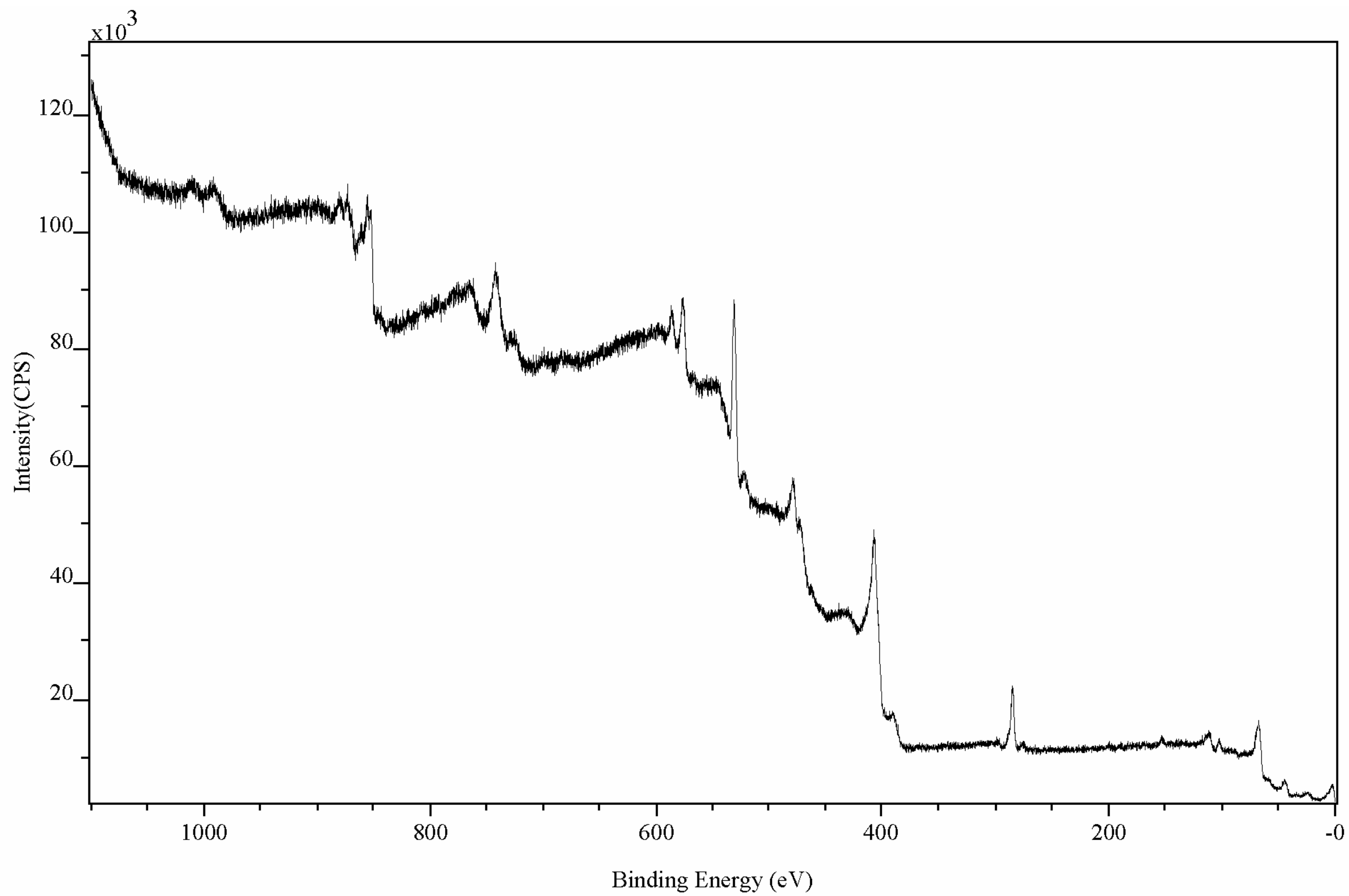

Fig. 7.6 Survey of Chromel Sample II.

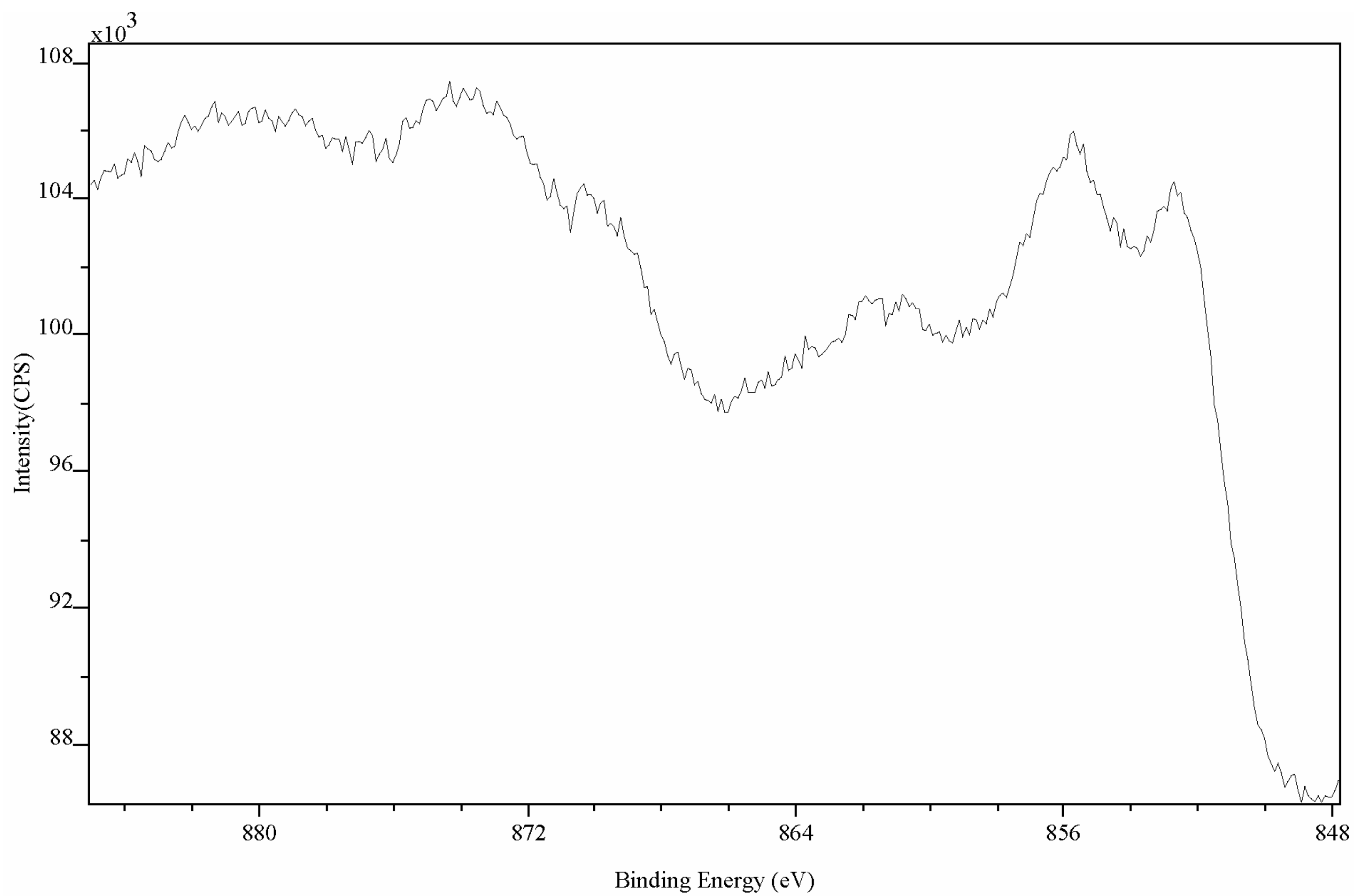

Fig. 7.7 Nickel Scan of Chromel Sample

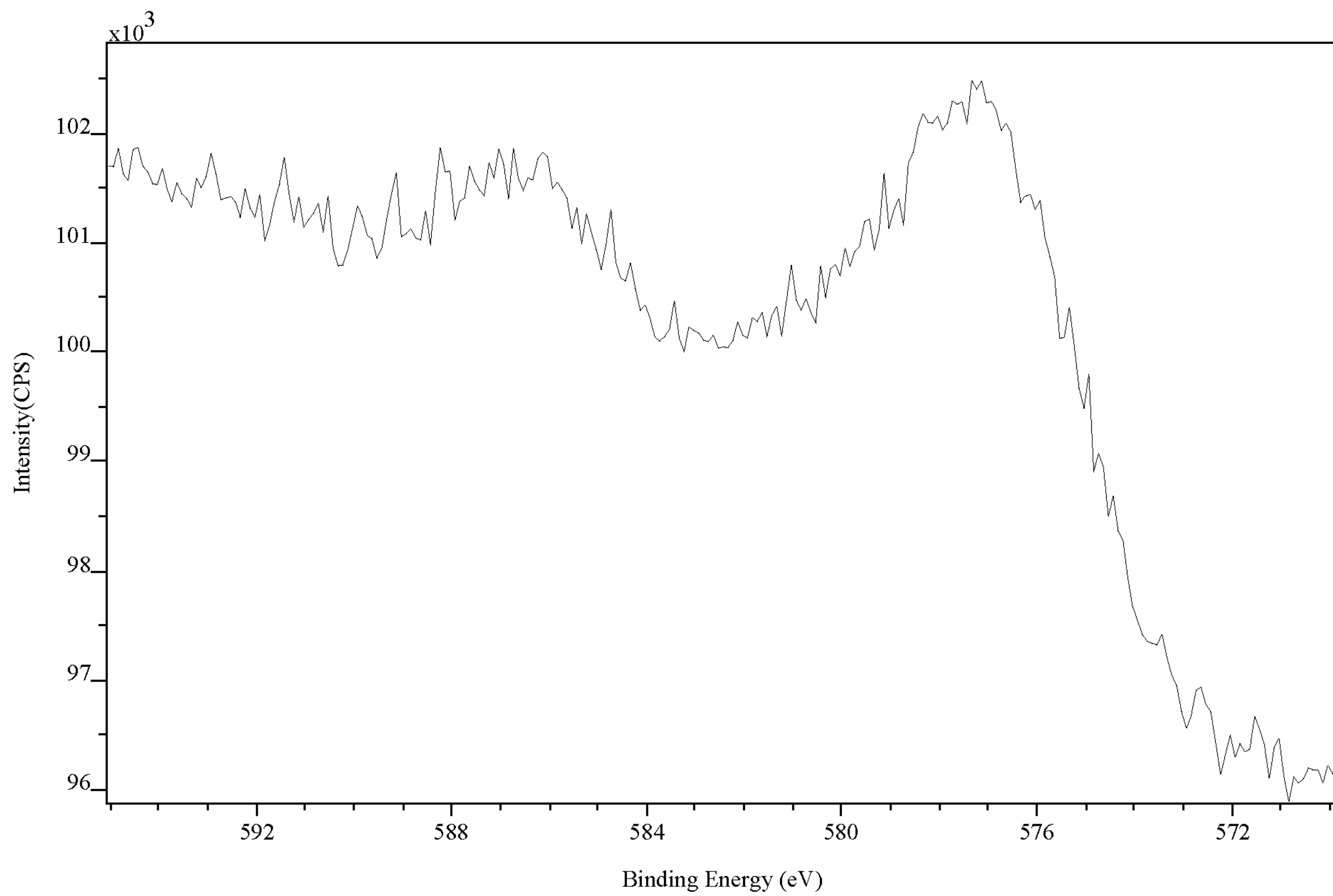

Fig. 7.8 Chromium Scan of Chromel Sample

7.1.2 Calibration Runs

The first calibration results were obtained from the thin film thermocouple packaged by wire bonding of Aluminum wire. These aluminum wires were connected to the alumel and chromel wires, for the corresponding bond pad. These alumel and chromel wires were connected to the data acquisition system.

Table 7.2
Results of Calibration of Thin Film Thermocouple Packaged by Wire Bonding

	Beaded Thermocouple	Micro Machined TFTC
0 Volts	26.67	41.51
5.01 Volts	38.25	49.62
9.7 Volts	62.94	65.89
15.04 Volts	103.89	94.42
18.84 Volts	135.37	115.62

Fig. 7.9 shows the calibration curve for the thin film thermocouples against a standard beaded thermocouple, when packaged using wire bonding. The slope of the calibration curve was 1.46. The major concern in this approach was the formation of a parasitic junction at the point of wire bonding. In this case, there exist three junctions instead of one. Junctions were formed by Alumel and Chromel, Alumel and Aluminum and Chromel

and Aluminum. To be able to compensate for the thermoelectric contribution of the two unwanted junctions, the junction temperatures were required. In typical multi-phase flow experiments these junction temperatures are unknown and therefore cannot be compensated for.

The results of the calibration run for the bent wire for resistance arc welding is as follows.

Table 7.3
Results of Calibration of Thin Film Thermocouple Using First Method of Resistance Arc Welding

	Beaded Thermocouple	Micro Machined TFTC
0 Volts	24.27	19.72
10 Volts	61.07	55.24
15 Volts	86.19	79.56
20 Volts	122.72	106.79
25 Volts	151.1	132.04

These results were plotted on a graph, Fig. 7.10. The temperatures of the thin film thermocouples are plotted on the x-axis and the temperatures obtained from the beaded thermocouples are plotted on the y-axis. The slope of the calibration plot is 1.14. The results of the calibration experiments for the second method of resistance arc micro welding (using combination of

thick and thin thermocouple wires) are shown in Table 7.4.

Table 7.4
Results of Calibration of Thin Film Thermocouple Using Second Method of Resistance Arc Welding

	Beaded Thermocouple	TFTC
0 Volt	23.85	19.04
5 Volts	31.37	27.38
10 Volts	50.47	46.87
15 Volts	81.49	75.16
22.5 Volts	137.45	133.78

The slope of the calibration plot is 1.0014 in Fig. 7.11. This is a definite improvement over the previous packaging methods which had a slope of 1.46 and 1.14.

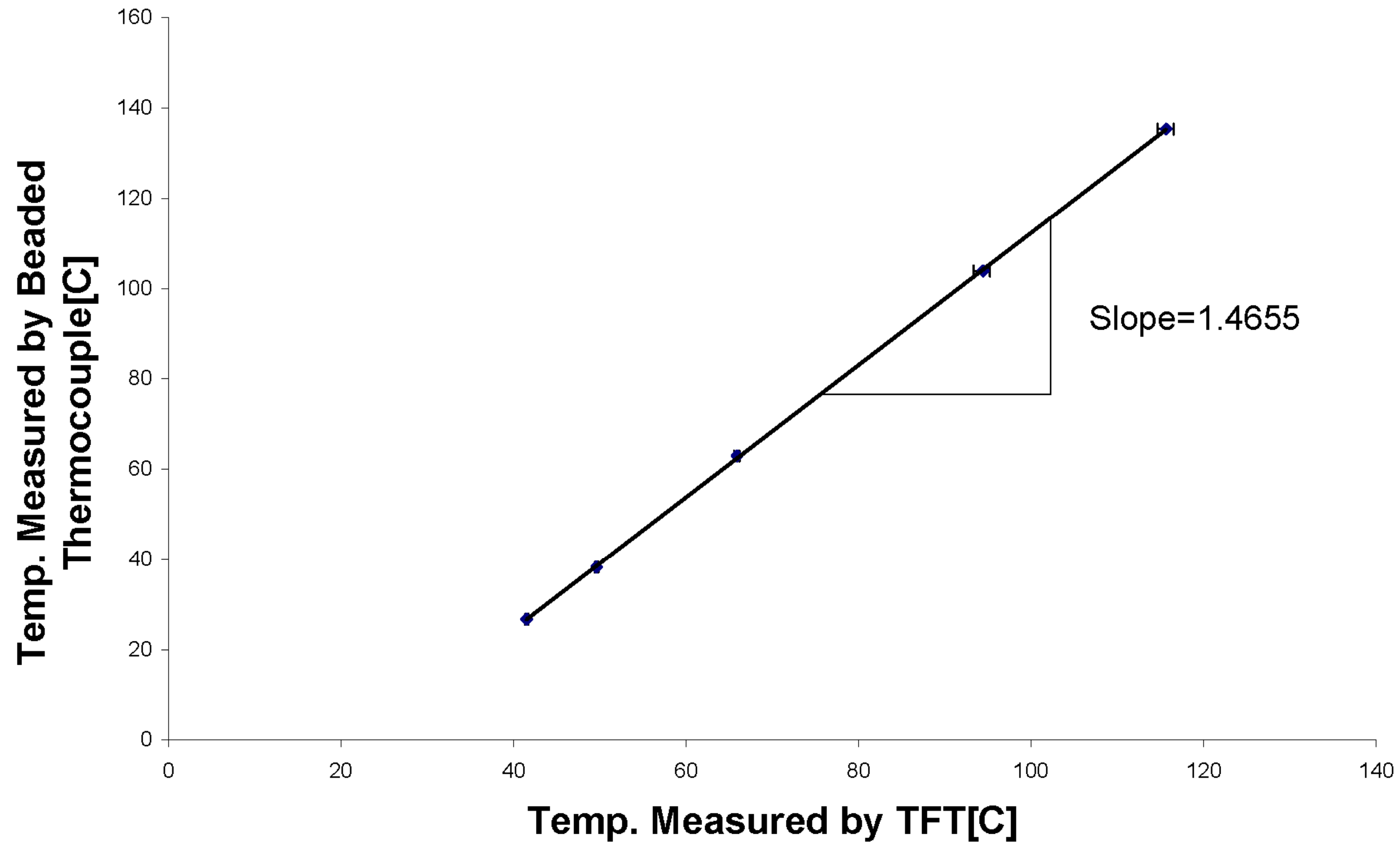

Fig. 7.9 Calibration Curve Obtained by Wire Bonding (Source: Sinha *et al.* [32])

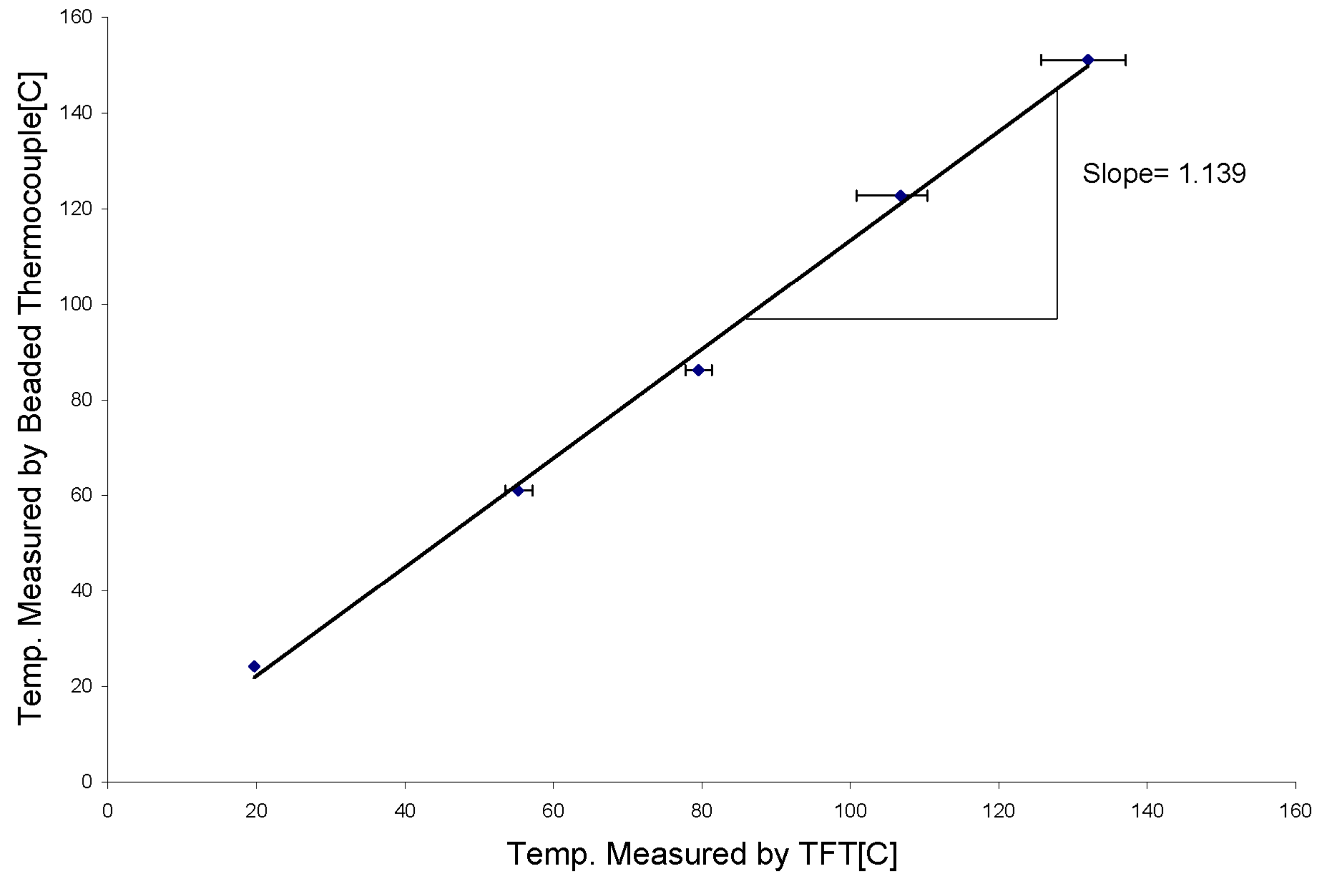

Fig. 7.10 Calibration Curve Obtained by the First Method of Resistance Arc Welding. (Source: Sinha *et al.* [32])

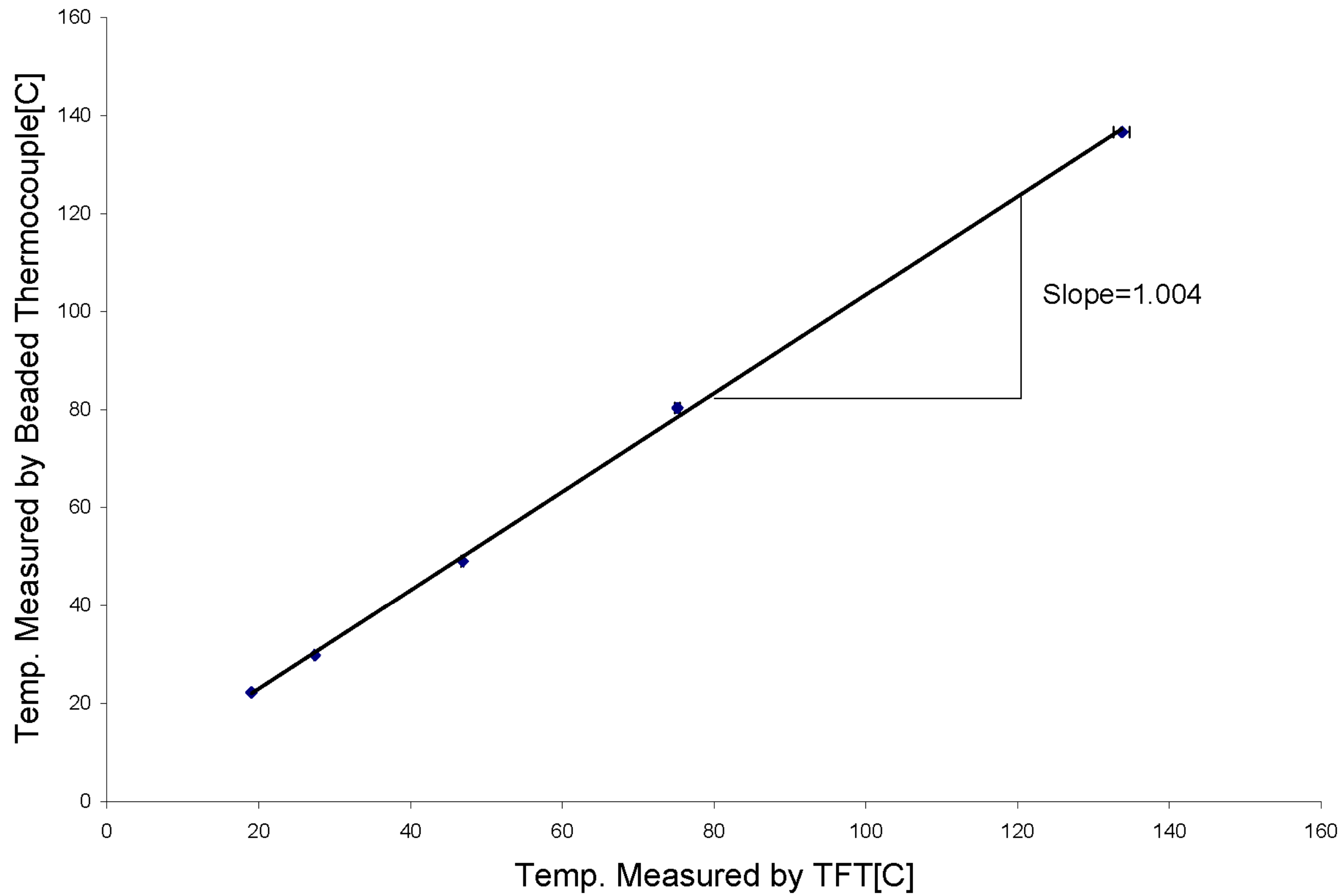

Fig. 7.11 Calibration Curve Obtained by Second Method of Resistance Arc Welding. (Source: Sinha *et al.* [32])

7.2 Boiling Experiments

Experiments were conducted in the viewing chamber using the wafers which had thin film thermocouples fabricated on them. Both Pyrex and silicon wafers were used for this testing and data for the surface temperatures during various boiling regimes was obtained. Using the data that was obtained from (1) the thin film thermocouples, (2) the thermocouples placed in the copper block and (3) the thermocouple placed in the liquid to measure the bulk temperature, the heat flux values were calculated. The following data (Table 7.5) was obtained from an experiment conducted using a Pyrex wafer.

Table 7.5
Data Obtained from the Pyrex Wafer Experiment

Wall Superheat (T_w-T_{sat}) (˚C)	4.68	15.78	16.09	18.80	21.38	23.81	27.12
Temperature of top of Copper Block ($T_{Cu,top}$) (˚C)	63.3	92.11	104.1	120.5	136.29	152.12	175.14
Temperature of top Silicon Wafer (T_w) (˚C)	60.6	71.78	72.09	74.80	77.38	79.81	83.12
Difference ($T_{Cu,top}$-T_w) (˚C)	2.63	20.33	32.06	45.71	58.91	72.31	92.02

As the wall superheat increases the difference in temperature between the top of the copper block and the silicon wafer surface also increases. Table 7.6 shows the Heat Flux and Heat Transfer Coefficient values, calculated using the method and formulas explained in Chapter VI.

Table 7.6
Heat Flux and Heat Transfer Coefficient Calculation from Thermocouple Data

Wall Temp (T_w) (˚C)	Wall Superheat (T_w-T_{sat}) (˚C)	Heat Flux (q”) (W/m^2)	Heat Transfer Coefficient (h) (W/m^2˚C)
60.68	4.68	2250	480
71.78	15.78	10756	681
72.09	16.09	16948	1053
74.80	18.80	25212	1340
77.38	21.38	33509	1567
79.81	23.81	41429	1739
83.12	27.12	51996	1916

As the wall superheat increases, the value of both the heat flux and the heat transfer coefficient should increase and this is what the data shows. Fig. 7.12 and Fig. 7.13 show a log-log plot of the heat flux and heat transfer coefficient values on the y-axis plotted against wall superheat on the x-axis. The heat transfer coefficient increases from 480 W/m^2˚C (at wall superheat 4.68˚C) to 1961 W/m^2˚C (at wall superheat 27.12˚C). The heat flux increases

from 1.08×10^4 W/m^2 (at 15.78˚C wall superheat) to 5.1×10^4 W/m^2 (at 27.12˚C wall superheat). The thermal resistance between the copper block and the wafer was also calculated. Table 7.7 shows the thermal resistance and rate of heat transfer data for the exposed area of the wafer in boiling.

Table 7.7
Thermal Resistance and Rate of Heat Transfer Values

Wall Superheat (T_w-T_{sat}) (˚C)	**Heat Flux (q") (W/m^2)**	**Temperature of the top of Copper Block ($T_{cu,top}$) (˚C)**	**Rate of Heat Transfer (Q) (W)**	**Thermal Resistance (R) (˚C/W)**
4.68	2250	63.32	7.13	0.37
15.78	10756	92.11	34.06	0.60
16.09	16948	104.16	53.67	0.60
18.80	25212	120.51	79.85	0.57
21.38	33509	136.29	106.12	0.56
23.81	41429	152.13	131.20	0.55
27.12	51996	175.15	164.67	0.56

The thermal resistance accounts for a thermal path covering a distance of nearly 1.5mm between the top of the copper block and the top of the silicon wafer. The cross sectional view of the gap between the two surfaces is shown in Fig. 4.8 in Chapter IV. The thermal resistance increases initially and then decreases as the wall superheat is increased. One possible explanation for this decrease in thermal resistance is the increase in

pressure between the surfaces because of the different thermal expansion coefficients of the materials that held them together, that is copper and stainless steel. The differential expansion might bring the two surfaces closer together and this would decrease the contact resistance between the two surfaces. Fig. 7.14 shows the thermal resistance values for the experiment.

A Kline and McClintock uncertainty analysis was performed for the data, as explained in Chapter VI. The uncertainty percentage in the heat flux decreased as the wall superheat was increased. The value of the uncertainty remained nearly same for the heat flux but as a percentage it decreased to nearly ±7.5% of the heat flux value (at 27.12°C wall superheat). For the heat transfer coefficient the uncertainty decreased to nearly ±7.6% of the value at 27.12°C wall superheat.

Fig. 7.15 shows pictures of various stages of boiling taken at steady state values during the experiment.

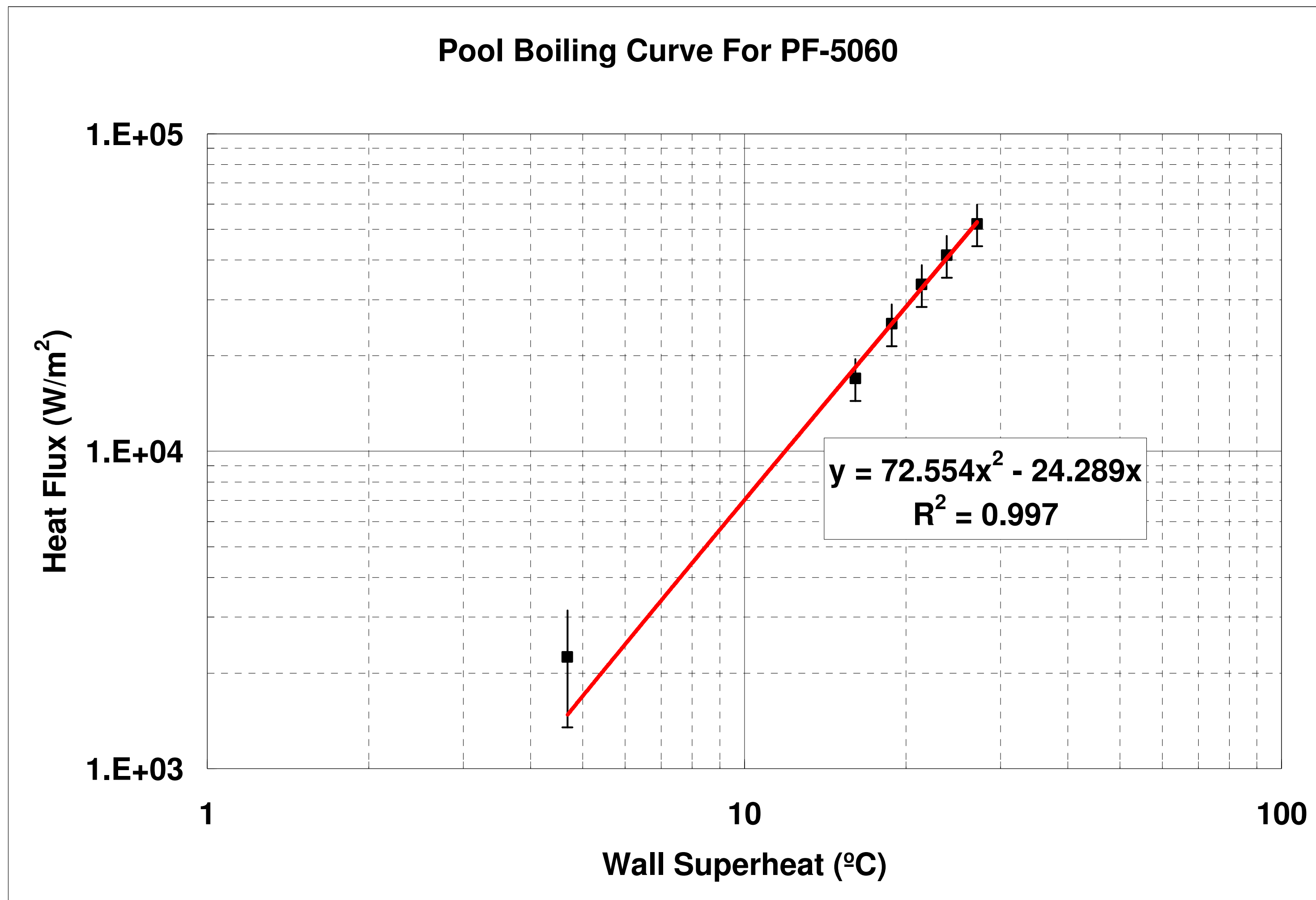

Fig. 7.12 Log-Log Curve Showing Heat Flux Values. (Source: Sinha *et al.* [32])

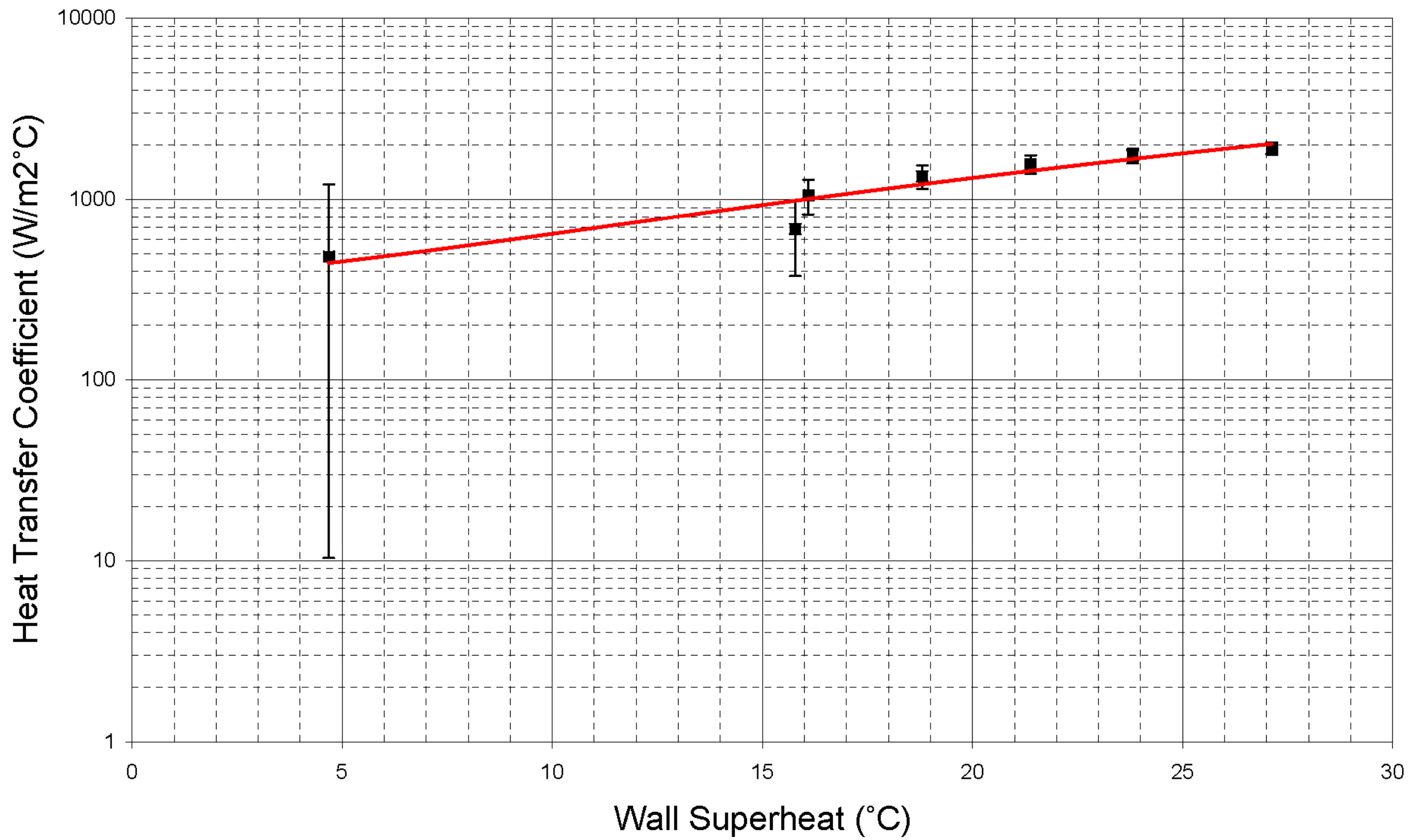

Fig. 7.13 Curve Showing the Heat Transfer Coefficient.

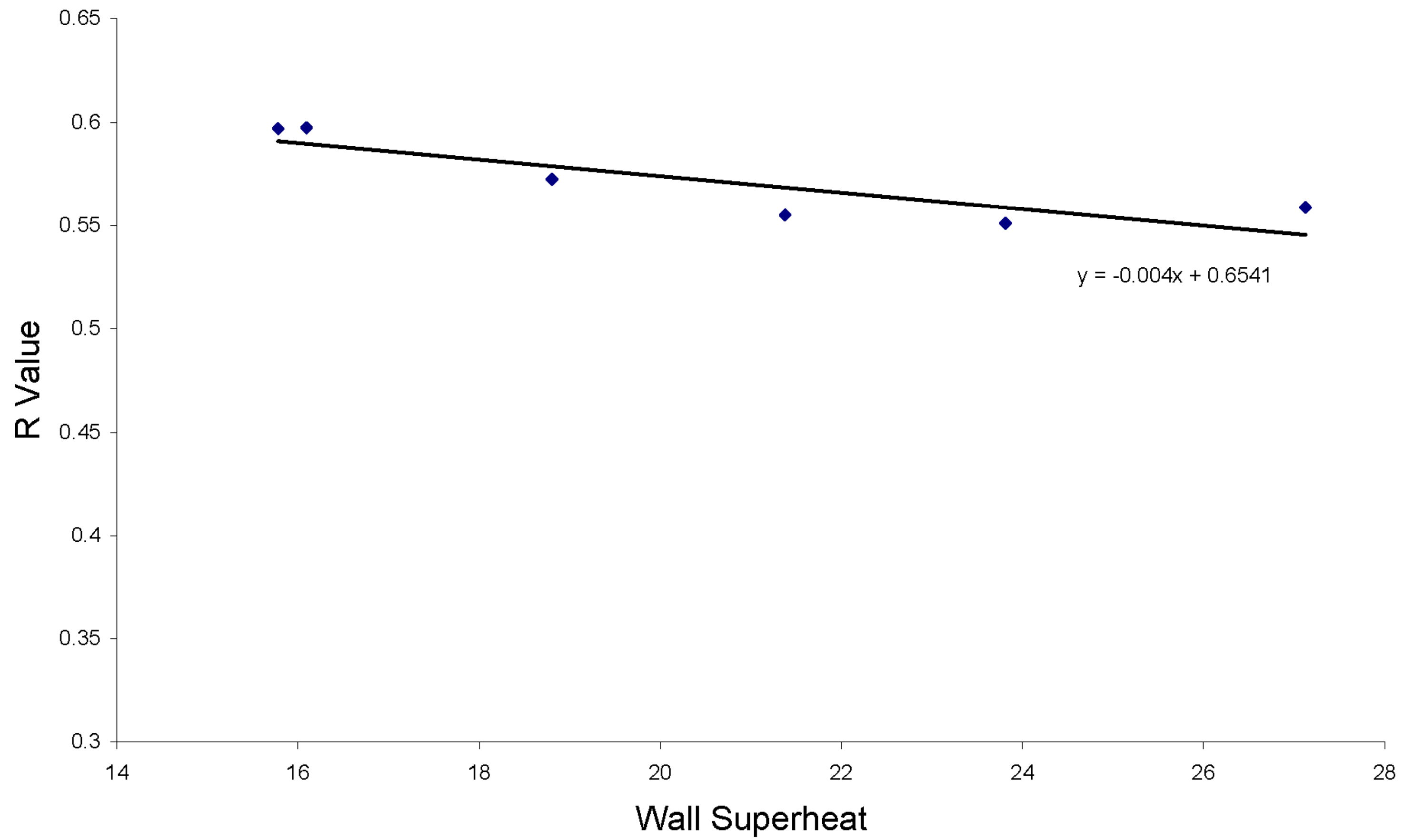

Fig. 7.14 Curve Showing the Thermal Resistance Values.

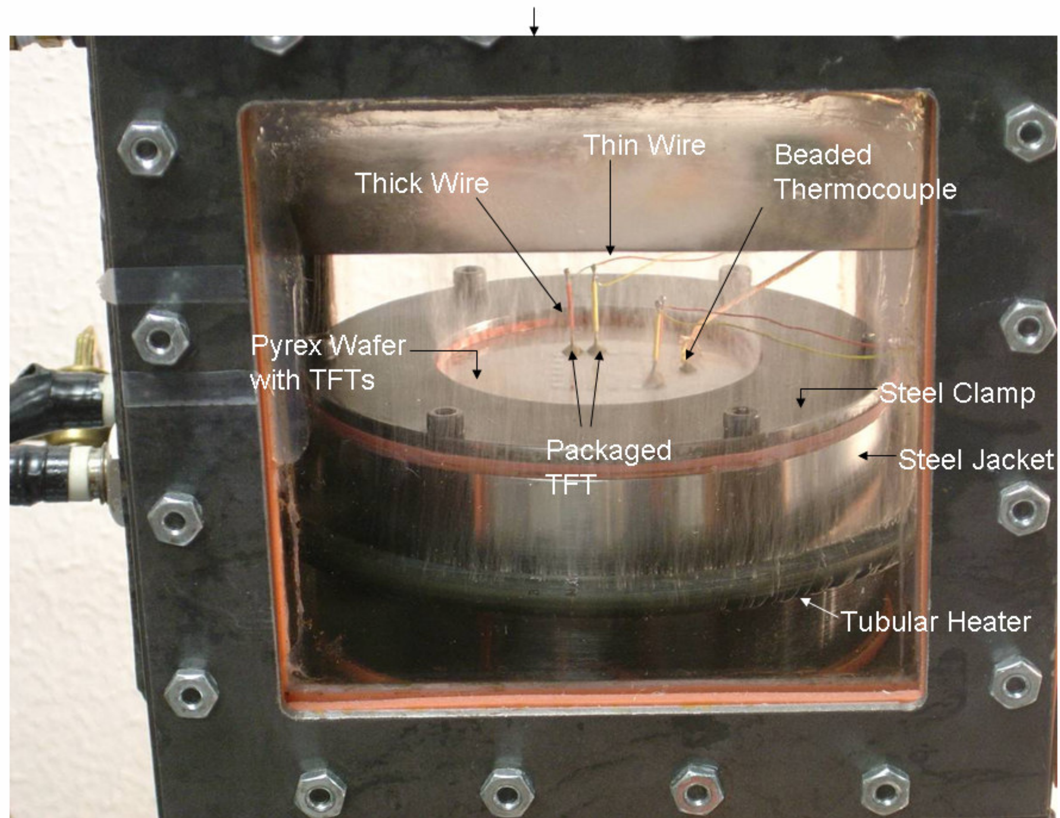

(a) At Saturation temperature (56 ˚C)

Fig. 7.15 Pictures of the Apparatus Showing Stages of Boiling at Various Superheats.

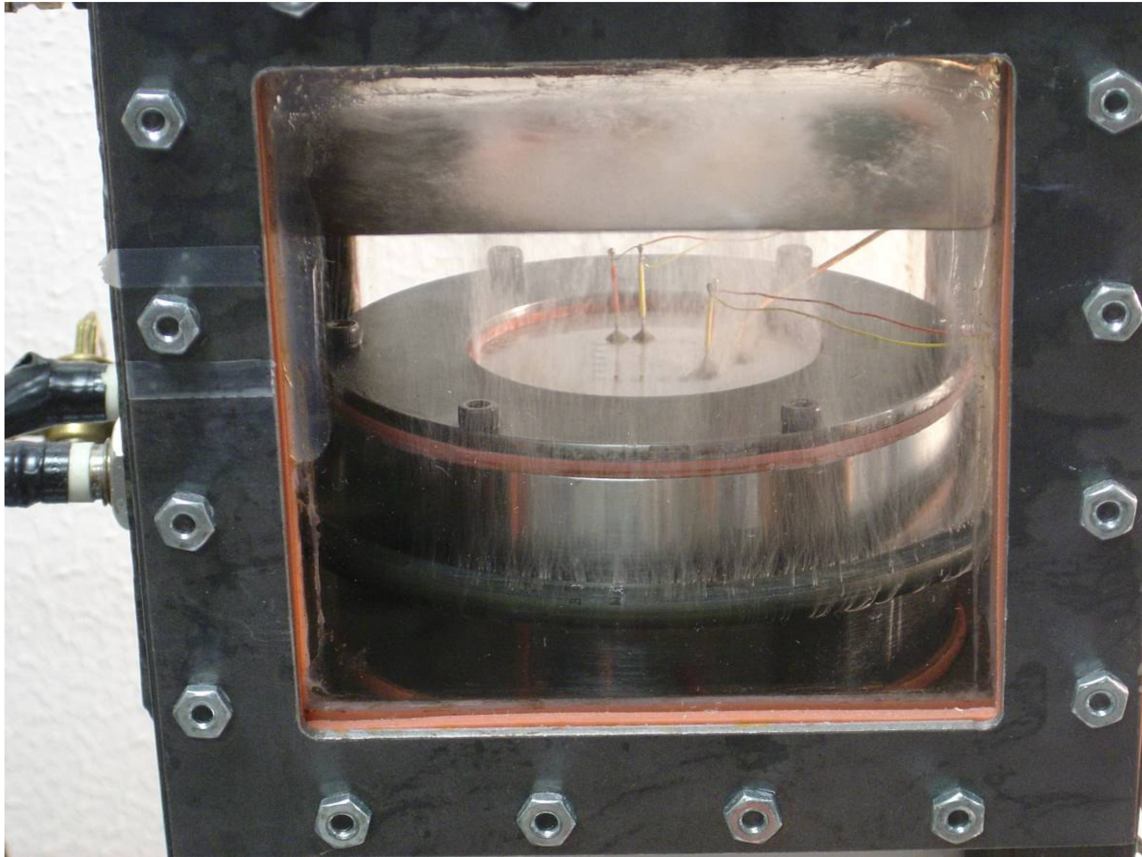

(b) At 4.7˚C Wall Superheat.

Fig. 7.15 Continued.

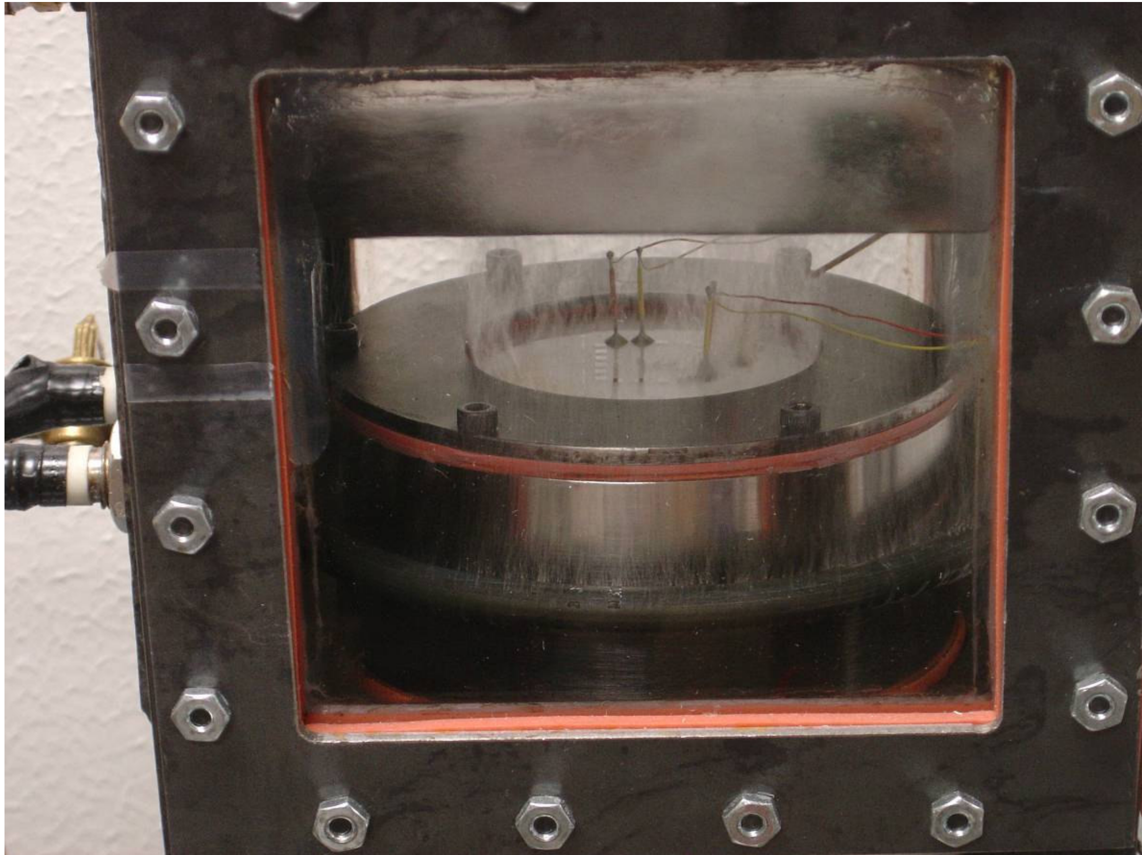

(c) At 15.8˚C Wall Superheat.

Fig. 7.15 Continued.

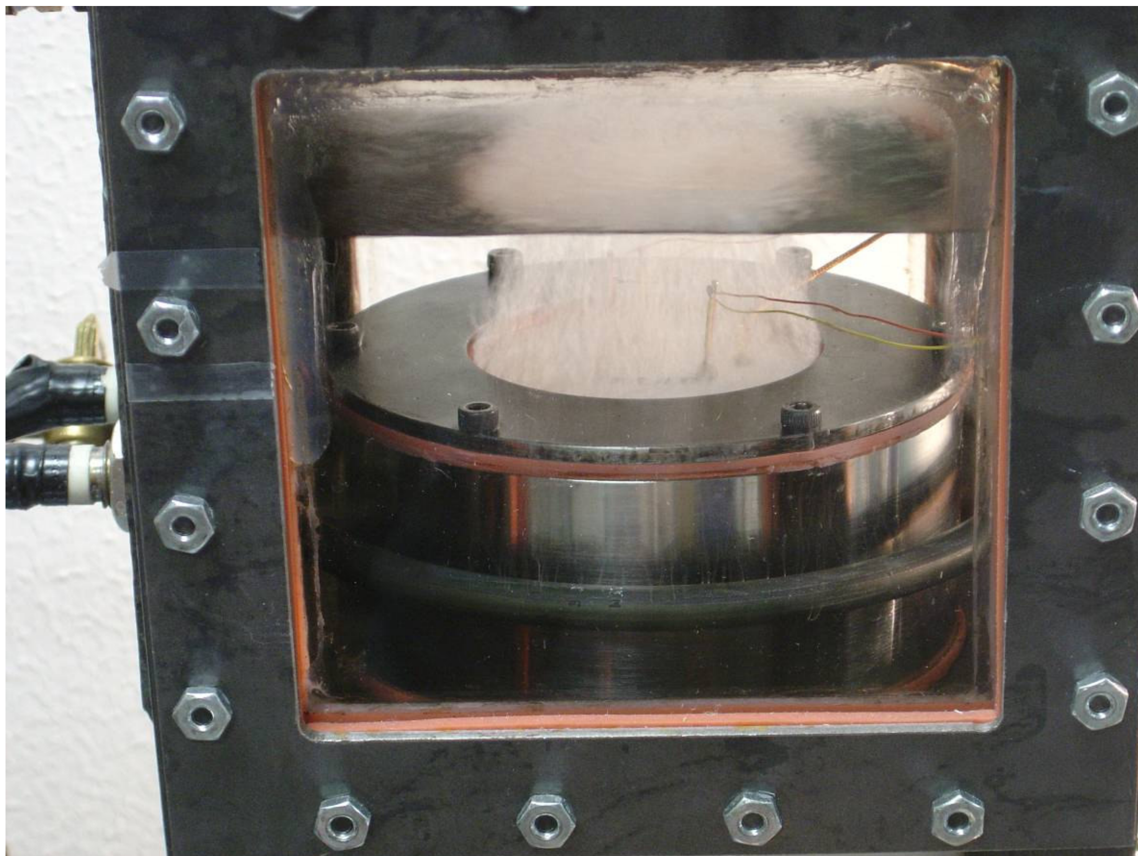

(d) At 16.1˚C Wall Superheat.

Fig. 7.15 Continued.

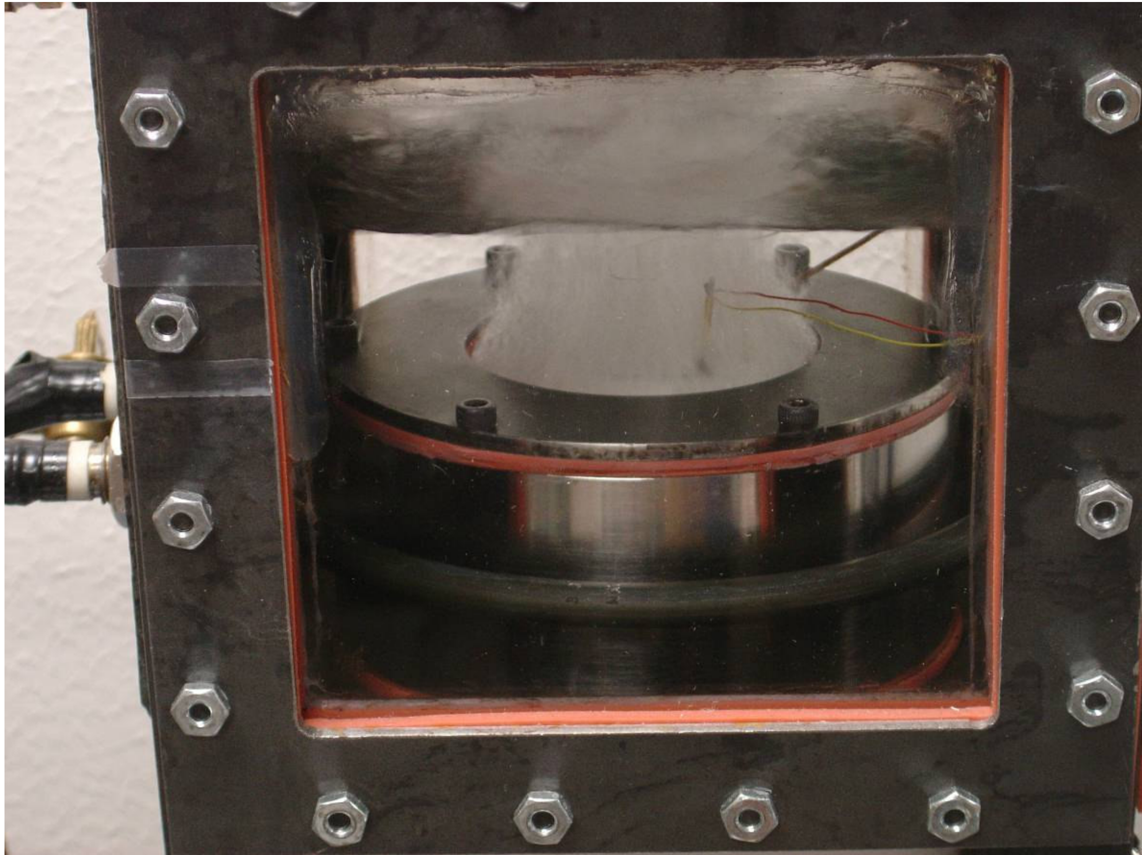

(e) At 18.8 ˚C Wall Superheat.

Fig. 7.15 Continued.

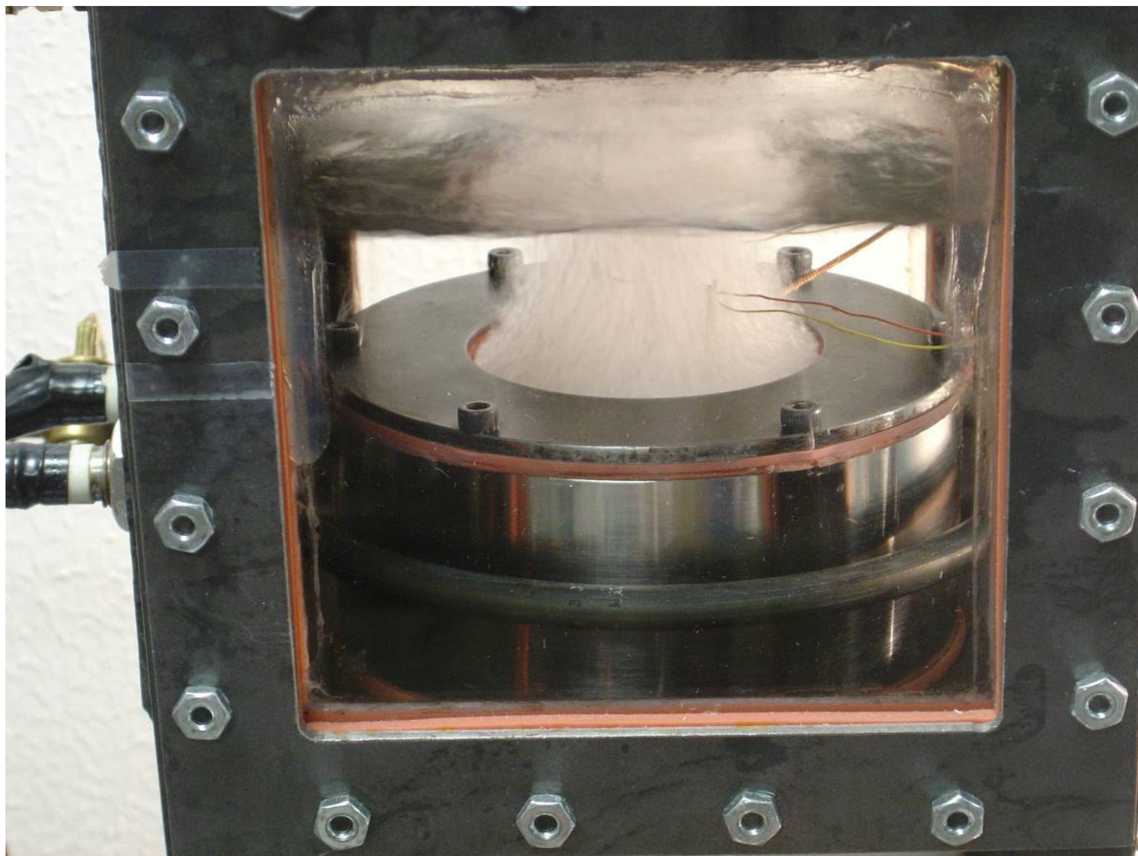

(f) At 21.4˚C Wall Superheat.

Fig. 7.15 Continued.

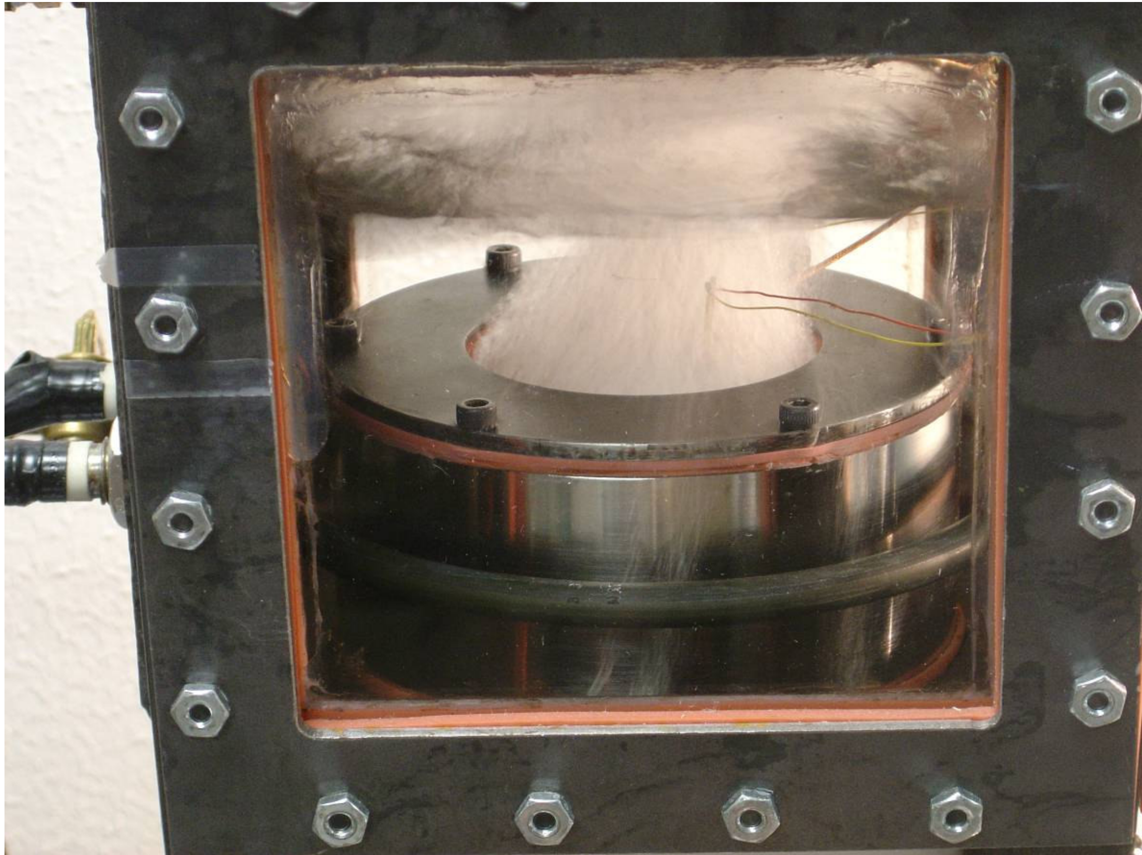

(g) At 23.8 ˚C Wall Superheat.

Fig. 7.15 Continued.

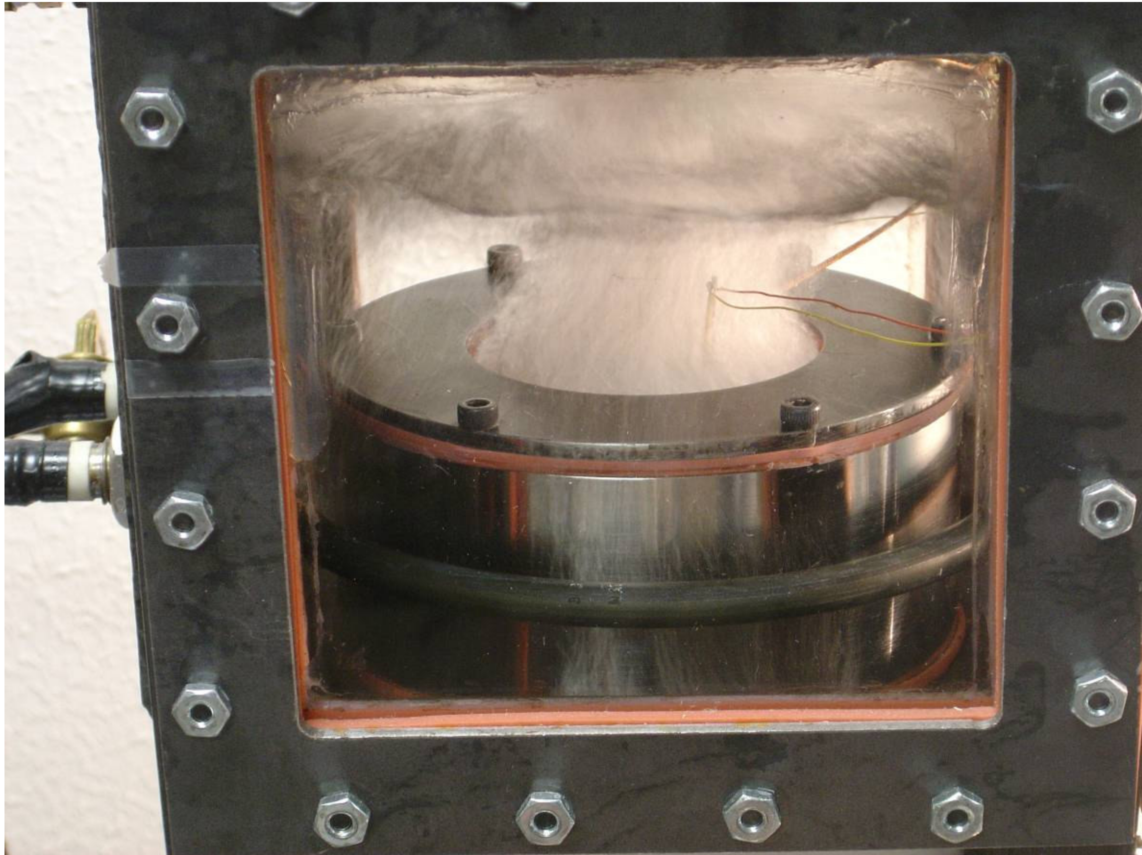

(h) At 27.1 ˚C Wall Superheat.

Fig. 7.15 Continued.

CHAPTER VIII

CONCLUSIONS

Thin film thermocouples were successfully fabricated and tested. Boiling experiments were conducted using these thin film thermocouples:

I. Calibration of the thin film thermocouples showed that there exists a linear relationship between the temperature of the thin film thermocouples and a standard K-Type thermocouple.

II. Various methods were explored for packaging. Finally, it was concluded that resistance arc micro welding of thermocouple wires to the bond pads provided better results compared to wire bonding of aluminum.

III. In welding, better bond strength of the wire was achieved by bending the tip of the wire to get multiple arcs and a larger melt zone. However, a setup using two different diameter wires was found to give the best performance.

IV. Thin film thermocouples were used to monitor and analyze surface temperature variations and fluctuations during various boiling regimes with better temporal resolution.

The procedure used for the microfabrication of thin film thermocouples has been described in Chapter II.

The major parameters that used to be given special attention during microfabrication are:

I. Over Exposure: Over exposure at the time of photolithography has been used. This does not affect the size of the features significantly and enables the formation of a conducive photoresist profile that facilitates in the lift-off process.

II. Oxygen Plasma Cleaning: This step helps to remove the residual photo resist. This step also helped in getting a good lift-off.

III. Base Layer of Chromium: The use of chromium adhesion layer of 5nm to 20nm before the deposition of Alumel or Chromel helped to enhance the yield of the thin film thermocouple in the chosen microfabrication process.

REFERENCES

1. Hirth, J. P., Hruska, S. J. and Pound, G. M., 1964, "Theory of Nucleation in Deposition on Substrates," *Single Crystal Films*, M. Francombe and H. Sato eds., Pergamon Press, New York, pp. 9-29.
2. Lewis, B., 1967, "Bond Energy Formulations of Heterogeneous Nucleation Theory," Thin Solid Films, **1**(2), pp. 85-107.
3. Sigsbee, R.A. and Pound, G.M., 1967, "Heterogeneous Nucleation from the Vapor," Advan. Colloid Interface Sci., **1**(3), pp.335-390.
4. Rhodin, T. and Walton, D., 1964, "Nucleation of Oriented Films," *Single Crystal Films*, M. Francombe and H. Sato eds., Pergamon Press, New York, pp.31-41.
5. Thompson, C. V., 1990, "Grain Growth in Thin Films," Annual Review of Materials Science, **20**, pp. 245-268.
6. Thompson, C. V., 2000, "Structure Evolution during Processing of Polycrystalline Films," Annual Review of Materials Science, **30**, pp. 159-190.
7. Sato, H., 1972, "Film Growth," Annual Review of Materials Science, **2**, pp. 217-252.
8. Maissel, L.I. and Glang, R., 1970 (Reissue 1983), *Handbook of Thin Film Technology*, McGraw Hill, New York.

9. “Thin and Thick,” 1968, Thin Solid Films, **2**(5-6), pp. 375. (http://www.sciencedirect.com/science/article/B6TW0-46PB4WF-23X/2/55c537d911f8b987be688c61a0e93897)

10. Editorial Statement, 1967, Thin Solid Films, **1**(1), pp. 1-2. (http://www.sciencedirect.com/science/article/B6TW0-46NYBS5-15V/2/67d3452c6f6f0f3933099f42d694a238).

11. Leaver, K.D. and Chapman, B.N., 1971, *Thin Films*, Wykeham Publications, London,.

12. Kay, E., 1971, “Solid Thin Films,” Annual Review of Materials Science, **1**, pp. 289-312.

13. Yaffe, L., 1962, “Preparation of Thin Films, Sources, and Targets,” Annual Review of Nuclear Science, **12**, pp. 153-188.

14. Monteiro, O. R., 2001, “Thin Film Synthesis in Energetic Condensation,” Annual Review of Materials Research, **31**, pp. 111-137.

15. Heavens, O.S., 1970, *Thin Film Physics*, Methuen & Co. Ltd. and Science Paperbacks, London.

16. Berry, R.W., Hall, P.M. and Harris, M.T., 1968, *Thin Film Technology*, D. Van Nostrand Company, Inc., Princeton,NJ.

17. Harris, L. and Johnson, E.A., 1934, “The Technique of Sputtering Sensitive Thermocouples,” Review of Scientific Instruments, **5**(4), pp. 153-158.

18. Marshall, R., Atlas, L. and Putner, T., 1966, "The Preparation and Performance of Thin Film Thermocouples," J Sci. Instrum., **43**, pp 144-149.

19. Bullis, L.H., 1963, "Vacuum-Deposited Thin-Film Thermocouples for Accurate Measurement of Substrate Surface Temperature," J Sci. Instrum., **40**(12), pp. 592-593.

20. Assanis, D. N. and Friedmann, F. A., 1993, "A Thin Film Thermocouple for Transient Heat Transfer Measurements in Ceramic-Coated Combustion Chambers," Int. Comm. Heat Mass Transfer, **20**, pp. 458-468.

21. Debey,D., Bluhm, R., Habets, N. and Kurz, H, 1997, "Fabrication of Planar Thermocouples for Real-Time Measurements of Temperature Profiles in Polymer Melts," Sensors and Actuators, **A 58**, pp. 179-184.

22. Tian, X., Kennedy,F. E., Deacutis, J. J. and Henning, A. K., 1992, "The Development and Use of Thin Film Thermocouples for Contact Temperature Measurement," Tribology Transactions, **35**, pp. 491-499,.

23. Laugier, M., 1980, "The Construction and Use of Thin Film Thermocouples for the Measurement of Surface Temperature: Applications to Substrate Temperature Determination and Thermal Bending of a Cantilevered Plate during Film Deposition," Thin Solid Films, **67**, pp. 163-170.

24. Chu, D., Bilir , D. T., Pease, R. F. W. and Goodson, K. E., 2003, "Thin Film Nano Thermocouple Sensors for Application in Laser and Electron Beam Irradiation," *Transducers '03, The 12th International Conference on Solid State Sensors, Actuators and Microsystems*, Boston, pp. 1112-1115.

25. Chu, D., Bilir , D. T., Pease, R. F. W. and Goodson, K. E., 2002, "Submicron Thermocouple Measurements of Electron-Beam Resist Heating," J. Vac. Sci. Technology, **B20**(6), pp. 3044-3046.

26. Park, J. J., and Taya, M., 2005, "Design of Micro-Temperature Sensor Array with Thin Film Thermocouples (TFTC)," J. of Electronic Packaging, **127**, pp. 286-289.

27. Kreider, K.G. and DiMeo, F. 1998, "Platinum/palladium Thin-Film Thermocouples for Temperature Measurements on Silicon Wafers," Sensors and Actuators, **A69**, pp. 48-52.

28. Kreider, K.G. and Gillen, G., 2000, "High Temperature Materials for Thin-Film Thermocouples on Silicon Wafers", Thin Solid Films, **376**, pp. 32-37.

29. Holanda, R., Kim, W.S., Pencil, E., Groth, M. and Danzey, G.A., 1990, "Attachment of Lead Wires to Thin Film Thermocouples Mounted on High Temperature Materials Using the Parallel Gap Welding

Process," *177th Meeting of the Electromechanical Society*, Quebec, NASA TM 102442.

30. Zupan, M., Hayden, M. J., Boehlert, C. J. and Hemker, K. J., 2001, "Development of High Temperature Microsample Testing," Experimental Mechanics, **41**(3), pp. 242-247.

31. Ahn, H. S., Sinha, N. and Banerjee, D., "Study of Spectral Response of Surface Temperature Fluctuation in Pool Boiling Using Surface Micro-Machined Thin Film Thermocouples (TFT)", Submitted to Journal of Heat Transfer (2005).

32. Sinha, N., Ahn, H. S., Williams, R. and Banerjee, D., "Packaging of Surface Micromachined Thin Film Thermocouples (TFT): Comparison of Resistance Arc Micro-Welding with Wire Bonding", Submitted to IEEE Transactions on Components and Packaging Technologies (2006).

VITA

Name: Nipun Sinha

Address: DII, 43/1, Andrews Ganj, New Delhi-110049, India

Email Address: nsinha@tamu.edu

Education: B.E., Mechanical Engineering, Panjab University, Chandigarh, India 2004

M.S., Mechanical Engineering, Texas A&M University College Station, Texas 2006